Extracellular vesicles and the quest for molecular biomarkers for amyotrophic lateral sclerosis

Charlotte Manser

Thesis submitted to the University of Ottawa

in partial fulfillment of the requirements for the MSc degree in Biochemistry

Department of Biochemistry, Microbiology, & Immunology

Faculty of Medicine

University of Ottawa

Abstract

Amyotrophic lateral sclerosis is a relentlessly progressive and fatal neuromuscular disease with no effective biomarkers, treatments or cure. In the early stages of ALS, it can be difficult to provide a diagnosis as patients do not meet diagnostic criteria until they become symptomatic, a sign of neuron degeneration. Early detection is therefore crucial to provide access to therapeutics prior to significant neuron loss. Extracellular vesicles are an ideal source of biomarkers as they contain a mix of proteins and nucleic acids reflective of the physiological state and are released from all cell types. We identified valosin-containing protein, integrin-beta 1 and gelsolin as potential biomarkers for ALS14 through proteomic analysis of EVs isolated from cell lines carrying the ALS-associated VCP-R155H mutation. My results indicate that EVs may serve as a valuable source of protein biomarkers in diagnostic, prognostic and predictive applications.

Acknowledgements

This thesis is written in dedication to my father Stephen Manser, who tragically died of ALS in 2013. It is gratifying that I have been able to honour my father with work which coincides with the research interests of my graduate supervisor, Dr. Robin Parks. Dr. Parks, I extend to you my sincere gratitude for your guidance, support and the numerous opportunities you have afforded me throughout my master's degree. I acknowledge and appreciate your time and efforts throughout the last two years. Thank you for your perceptive comments on various drafts of this manuscript and for bringing my attention to gaps in my knowledge and holes in my logic. Under your supervision I have learned the true value of integrity and leadership.

I express my deepest appreciation to my thesis advisory committee members, Dr. Dylan Burger and Dr. Johnny Ngsee. You have been selfless with your time, wisdom and advice. Your roles have extended far past what is typically expected of committee members; I can't even begin to express how grateful I am for your mentorship. Without your support, this manuscript may never have seen the light of day (mostly because I would have burned it…or buried it…or something far less dramatic like just deleting the file).

Dr. Ngsee, you have inspired me since the first day I walked into your lab. Thank you for introducing me to the world of ALS research and for continuing to stick by me after my time in your lab had concluded. Thank you for always making time for me and for providing thoughtful and sound advice.

Dr. Burger, thank you for your honesty, mentorship and time. Your candour is unparalleled; what I value most about your advice is that you have never, under any circumstances, told me what I wanted or felt I needed to hear. Your guidance has strengthened my abilities as a scientist and a person.

To the Parks lab: I would like to acknowledge my “lab mom”, Kathy Poulin, for your technical (and emotional) support the past two years. You’re my go-to source for all the hot gossip, you have better intel than anyone I know. My comrades in arms: Josh, Leslie, Charlie #2, Morgan, thank you for everything; your friendship has made graduate school worthwhile. I will never forget our countless coffee breaks, drinks and hilarious lab conversations. Thank you for your commiseration and participation in all of the lab shenanigans. I like to think I’ve inspired you to start shenanigans of your own. I hope we never lose touch.

Finally, I would like to acknowledge my wonderful family and friends. Mom, Ev, Greg, Katrina, MK, Morgan and Mike: I can’t even begin to thank you for your patience, kindness and support. You guys are my rocks and I wouldn’t be standing here without you. Thank you for being here for the highs and lows, for not kicking me when I’m cranky and if I haven’t said it yet: I’m sorry for anything I said while I was writing this manuscript (I swear it won’t happen again for like, another few years). Thank you for always being there.

Table of Contents

List of Abbreviations

ALIX: ALG-2 interacting protein X
ALS: Amyotrophic lateral sclerosis
ALSFRS-R: Revised amyotrophic lateral sclerosis functional rating scale
APOE-4: Apolipoprotein-E
ARF6: ADP-ribosylation factor 6
ARMMS: Arrestin domain containing protein 1-mediated microvesicles
ARRDC1: Arrestin domain containing protein 1
ATF6: Activating transcription factor 6
BiP: Binding immunoglobulin protein
CAV-1: Caveolin-1
CHOP: CCAAT-enhancer-binding protein homologous protein
CNS: Central nervous system
CSF: Cerebrospinal fluid
DAPI: 4'-6' diamidino-2-phenylindole
eIF2a: Eukaryotic initiation factor 2-alpha
ER: Endoplasmic reticulum
ERAD: ER-associated protein degradation
ESCRT: Endosomal sorting complexes required for transport
EV: Extracellular vesicle
FBS: Fetal bovine serum
FGM: Fibroblast growth media
FTD: Frontotemporal lobe dementia
FUS: Fused in sarcoma
GO: Gene ontology
H3: Histone 3
IBM: Inclusion body myopathy
IBMPFD/ALS: Inclusion body myopathy associated with Paget disease of bone (PDB) and/or frontotemporal dementia and/or ALS
ILV: Intraluminal vesicle
IRE-1: Serine/threonine-protein kinase/endoribonuclease
L/C: Liquid chromatography
LBD: Lewy body dementia
LMN: Lower motor neurons
LMV: Leukocyte-derived microparticles
LN: Lupus nephritis
MEM: Minimal Essential Medium
miRNA: MicroRNA
mRNA: Messenger RNA
MS: Multiple sclerosis
MSA: Multiple system atrophy
MVB: Multivesicular body
NfL: Neurofilament light chain
NTA: Nanoparticle tracking analysis
PDB: Paget's disease of the Bone

PERK: Protein kinase RNA-like endoplasmic reticulum kinase
PrP: Prion protein
RBP: RNA binding protein
ROI: Pegions of interest
ROS: Reactive oxygen species
SOD1: Superoxide dismutase 1
TARDBP: Tar DNA binding protein
tgG: Truncated rabies glycoprotein
TSG101: Tumor susceptibility gene 101
UPDRS: Unified Parkinson's Disease Rating Scale
UPM: Upper motor neurons
UPR: Unfolded protein response
UPS: Ubiquitin-proteasome system
VCP: Valosin containing protein
XBP-1: X-box binding protein 1

List of Figures

List of Tables

Chapter 1: Introduction

1.1 Amyotrophic lateral sclerosis

Amyotrophic lateral sclerosis (ALS) is a relentlessly progressive neuromuscular illness characterized by the gradual loss of motor neurons in the motor cortex (upper motor neurons) as well as those in the brain stem and spinal cord (lower motor neurons). ALS is fatal within 2-5 years of symptom onset with an estimated prevalence of 5 in 100,000 and an incidence of 3.8 per 100,000 people [1]. In Canada, ALS currently affects approximately 3000 individuals [2]. ALS was first clinically described by French neurologist Jean-Martin Charcot and named based on disease pathogenesis and progression; “amyotrophic” is derivative of the Greek phrase “amyotrophia” translating to “lack of muscle nourishment”, which refers to the denervation of muscle fibers accompanying neuron death, “lateral” refers to the area of the spinal cord affected, and “sclerosis” describes the hardening and scarring of the spinal cord as the nerves degenerate [3].

The etiology of ALS remains elusive; 90-95% of cases are sporadic, with no known cause or origin, and the remaining 5-10% are familial, with a genetic basis for the disease. Despite differences in subtype, patients with ALS generally show similar symptoms: disease generally begins with focal muscle weakness and atrophy that progressively worsens and spreads throughout the body. ALS disease progression is rapid, eventually leading to paralysis and death, usually by respiratory failure. Currently, there are over 30 subtypes of familial ALS that present with a range of phenotypes from juvenile to adult onset, bulbar vs. limb-onset and mild vs. aggressive disease progression

(Table 1.1) [4-15]. Regardless of onset or phenotype, affected individuals experience debilitating symptoms that lead to a loss in independence and quality of life, and ultimately loss of life.

Table 1.1: Characterization of familial ALS

Disease Subtype	Gene Implicated	Onset	Inheritance
ALS1	SOD1	Adult	AD; AR; De novo
ALS2	Alsin	Juvenile	AR
ALS3	SQSTM1	Adult	AD
ALS4	SETX	Juvenile	AD
ALS5	SPG11	Juvenile	AR
ALS6	FUS	Adult	AD; AR; De novo
ALS7	Unknown	N/A	AD
ALS8	VAPB	Adult	AD
ALS9	ANG	Adult	AD
ALS10	TARDBP	Adult	AD; AR
ALS11	FIG4	Adult	AD
ALS12	OPTN	Adult	AD; AR
ALS13	ATXN2	Adult	AD
ALS14	VCP	Adult	AD
ALS15	UBQLN2	Adult	XD
ALS16	SIGMAR1	Juvenile	AD
ALS17	CHMP2B	Adult	AD
ALS18	PFN1	Adult	AD
ALS19	ERBB4	Adult	AD
ALS20	hnRNPA1	Adult	AD; De novo
ALS21	MATR3	Adult	AD
ALS22	TUBA4A	Adult	AD
ALS23	ANAX11	Adult	AD
ALS24	NEK1	Adult	AD
ALS-CCNF	CCNF	Adult	AD
ALS-CHCHD10	CHCHD10	Adult	AD
ALS-DAO	DAO	Adult	AD
ALS-DCTN1	DCTN1	Adult	AD; AR; De novo
ALS-EWSR1	EWSR1	Adult	De novo (somatic)
ALS-FTD	C9ORF72	Adult	AD
ALS-hnRNPA2B1	hnRNPA2B1	Adult	AD
ALS-KIF5A	KIF5A	Adult	AD
ALS-PRPH	PRPH	Adult	AD; AR
ALS-TBK1	TBK1	Adult	AD

AD; Autosomal dominant, AR: autosomal recessive, XD: X-linked dominant, De novo: no evidence of inheritance

Some familial subtypes of ALS are more common than others. Pathogenic variants in C9ORF72 account for approximately 30-40% of all familial cases, superoxide dismutase 1 (SOD1) approximately 20%, while fused in sarcoma (FUS*)* and Tar DNA binding protein (TARDBP) each account for 5% [8,16,17]. Although SOD1-positive inclusions are common in sporadic and SOD1-associated familial ALS, TDP-43+ cytoplasmic inclusions are far more prevalent and are found in 95% ALS cases regardless of their genetic subtype [1,17-21]. As with other ALS-associated genes, there remains a question of whether or not mutations may play a role in sporadic cases of ALS; although rare, mutations in genes such as FUS and C9ORF72 have been identified in sporadic cases of ALS but are estimated to account for a very small proportion [17,22,23]. The large number of genes associated with ALS suggests that there is a downstream convergence at the molecular level that ultimately results in similar pathological consequences and phenotype, hence the disease state.

1.1.2 Amyotrophic lateral sclerosis and the multistep hypothesis

With over thirty familial subtypes in addition to sporadic cases, there is truly no simple answer to the question of what gives rise to the diversity and heterogeneity of ALS. The multistep hypothesis is a theory that derives from early cancer research, stating that disease development occurs through a number of molecular “steps” and incidence of disease can predict the number of “steps” required for development [24]. Each step can be defined as an event that perpetuates the toxic disease state; mutations, aberrant posttranslational modifications and environmental insults are all proposed mechanisms that could bring an individual closer to the disease state. The number of “steps” required for disease to develop can be mathematically determined by the incidence of the disease

itself. For instance, if disease was caused by a single event, the incidence would be directly proportional to the probability of exposure to the disease-causing element and the probability that the molecular event would occur within a given year [25]. As multiple steps become involved, the calculations become increasingly complex and an algorithm is applied. Like cancer, development of ALS is a multistep process, with six steps to disease onset [25]. Although these steps are not clearly defined, recent evidence suggests that genetic mutations account for one or more steps of these steps, thus requiring fewer steps prior to disease onset [26]. A cohort of 1077 patients was tested for mutations in genes associated with common familial ALS subtypes and the number of steps associated with each mutation was determined by performing a regression of the log of age-specific incidence versus the log of age with least-squares regression for the subpopulation carrying disease-associated mutations for each gene [26]. Individuals carrying mutations in C9ORF72 (3 steps), SOD1 (4 steps) and TARDBP (2 steps) had fewer remaining steps until disease onset compared to individuals who did not possess any known disease-associated mutation (6 steps) [26]. Thus, patients who carried disease-associated mutations had fewer steps in the preclinical stages of disease, supporting the idea that the ALS development is a multistep process in which environmental factors and epigenetic changes play a significant role. The question remains of what epigenetic, molecular or environmental processes contribute to the disease state and how positively associated risk factors may contribute to these processes. Accelerated DNA-methylation and aberrant histone modifications, two epigenetic processes, appear to play a role in early ALS pathogenesis and are likely triggered by environmental variables [27,28]. The exact environmental variables remain largely elusive; risk factors for ALS include aging,

military service and cigarette smoking, although these are largely based on positive association [29,30]. Indeed, while not completely elucidating the mechanism behind ALS pathogenesis, the multistep hypothesis helps account for a certain degree of phenotypic heterogeneity seen in ALS. Indeed, the multistep hypothesis highlights the importance of identifying relevant pathological variables and in turn, what cellular processes are triggered in the ALS disease state.

1.2 Mutations in VCP cause ALS14

Mutations in *valosin containing protein* (VCP) are causative in a rare form of familial ALS termed ALS14 (Table 1.1). VCP mutations account for approximately 1-2% of familial cases of ALS (Figure 1.1, Table 1.1) [31]. Currently, eight (R155H, R159C, R159G, R191Q, N387T, D592H, D529M, R662C) out of the twenty identified pathogenic VCP mutations have known associations with the development of the ALS phenotype, while the remainder are associated with other VCP-associated disorders, as discussed in section 1.2 (Figure 1.1) [31,32]. VCP has also been implicated in at least some instances of sporadic ALS: whole exome screening for documented pathogenic VCP mutations (R159C, N387T, R662C) in a large cohort (n=701) of sporadic ALS patients revealed identified mutations in 3 out of 701 cases screened. Therefore, similar to other forms of ALS, VCP mutations are associated with rare forms of familial and sporadic ALS.

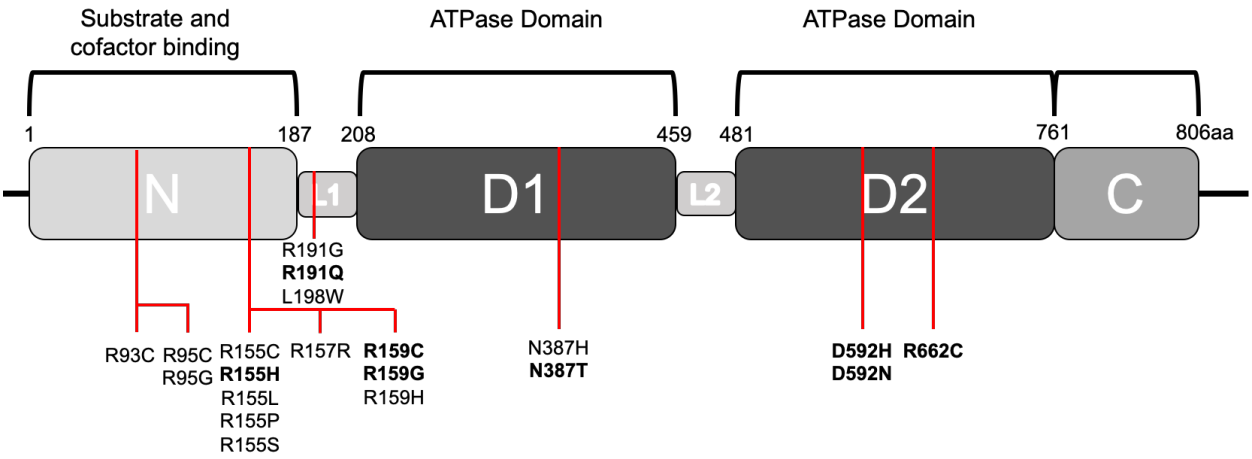

Figure 1.1: Schematic representation of the VCP gene and pathogenic mutations associated with IBMPFD/ALS. The VCP protein is comprised of 806 amino acids and is divided into four distinct regions: An N domain, two ATPase domains, D1 and D2 with linkage regions L1 and L2, and a C terminal domain. Mutations associated with ALS are indicated by bold typeface.

1.2.1 Mutations in VCP cause a complex multi-system proteinopathy

Mutations in the VCP gene cause an autosomal dominant, multisystem proteinopathy known as inclusion body myopathy (IBM) associated with Paget disease of bone (PDB) and/or frontotemporal lobe dementia (FTD) and/or ALS (IBMPFD/ALS). IBMPFD/ALS is a highly complex and rare disease, affecting multiple organ systems and causing widespread debilitating symptoms. The incidence of IBMPFD/ALS is between 1:300,000 and 1:600,000, although these estimates are based on patient cohorts from England and Scotland; worldwide incidence has yet to be determined [33]. Named after the most common phenotypes associated with the disease, individuals with IBMPFD/ALS may present with IBM, PDB, FTD and/or ALS [34]. Although rare, individuals with IBMPFD/ALS can display a number of other phenotypes including Charcot Marie Tooth Disease, hereditary spastic paraplegia and Parkinson's Disease, in addition to those previously mentioned [34]. Regardless of phenotype, IBMPFD/ALS patients typically die of

respiratory or cardiac failure and cardiomyopathy [35]. Post-mortem and *in vitro* studies reveal that VCP disease typically results in a number of distinct cellular characteristics including ubiquitin and TDP-43-positive inclusions in the brain, muscle and heart, and rimmed vacuoles in the cytoplasm of skeletal muscle cells [36,37]. The age of disease onset is highly variable and largely dependent on phenotype but, similar to other forms of ALS, typically occurs around middle age (50 years) [34].

Phenotypes of IBMPFD/ALS have variable penetrance and thus affected individuals within the same family can display a multitude of phenotypes with varying degrees of severity despite possessing the same mutation [34]. Modifier genes may account for much of the phenotypic variability in IBMPFD/ALS, as individuals with sharing the same mutations display such a large degree of disease heterogeneity. The epsilon-4 allele of apolipoprotein-E (APOE 4) is proposed as a potential modifier in a number of diseases including late onset Alzheimer's disease, Lewy body dementia (LBD) and IBMPFD/ALS [16,38]. Apolipoproteins mediate lipid transport and metabolism and exist in three isoforms: APOE2, the rarest isoform is considered "protective", APOE3, the most common isoform which has been deemed "neutral" and APOE4 [39]. Each APOE isoform differs by only two amino acid residues [40]. In IBMPFD/ALS, APOE4 is thought to contribute to the development of FTD [16]. Although the precise mechanism has not been fully elucidated, APOE4 has been found to impair phagocytosis, migration, and metabolic activity in microglia and is thought to increase the risk of dementia as a direct regulator of α-synuclein and amyloid-β [38-40]. Although uncommon, α-synuclein-positive inclusions have been documented in a number of patients with IBMPFD/ALS during post-mortem

studies [41]. Regardless, a study of APOE genotypes in a cohort of 174 individuals from fifteen documented IBMPFD/ALS families found that presence of the APOE4 genotype is associated with the FTD phenotype when in possession of a VCP mutation [16].

1.3 VCP function at a cellular level

VCP is a versatile protein with broad functions that extend to many areas of cell physiology, with an overarching role in maintenance of protein homeostasis. Through interactions with cellular binding partners (referred to as cofactors), VCP plays vital roles in protein and DNA quality control such as chromatin-associated degradation, ER-associated protein degradation (ERAD), cytosolic degradation, autophagy and the ubiquitin-proteasome system (UPS) [42-49]. Under physiological conditions, VCP mitigates cellular stress by extracting and ubiquitinating misfolded proteins from membranes, unfolding mature proteins targeted for proteasomal degradation and segregating proteins for elimination or activation by binding proteins [50]. It is therefore unsurprising that the loss or reduction of VCP causes numerous deleterious effects that actively contribute to the IBMPFD/ALS disease state, including the accumulation of misfolded protein that can lead to loss-of-function phenotypes and formation of protein aggregates that can have toxic gain-of-function phenotypes [49].

1.3.1 VCP in proteostasis

Proteostasis is maintained by three cellular processes: regulated protein synthesis, chaperone-mediated protein folding and protein degradation pathways. VCP plays an integral role in protein degradation, especially at the endoplasmic reticulum (ER),

where it participates in the coordinated responses of the unfolded protein response (UPR), ERAD and autophagy. ERAD and autophagy are pro-cell survival processes that help maintain cell proteostasis by degrading misfolded and aggregated proteins from the ER. Failure to do so leads to the accumulation of misfolded proteins in the ER-lumen causing the chaperone protein BiP to dissociate from the three membrane-bound UPR sensors, IRE-1, PERK and ATF6, to activate the UPR [51]. As a coordinated signaling cascade, the UPR has three main objectives: 1. Halt translation of new proteins, 2. Upregulate the production of chaperones to refold misfolded proteins and 3. Degrade misfolded proteins through upregulation of ERAD and autophagy [51]. The signaling cascades activated by the UPR, although initially independent, are overlapping and their responses are coordinated in an attempt to reestablish proteostasis. VCP, despite its many functions, is not necessarily a direct player in the UPR but plays a vital role in the process as a direct regulator of ER stress [42]. This notion is emphasized by the fact that a reduction of VCP leads to increased expression of the UPR machinery, specifically chaperone protein BiP and downstream effector of the PERK pathway, CHOP and increased downstream UPR activity though the phosphorylation of eIF2α and splicing of XBP-1 mRNA [52].

The first two UPR sensors, IRE-1 and ATF6, upregulate pro-cell survival signaling pathways to increase ERAD and clear misfolded proteins from the ER [51,53]. ERAD is constitutively active but upregulated in times of ER-stress, working to remove misfolded, unwanted or superfluous proteins from the ER to be degraded by the proteasome via the ubiquitin proteasome system (UPS) [50,53,54]. During ERAD, VCP is recruited to the ER by

ER-localized protein VIMP, where they form a complex with Derlin and gp78 [50]. VCP then uses ATP-hydrolysis to extract the substrate from the ER and recruits proteins Ufd2, Rad23 and Dsk2 to form a complex to facilitate the transfer of the ubiquitinated substrate to the proteasome for degradation [50,55]. Reduction of VCP levels by RNAi in HeLa cells results in incomplete clearance and accumulation of proteins in the ER, promoting activation of the UPR [42]. Therefore, reduction of VCP not only has detrimental effects on ERAD but leads to accumulation of proteins in the ER and sustained activation of the UPR.

ERAD is tightly linked to the process of autophagy, where decrease or inhibition causes the compensatory upregulation of autophagy to clear proteins from the ER. Induction of autophagy, in addition to upregulation of chaperone proteins, are two of the short-term consequences of the activation of the third arm of the UPR, mediated by the protein kinase PERK (protein kinase RNA-like endoplasmic reticulum kinase). Upon activation, PERK causes the phosphorylation of eIF2α to halt translation and initiate pro-cell survival responses [51]. Autophagy is a highly conserved cellular process in which the cell degrades superfluous or damaged intracellular components in an effort to maintain homeostasis [56]. Among these cellular components are organelles, soluble and misfolded/aggregated proteins, stress granules and pathogens, and other cytosolic content [56]. Although many aspects of autophagy have been studied extensively, the exact role of VCP in autophagy has not been fully elucidated. Some research suggests that VCP is involved in autolysosome maturation; loss of VCP activity results in the

accumulation of autophagosomes in the cytoplasm and impaired clearance of cytoplasmic structures called stress granules [45,46,57].

While activation of the UPR in the short term is beneficial to the cell and serves as a means to remedy cellular stress, sustained UPR activity can be fatal. When the UPR fails to re-establish proteostasis through increased chaperone activity, ERAD and autophagy, the PERK and IRE-1 arms of the UPR activate the downstream effectors to initiate pro-apoptotic pathways. Sustained activation of PERK leads to upregulation of the pro-apoptotic protein CHOP, while IRE-1 activates JNK signaling that ultimately leads to induction of programmed cell death [51]. Thus, the consequences of prolonged ER stress are great, leaving little room for error. VCP is highly involved in the maintenance of proteostasis, the loss of which results in the accumulation of protein aggregates, defects in ERAD and autophagy and increased UPR activity [42,55,57,58]. All pathogenic VCP mutations have a dominant negative mechanism of action and thereby reduce the levels of functional VCP within the cell, which ultimately causes the IBMPFD/ALS disease state [34,59,60]. Fully elucidating the cellular role of VCP may aid in the development of targeted therapeutic approaches to slow progression or eradicate disease.

1.3.1 Impact of VCP on RNA Metabolism

Although there is evidence for a number of pathogenic mechanisms that are characteristic of the ALS disease state, two of the most widely accepted are dysfunctional proteostasis and disruptions of RNA metabolism [61]. RNA metabolism and proteostasis are intrinsically linked, exemplified by the stress granule formation in response to

inhibition of general translation as a means to stabilize mRNA [62]. Stress granules are membrane-less, cytoplasmic structures that form in response to cellular stress (e.g. heat shock, oxidative stress, UV radiation, external chemicals) [63]. Primarily thought to be protective, stress granules serve to stabilize mRNA and sequester apoptotic proteins to help the cell adapt to stress conditions [64]. The formation of stress granules can be simplified to three steps: Firstly, translation is halted and accompanied by primary aggregation: RNA binding proteins with prion-like/intrinsically disordered domains bind untranslated mRNA to form multimeric complexes, their low complexity domains facilitating the formation of multimeric complexes through the process of liquid-liquid phase separation [65]. Interestingly, the RNA binding proteins (RBPs) in stress granules include ALS-associated proteins TDP-43, FUS and Matrin 3. Secondly, secondary aggregation occurs and stress granule nucleators such as ATX2 and G3BP, are recruited to stabilize the stress granule structure. Lastly, proteins at the core of the stress granules recruit a number of signaling molecules including scaffold proteins such as TRAF2 and RACK1, which serve to integrate various stress signaling cascades to mediate cross-talk during the cellular response to stress [66]. Generally, stress granules will disassemble as the cell recovers and are cleared from the cytosol via autophagy.

Mutations in a number of RBPs found in stress granules are linked with familial ALS including TDP-43, FUS, TAF15, EWSR1, hnRNPA1, hnRNPA2B1, ATXN2 and TIA1 (Table 1.1). Furthermore, the characteristic cytoplasmic TDP-43 aggregates observed in cells in most ALS disease models and in patient tissue are thought to be due to increased production of stress granules or the production of more stable stress granules that cannot

be cleared from the cytosol [65,67,68]. TDP-43 is a key modulator of stress granule formation, and is required for stress granule formation in astrocytes as well as primary motor and cortical neurons [69]. As previously described, VCP directly contributes to interruptions in RNA metabolism through its regulatory roles in proteostasis and stress granule clearance via autophagy. VCP knock-down via siRNA or chemical inhibition in HeLa cells results in decreased stress granule clearance and increased cytoplasmic TDP-43 [46]. Therefore, in the case of VCP-related disease, the dominant-negative mechanism of action of VCP mutations and subsequent defects in autophagy directly translate into the accumulation of ubiquitinated protein aggregates and stress granules characteristic of the ALS disease state [57,59].

1.4 ALS Therapeutics

ALS is the most common adult-onset neuromuscular disease and despite the large demand for a cure, there are limited therapeutic options for patients and treatment largely consists of symptom management and comfort measures. ALS-targeted therapeutics are currently restricted to two drugs, riluzole and edaravone, which are modestly effective in slowing ALS disease progression but ultimately unsuccessful in increasing life expectancy by more than a few months. Thus, many trials rely on the Revised amyotrophic lateral sclerosis functional rating scale (ALSFRS-R), a questionnaire designed to stratify the severity of ALS and provide an indirect measure of therapeutic efficacy to clinicians, as the primary endpoint of their studies. Riluzole, a glutamatergic antagonist, is the best recognized treatment for ALS and was first approved in Canada in the year 2000 [70]. Riluzole targets excitotoxicity in the brain, although the exact molecular

targets have not been fully elucidated. Riluzole may function through preventing the uncurbed release of excitatory neurotransmitter into the synapse, thereby preventing subsequent detrimental cellular signaling cascades that leads to excessive intracellular calcium, mitochondrial dysfunction, the release of reactive oxygen species (ROS) and ultimately cell death [71]. The ability of riluzole to delay disease progression is surprisingly modest; outcomes of randomized clinical trials indicate that although riluzole does not vastly improve the maintenance of overall muscle strength, it may reduce or delay the severity of bulbar and limb dysfunction [72]. Clinical trials showed that riluzole increased mean survival by 2-3 months and ultimately delayed the need for a tracheostomy [72]. Therefore, riluzole not only increases life expectancy but it also may prolong the quality of life of ALS patients.

Previously used to treat acute cerebral infarction and ischemic strokes in Japan and the United States, edaravone was first approved for the treatment of ALS in Canada in October 2018 [70]. Treatment of a hypoxia/ischemic mouse model with edaravone reduced ER dysfunction and stress, making it an attractive treatment option for ALS [73]. Although the specific molecular targets of edaravone in the treatment of ALS have not been fully elucidated, it may act as a powerful antioxidant, scavenging harmful free radicals from circulation [74]. Edaravone was subsequently studied as a potential treatment for ALS using the popular SOD1-G93A mouse model, which were treated with edaravone daily via intraperitoneal injection from the time of disease onset [74]. Edaravone significantly slowed disease progression in the mice and mean survival was extended by 4-11 days, which researchers approximate would clinically correspond to 7-20 months in human

subjects [74]. Unfortunately, this prediction has yet to be validated; a meta-analysis of clinical trial data was performed in 2019, finding that despite improved scores in the ALSFRS-R, there was no significant improvement in the life expectancy of patients treated with edaravone [75]. Therefore, treatment with edaravone can improve the quality of life for patients with ALS by slowing disease progression, however further research must be done to ascertain its mechanism of action.

Despite limited efficacy, these two drugs provide hope for the ALS community that viable treatments may be within reach. However, the road to a treatment is long and full of many challenges. The ability to custom tailor therapeutics for ALS is greatly encumbered by the heterogeneous nature of the disease and lack of understanding of the underlying cause of ALS pathology. Recent work suggests active immunotherapy (vaccination) may be an effective strategy to prevent and slow overall disease progression in ALS, Parkinson's and Alzheimer's disease [76-78]. As with prion diseases, certain non-native pathogenic configurations of proteins such as amyloid-β, tau, α-synuclein and SOD1 are hypothesized to spread via seeding mechanism resulting in a progressive neurodegenerative disease state [77-80]. The use of prophylactic immunotherapy in prion and prion-like diseases aims to impair the interaction between the diseased and natively conformed proteins to limit recruitment and conversion, alter trafficking of diseased proteins and prolong the stage of peripheral amplification by depleting the availability of natively conformed proteins [81]. In the context of ALS, vaccines were designed using a disease-specific epitope (DSE) strategy to target regions of the SOD1 protein that are highly amyloidogenic and prone to misfolding in destabilizing

conditions[76]. Researchers used a truncated rabies glycoprotein (tgG) as a carrier protein in SOD1 vaccines, which have previously been shown to elicit a strong Th2-biased humoral response in vaccinated mice [82]. The vaccines, tgG-DSE2lim and tgG-DSE5b were then administered to transgenic SOD1-G37R mice at 0 and 3 weeks. Both vaccines proved successful and significantly improved the life expectancy of SOD1 transgenic mouse models; tgG-DSE2lim was most effective in the preclinical stages prior to symptom onset while tgG-DSE5b significantly delayed disease onset and progression [76]. With such promising results, there is hope that combinatorial treatment including prophylactic immunotherapy for familial ALS will be an innovative treatment option for ALS.

Many experimental treatments currently under development act through a general mechanism, and aim to prevent motor neuron death, which, in theory, can be achieved a number of ways. Anti-apoptotics, antioxidants, anti-aggregates, anti-inflammatories and anti-excitotoxic agents could, potentially, all slow disease progression. Testing the efficacy of these therapies in sporadic and familial ALS is severely limited by the lack of sensitive biomarkers, which could predict who is facing increased risk of developing disease and allow for early enrolment into clinical trials. For this reason, researchers and clinicians rely heavily on patients with familial ALS and preclinical models such as transgenic mice, zebrafish and cell culture for which disease onset and progression can be more easily predicted. Focusing on specific familial ALS subtypes can control for environment and genetic background, while elucidating the underlying disease pathology and determining the best treatment strategy [83,84]. The hope is that, once there is a viable

treatment for a specific subtype, the same knowledge or process can be applied for all subtypes, leading to the development of a successful treatment for ALS.

1.5 Clinical biomarkers for ALS

One of the central limitations in the development of therapeutics for ALS is the lack of sensitive biomarkers. A biomarker consists of any measurable parameter that is indicative of a certain biological state such as health, infection or disease [85]. Biomarkers can be broadly classified into three categories: diagnostic, prognostic and pharmacodynamic/predictive (Figure 1.2). Diagnostic biomarkers, the primary indicators of disease, are used to identify an individual in the midst of a particular disease state, helping to distinguish affected individuals from the rest of the population [85]. Prognostic biomarkers are used to predict the probability of future clinical events such as death or relapse, determine who is at risk, monitor disease progression and predict outcome in an identified population regardless of therapeutic intervention [85]. The third type of biomarker is predictive or pharmacodynamic. Predictive biomarkers are used to examine treatment efficacy in comparison to a control population or the condition of the patient prior to treatment [85]. In ALS, clinicians rely on a number of biomarkers to evaluate the overall well-being of the patient while progressing through the disease state; functional rating scales, biometric measurements, laboratory tests, electrophysiology and a variety of imaging techniques are all among the current strategies used for the diagnostic, prognostic and predictive applications for ALS (Table 1.2) [84,86,87].

Table 1.2 Summary of select clinical biomarkers for ALS

Biomarker		Key findings	Interpretation
Biometric			
Body Weight		5-10% weight loss from established baseline	Indicator of poor prognosis, correlates with faster disease progression
Forced/slow vital capacity (FVC/SVC)		Reduced with disease progression	Non-invasive, limited use in bulbar illness, used as a clinical marker of respiratory function
Imaging			
Structural MRI		Focal atrophy, cortical hyperintensities	Excludes ALS mimics
PET Scan		Changes in serotonergic neurotransmission, increase in microglial activation and oxidative stress	Excludes ALS mimics
Electrophysiology			
Motor unit number estimation (MUNIX)		Declines with disease progression	Sensitive marker of disease progression, identifies pre-clinical LMN degeneration
Biofluids			
Neurofilament light chain (NfL)	Blood	Steady increase in levels over time	Sensitive marker of disease progression (neurodegeneration)
	CSF	Elevated levels	Diagnostic biomarker, non-disease specific
Creatinine kinase (Blood)		Reduction of creatinine kinase	Indicator of muscle denervation, predictor of slow vs. fast disease progression
Rating scales			
Revised ALS Functional Rating Scale		Scores decline throughout disease progression	Indicator of poor prognosis, used to monitor treatment efficacy and disease progression

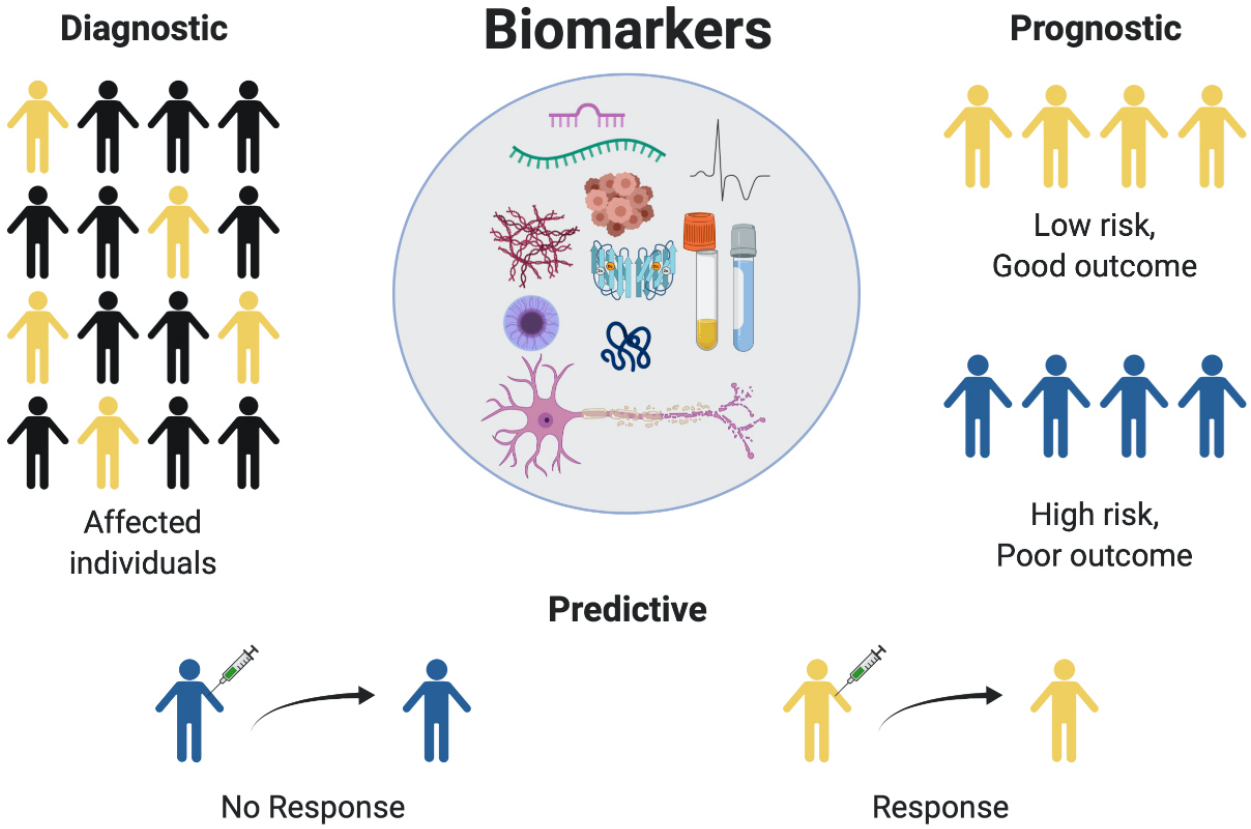

Figure 1.2: Summary of biomarker types. Biomarkers can be broadly classified into three categories: diagnostic: the primary indicators of disease, prognostic: indicators of what is to come, and pharmacodynamic/predictive: indicators of treatment efficacy.

Throughout the natural progression of disease, ALS is distinct relative to many neuromuscular disorders due to the involvement of both upper and lower motor neurons yet presents with significant phenotypic variation in the initial disease stages. Despite recent advances to improve the sensitivity and accuracy of medical imaging techniques and electrophysiology for early diagnosis, test accuracy and specificity largely depends on disease manifestation in the early stages, varying greatly depending on the presence of UMN vs. LMN signs [88-92]. As such, the median diagnostic delay, referred to as the time between symptom onset and positive diagnosis, for patients with ALS is approximately 1

year, by which time patients have experienced significant physical decline and irreversible motor neuron degeneration [61,83,88]. The resulting lag between disease onset and diagnosis prevents early therapeutic intervention and enrolment in clinical trials, impeding the evolution and improvement of clinical care for ALS [88]. Earlier detection of ALS would allow for expeditious medical intervention and possible enrolment in clinical trials perhaps even prior to the manifestation of overt symptoms, which may improve the efficacy of current therapeutics [88]. Thus, there is an urgent need for a sensitive and disease-specific biomarker that could differentiate between individuals who are healthy and those in the very early or preclinical stages of ALS.

1.5.1 Molecular Biomarkers in ALS

The exact timing of when patients transition from the preclinical stage of disease to the clinical stage of disease is difficult to pinpoint. Subtle pathological changes likely begin at the cellular level in the preclinical disease phase, evolving and manifesting into the visible symptoms characteristic of the clinical stage of disease [31,93,94]. To be efficacious, treatment likely must be initiated prior to significant motor neuron death, or, more simply, prior to symptom onset. Aside from those with a history of familial ALS, most individuals are unaware of their risk or predisposition to disease [88]. As many of the physical symptoms of ALS are the result of upstream changes at the cellular level, molecular biomarkers may hold the key to early detection. Consisting of any quantifiable biophysical constituent, potential molecular biomarkers may include nucleic acids (e.g. DNA, RNA, miRNA), small molecules (lipids, glycans, etc.), proteins and peptides that are indicative of the physiological state of the patient. Moreover, molecular biomarkers

can be detected in a number of bodily fluids such as urine, blood, cerebrospinal fluid (CSF) and saliva, and are minimally invasive candidates for use in diagnostic, prognostic and predictive applications.

One of the most widely investigated examples of a molecular biomarker for neurological conditions is neurofilament light chain (NfL). Exclusive to neurons and concentrated in the axon, neurofilaments serve to maintain structural integrity and enable high conduction speeds within the central nervous system (CNS) [95]. First observed in ALS and Alzheimer's disease in 1996, elevations of NfL in blood and CSF are commonly observed in many neurodegenerative diseases, including Huntington's, spinal muscular atrophy, Parkinson's, multiple sclerosis and spinal cerebellar ataxia [86,96-100]. Under physiological conditions, NfL is slowly released into the interstitial fluid and passes freely into the CSF and, to a lesser extent, blood [96]. As the most abundant of the neurofilament subunits in the body, NfL is the most reliably quantified, making it an ideal candidate for a biomarker [96]. The concentration of NfL in the CSF and blood are initially high in neonates and decrease throughout childhood [101]. Although NfL levels gradually increases in healthy populations with age, axonal damage due to inflammatory processes and neurodegeneration cause these levels to increase dramatically [96]. Throughout ALS disease progression, the gradual degeneration of motor neurons results in a progressive increase in plasma and CSF NfL levels, emphasizing its utility as a prognostic biomarker [95]. The diagnostic value of NfL has been highlighted by its ability to discriminate between healthy and preclinical patients in the process of developing ALS [93]. While no significant difference in levels of NfL between asymptomatic and controls was observed, NfL levels

in individuals who were in the process of transitioning into the clinical stages of disease (phenoconversion) were significantly elevated in CSF for almost a year prior to disease onset [93]. Additional information shows that including the measurement of TDP-43 in and NfL in CSF samples can increase disease specificity and diagnostic performance for ALS [102].

The current diagnostic process for ALS is one of exclusion; relying heavily on the ability of experienced neurologists to exclude ALS mimic diseases through the collection of supporting data from biofluid analysis, electrophysiological studies, muscle biopsies and diagnostic imaging such as MRI [87]. To be incorporated into the clinical standard of care for ALS, further investigations must be performed to obtain a more comprehensive understanding of NfL levels at defined stages of disease and in overlapping phenotypes [103]. Furthermore, despite the advances in the study of NfL, its utility as a biomarker for ALS remains in question; NfL is a marker of axon degeneration, where elevations in levels are seen across a spectrum of neurodegenerative diseases. Moreover, NfL levels do not readily correlate with disease progression. Thus, there is a demand for sensitive, disease-specific biomarkers to stratify the ALS disease state.

1.6 Extracellular vesicles

Extracellular vesicles (EVs) are small, spherical particles that are secreted by cells into the extracellular space. Evidence for the existence of EVs was first proposed in 1967 by Peter Wolf while studying blood coagulation; however, the idea of EVs extends back to Charles Darwin, who in 1868, proposed that every cell type in the body secretes minuscule-sized particles he dubbed “gemmules” [104,105]. Darwin hypothesized that

gemmules were susceptible to environment-mediated modifications, were used for paracrine signaling and helped mediate the maternal-fetal transfer of heritable information [104]. Although some of Darwin's predictions turned out to be true, unfortunately his theory was not accepted during his time and was largely disregarded. We now know that cells release a variety of EVs that are classified based on biogenesis, size and content (Table 1.3). Previously, EVs were thought to act as a "garbage disposal", ridding the cell of unwanted proteins and debris [106]. EVs serve a much greater purpose, helping to mediate intercellular communication with targets both near and far. The largest subtype (>1000nm), named apoptotic bodies, are produced as the cell undergoes the final stages of apoptosis and are arise from blebbing from the plasma membrane [107]. Microparticles or microvesicles, are the second largest vesicle subtype (200-1000nm) and form in response to cellular stress [107,108]. Microparticles originate directly from the plasma membrane; protrusions bud from the plasma membrane and are shed into the extracellular space. Arrestin domain containing protein 1 (ARRDC1)-mediated microvesicles (ARMMs; <100nm) are a type microparticles that originate from the plasma membrane via interactions with tumor susceptibility gene 101 protein (TSG101) [109]. The fourth type of extracellular vesicle, exosomes (30-150nm), are formed as intraluminal vesicles via the invagination of the endosomes to form the multivesicular body (MVB) and are released from the cell when MVB fuses with the plasma membrane [107].

Table 1.3: Extracellular vesicle subtypes

	Size	Mechanism of biogenesis	Content
Exosomes	30-150nm	Fusion of MVB with plasma membrane	Protein, RNA, miRNA, lncRNA, mRNA
ARMMs	<100nm	Budding of the plasma membrane	Protein, RNA*
Microparticles	200-1000nm	Budding of the plasma membrane	Protein, RNA, miRNA, lncRNA, mRNA
Apoptotic Bodies	>1000nm	Membrane blebbing during apoptosis	Protein, RNA, miRNA, organelles, DNA, lncRNA

Asterisk (*) indicates content not yet confirmed

1.6.1 Biogenesis

Microparticles, and exosomes fall into two separate categories based on their biogenesis; microparticles are ectosomes and are formed by the outward budding of the plasma membrane while exosomes are formed from the invagination of endosomes to form intraluminal vesicles [107,109]. Microparticles are shed from the cell in response to stress or activation; the plasma membrane buds outwards and pinches off, releasing vesicles into the extracellular milieu [110]. During this process, cargo (proteins, RNAs) is trafficked to the cell surface by proteins ARF6 and Rab22a, the lipids at the membrane redistribute and contractile machinery, largely mediated by the protein ARF1, is used to pinch off and form vesicles [110]. Exosomes are formed intracellularly through the inward budding of the endosomal membrane [107]. Formation of intraluminal vesicles (ILVs), exosome precursors, requires the participation of the endosomal sorting complexes required for transport (ESCRT). The ESCRT machinery is composed of four proteins: ESCRT-0, ESCRT-I, ESCRT-II and ESCRT-III and helps recruit a variety of accessory proteins such as Vps4, ALG-2 interacting protein X (ALIX), TSG-101 and CHMP4 to cooperatively aid in the abscission of the endosomal membrane. The ILVs, contained

within the MVB, will then be transported to the plasma membrane where the MVB will fuse and release its contents as exosomes. Alternatively, the MVB can also be transported to the lysosome, where it is subject to degradation [107]. Like microparticles, ARMMs are formed by the budding of the plasma membrane, driven by the interaction of ARRDC1 and TSG101, which is recruited from endosomes to the plasma membrane by ARRDC1[109]. Although ARMMS are enriched for ARRDC1, TSG101 and proteins associated with ESCRT complexes, very little is currently known about their content [109].

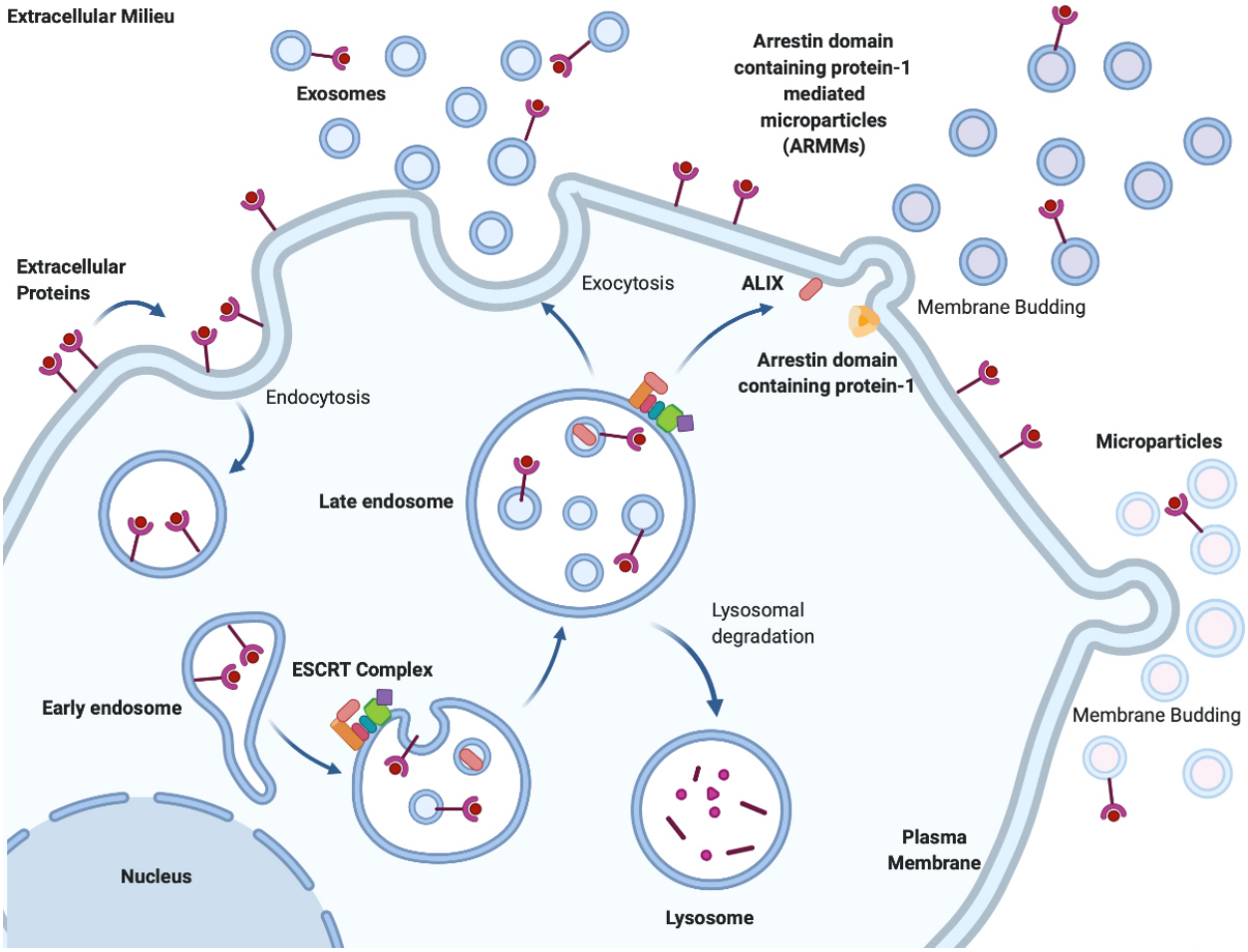

Figure 1.3: Schematic representation of exosome, ARMMS and microparticle biogenesis. Exosomes are formed through a series of membrane invaginations resulting in the formation of the endosome and intraluminal vesicles, which are then released into the extracellular milieu as exosomes by exocytosis. Microparticles are formed through the outward budding and pinching off of the cell membrane into the extracellular milieu. Figure created with BioRender.com.

1.6.2 EV isolation and characterization

Many current EV isolation strategies such as PEG-precipitation, differential ultracentrifugation and tangential flow filtration rely primarily on size classification. Despite differences between microparticles and exosomes, these distinct EV subpopulations frequently overlap in size [106]. Exosome and microparticle size can range from 30-200nm

and 100-1000nm, respectively, thus complicating the ability to isolate discrete populations of vesicles [106,111]. Recent guidelines established by the *International Journal for extracellular vesicles* (2018) [112] recommend extensive characterization of EVs, including the use of protein markers to provide evidence for biogenesis, single vesicle characterization through the use of electron microscopy and non-electron microscopy based single particle analyzers (nanoparticle tracking analysis [NTA]) [112]. Positive markers for EVs include proteins that are enriched in EVs such as flotillin-1 and -2, ALIX, TSG-101, CD81, CD63 and CD9 [106]. A cytosolic marker, such as tubulin or GAPDH is also recommended to ensure that vesicles are present within the sample and not just fragments of membranes. Differences in discrete populations of EVs can be distinguished by negative control protein markers, as these serve as a good indicator of biogenesis and sample purity. Proteins from different subcellular compartments may be present or absent due to the nature of how the different vesicle subtypes are produced [112]. Nuclear proteins, such as histone 3 (H3), for instance, are present in apoptotic bodies due to nuclear fragmentation in late stage apoptosis but are typically absent from both microparticles and exosomes. Despite the use of positive and negative EV markers to maximize the confidence of sample purity, the size-based nature of EV isolation does not exclude protein complexes and membrane fragments of similar target size from contaminating a sample. Moreover, EV protein markers cannot prove biogenesis, which prevents the definitive identification of vesicle subtypes [112]. NTA, although informative, has a limited ability to quantify EVs of very large (<400nm) and small (>50nm) sizes. Therefore, all samples isolated are assumed to be a mixed population of vesicles, centered around a certain size parameter.

1.6.3 Extracellular vesicle cargo sorting

Although the precise mechanism of EV cargo sorting has yet to be fully elucidated, EV content is determined by selective and passive processes during microparticle and exosome formation [110,113-117]. Some elements are incorporated into EVs by chance due to their proximity to the endosomal or plasma membrane, others are selectively trafficked to these areas and targeted for export from the cell [113,118]. In exosome biogenesis, beyond promoting the formation of ILVs, the ESCRT machinery and a number of accessory proteins, including ALIX and TSG-101, participate in protein and nucleic acid sorting for exosomal cargo [119-122]. ESCRT-0 binds proteins ubiquitin-tagged proteins and recruits them to the membrane of the late endosome/MVB, where ESCRT-I and -II are responsible for sequestering ubiquitinated cargo into buds and ESCRT-III then mediates membrane scission to form the ILVs [123,124]. In addition to membrane scission, ESCRT-III can be recruited by ALIX to the endosome to mediate the sorting of tetraspanins into exosomes [125]. ESCRT-independent mechanisms for cargo sorting may involve tetraspanins such as CD63 which has been implicated in the sorting of cargo in melanocytes and Tspan8, to selectively recruits mRNA and proteins into exosomes [117,118,124]. Selective recruitment of cargo during biogenesis is also evident in the case of microparticles. Proteins such as ADP-ribosylation factor 6 (ARF6) and Rab22a mediate selective protein recruitment during microparticle biogenesis [126,127]. Furthermore, conserved “zip code” RNA in the 3’ untranslated region and miR-1289 may function to enrich certain mRNAs in microparticles [128]. Additionally, recent work suggests that

ARMMs are capable of actively recruiting certain proteins during biogenesis, such as surface receptors, which can be transmitted to other cells [129]. Thus, since EVs are important mediators of intercellular signaling, the selective incorporation of protein and RNA cargo is integral in message transmission and induction of important cellular processes.

1.6.4 The role of extracellular vesicles in the spread of disease

Selectively imported cargo allows EVs to control the types of messages that are communicated to surrounding cells. In the context of disease, these mechanisms for cargo selection can be exploited to transport and spread pathogenic material to induce pathological changes in surrounding cells [130]. There is evidence that SOD1 and TDP-43, which appear as characteristic insoluble cytoplasmic inclusions in muscle and upper and lower motor neurons of ALS patients, can spread from one cell to another [18,19,21,67,74,131-135]. Pathological SOD1 and TDP-43 are enriched in EVs from ALS cell culture models and ALS patients' plasma and brain tissue, suggesting a prion-like seeding mechanism for the spread of pathological proteins in ALS [136-138]. In this model, the misfolded protein is packaged into extracellular vesicles and transmitted to other cells and the diseased protein converts natively-conformed proteins into the diseased subtype [80,139-143].

Like prion protein (PrP), TDP-43 and SOD1 possess inherent properties that cause them to become disordered in the disease state. TDP-43 has a prion-like, low complexity domain and certain environmental insults or mutations in SOD1 can destabilize the protein, leading to fibril formation, aberrant post translational modifications and oxidative

stress [21,79,140,141,144]. While cell culture studies are the primary evidence for the prion-like spreading of pathological proteins in ALS, there is mounting *in vivo* evidence of misfolded and nonnative disulfide-cross-linked aggregated SOD1 in brain- and spinal cord-derived EVs from human ALS patients and $SOD1^{G93A}$ transgenic mice, and enriched exosomal TDP-43 in human brain samples [80,137,139,140]. A previously discussed study in which researchers designed vaccines to target misfolded versions of pathological SOD1 provides further proof of concept. Vaccinated mice lived substantially longer than mice that were not vaccinated [76], suggesting that neutralizing extracellular levels of misfolded SOD1 could be beneficial. It also suggests that mutant SOD1 present in EVs of ALS patients may spread via a prion-like seeding mechanism. The presence of SOD1 and TDP-43 in EVs derived from ALS patient samples provides evidence to suggest these proteins may serve as good potential biomarkers of the ALS disease state. Further elucidation of the role of EVs in the of pathological spread of proteins SOD1 and TDP-43 in ALS will explain how these proteins can be exploited as biomarkers of disease and identify novel therapeutic targets.

1.6.5 Extracellular vesicle biomarkers for disease

EVs mediate intercellular communication and are implicated in carcinogenesis and the spread of disease. Their cargo, comprised of a mix of nucleic acids and proteins that are both selectively and non-selectively incorporated during biogenesis, provide a valuable, time-sensitive snapshot into the inner state of the cell [114,115,145]. The continuous release of EVs into blood (plasma and serum), CSF, saliva, seminal fluid and breast milk, among other fluids, make EVs an ideal candidate for non-invasive and readily accessible

molecular biomarkers [145-150]. In addition to cancer, EV biomarkers are being investigated in diagnostic, prognostic and predictive applications for many different congenital and acquired diseases. In patients with lupus nephritis (LN), urinary exosomes provide a non-invasive alternative to renal biopsies, which are used to diagnose, classify scarring and assess renal inflammation [151]. Examination of vesicle contents from patients with LN revealed that expression of three miRNAs miR-135b-5p, miR-107, and miR-31-5p were significantly elevated in patients during a renal flare relative to healthy controls [151]. Moreover, miR-135b-5p, miR-107, and miR-31-5p were able to discriminate between responders and non-responders after clinical intervention [151]. Patients with Parkinson's disease had elevated levels of neuron-derived extracellular vesicles in plasma relative to patients with multiple system atrophy (MSA) and healthy controls [152]. Additionally, the ratio of EVs derived from neurons versus oligodendrocytes showed a significant correlation with scores from the Unified Parkinson's Disease Rating Scale (UPDRS) in patients with MSA [152]. Individuals with Parkinson's disease were found to have elevations in proteins SNAP23 and calbindin in urinary EVs, with 86% prediction success for disease diagnosis [153]. In patients with multiple sclerosis (MS), serum exosome profiling identified miRNAs characteristic of the MS disease state that could be used to differentiate between patients with MS and healthy controls [154]. A total of nine characteristic miRNAs were then further identified to differentiate between relapse-remitting and progressive MS disease subtypes with a very high degree of accuracy [154]. Therefore, EVs can be used in a variety of clinical applications to diagnose, predict and monitor a disease state. Given the great success in biomarker identification for other diseases, EVs may serve as a valuable source of biomarkers for ALS.

1.6.6 Extracellular vesicles as biomarkers of ALS disease pathology

ALS is non-cell autonomous disease; the convergence of numerous disease-associated gene products provoking damage within the highly vulnerable motor neuron and a number of other cell types [155]. As previously discussed, EVs are uniquely reflective of the disease state and their content can be a valuable source of biomarkers for diagnostic, prognostic and predictive applications. In ALS, EVs have been implicated in ALS disease pathogenesis through the transport and spread of toxic proteins SOD1 and TDP-43 and the investigation of EV content for patients with ALS is likely to yield further clinical biomarkers [76,136,137,139,147,156]. In a recent pioneering study, a comprehensive analysis of CSF mRNA content of patients with sporadic ALS was performed with high-throughput next generation sequencing [157]. Analysis of exosome mRNA content identified a total of 543 genes that were significantly changed in patients with ALS, the most dramatic being CUEDC2 which has been implicated previously in tumorigenesis and inflammation [157,158]. The use of leukocyte-derived microparticles (LMV), otherwise known as CD45+ microparticles, in CSF and plasma have also been investigated as a potential biomarker for ALS [147,159]. LMVs were initially described in a case study in which a patient with ALS displayed significant enrichment of CD45+ microparticles in isolated CSF [159]. Recent work suggests that LMVs are also significantly enriched in sporadic ALS patient plasma and levels are correlated with disease progression in patients with slow progressing forms of ALS [147]. Additionally, LMV levels of misfolded SOD1 are strongly correlated with disease progression in slow-progressing forms of sporadic ALS [147]. Neither LMV nor SOD1 levels showed any association in the plasma of patients with fast-

progressing ALS [147]. Exosomes derived from patients with ALS CSF show marked changes in miRNA profiles relative to healthy controls, including substantial increases in miR-486-5p, miR-26a-5p and let-7a-5p [160]. Analysis of miRNAS from EVs in peripheral blood in patients with sporadic ALS showed substantial changes in the miRNAS miR-24-3p, miR- 1268a, miR-3911 and miR-4646-5p [161]. Among the gene targets for the identified miRNAs was UNC13A, which has been implicated in the development of sporadic ALS [161-163]. EVs can therefore provide particular insight to the ALS disease state, which in turn can be harnessed to monitor, diagnose and determine therapeutic efficacy.

Rationale

ALS is a fatal neuromuscular disease known for its rapid progression. While some progress has been made in treatment, many therapeutic advances are thwarted by the lack of sensitive biomarkers. EVs, microparticles and exosomes specifically, are released from all cell types and contain a mixture of proteins, lipids and nucleic acids that provide unique insight into the physiological state. Their continuous release into biofluids, heterogenous cargo and role in the spread of pathology in ALS disease makes EVs an attractive, non-invasive source of potential molecular biomarkers for ALS. VCP plays a critical role in EV production due to its involvement in MVB biogenesis, which may lead to changes in EV content. Moreover, progressive deterioration of cellular functions caused by dysfunctional proteostasis in ALS14 will likely lead to additional changes in EV content over time. Taken together, cells harbouring mutations in VCP are good models from which to identify EV biomarkers of early onset and progression for ALS, which may have applicability to other forms of sporadic or familial ALS.

Hypothesis

I hypothesize that the analysis of the protein content of EVs isolated from fibroblasts cell lines carrying the VCP-R155H mutation, compared to normal controls, will lead to the identification of potential diagnostic, prognostic and predictive biomarkers for ALS.

My objective is to investigate the utility of using extracellular vesicles (EVs) as source of protein biomarkers and to identify EV-derived protein biomarkers for ALS14.

I) Identify prospective biomarkers for ALS14 using a biased method using a literature-based candidate approach.

II) Identify prospective biomarkers for ALS14 using an unbiased methodology using label-free liquid chromatography mass spectrometry analysis.

Chapter 2: Methods

2.1 Cell line selection

To begin our biomarker study, we selected primary fibroblast cell lines carrying the VCP-R155H mutation from Coriell Cell Repository as a cell culture system for preliminary analysis. The three cell lines derived from patients with the VCP-R155H mutation we selected for use in our study and their phenotypic characteristics are shown in Table 2.1. We selected fibroblasts carrying the VCP-R155H mutation, the most common cause of familial IBMPFD/ALS, otherwise referred to as ALS14. The R155H mutation is an autosomal dominantly inherited missense mutation that is caused by a G>A transition at nucleotide 464 in exon 5 of the VCP gene, resulting in an arginine to histidine substitution at position 155 of the protein (Figure 2.1). The clinical description of the patients from which these cell lines were derived did not include an explicit diagnosis of ALS, but two of the 3 patients had noted atrophy and muscle weakness. Nonetheless, selected cell lines carry the desired mutation and are affected with IBMPFD/ALS with variable phenotypes including IBM, FD and PD. Cell lines derived from patients with various ages, disease progressions and both sexes were included to address any potential age or sex differences. All affected individuals were matched with a sex- and age-matched control fibroblast cell line that are wild-type with respect to the VCP allele. The fibroblast cell lines will be referred to by the corresponding number listed in Table 3.1 (e.g.: VCP-R155H #1, Control #1) throughout this study.

Table 2.1: Phenotypic characteristics of fibroblast cell lines

Coriell Catalogue Number	Age of sampling	Sex	Mutation (VCP)	Phenotype
GM21752 (VCP-R155H #1)	57	M	R155H	Clinically affected; myopathy with onset at 45 years of age; Paget and muscle disease with onset at age 32; signs of depression and substance abuse; dementia with onset at age 47;
GM23284 (VCP-R155H #2)	57	M	R155H	Clinically affected; myopathy symptom onset at age 40 years; back pain; hip pain; proximal muscle weakness; limb weakness/atrophy; pelvic girdle weakness/atrophy; gait abnormalities; difficulty walking up stairs
GM23268 (VCP-R155H #3)	38	F	R155H	Clinically affected; myopathy symptom onset at age 35 years; Paget disease symptom onset at age 38 years; winged scapulae; proximal muscle weakness; shoulder weakness/atrophy; limb weakness/atrophy; pelvic girdle weakness/atrophy; gait abnormalities; difficulty walking up stairs
GM23248 (Control #1)	55	M	N/A	Participant #1 (hu43860C) in the Personal Genome Project: http://www.personalgenomes.org
GM23249 (Control #2)	44	M	N/A	Participant #4 (huE80E3D) in the Personal Genome Project: http://www.personalgenomes.org
GM01650 (Control #3)	37	F	N/A	None noted

Figure 2.1: Schematic representation of the VCP protein showing the position of the R155H mutation.

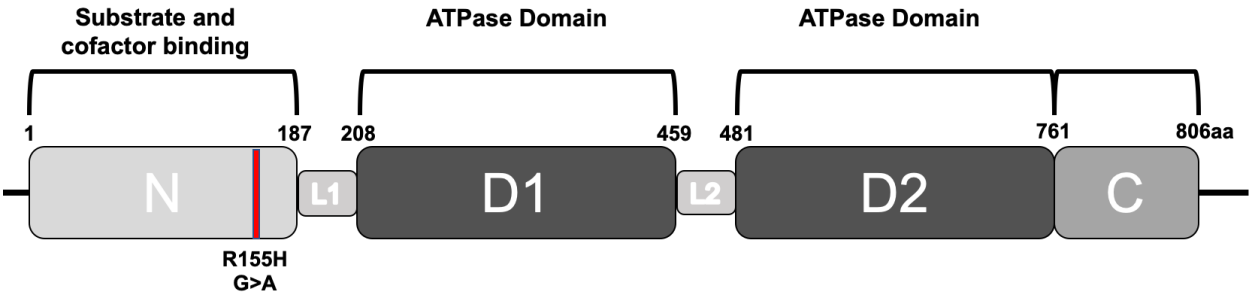

2.2 Cell Culture

Human fibroblast cells (GM23248, GM23249, GM01650, GM21752, GM23284 and GM23268, Coriell Cell Repository) were maintained in Minimal Essential Medium (MEM) (Sigma Aldrich, Oakville, ON, Canada) supplemented with 15% fetal bovine serum (FBS) (Sigma Aldrich), 2 mM GlutaMAX (Invitrogen, Waltham, MA, USA), X1 Antibiotic-Antimycotic (Invitrogen). All cell lines were cultured at 37°C with 5% CO_2. For isolation of EVs, fibroblasts were cultured in Fibroblast Growth Media (FGM; Promocell, C-23010, Heidelberg, Germany).

2.3 DNA Isolation

Genomic DNA from VCP-R155H and control fibroblasts was isolated as per Ross and Parks [164]. Genomic DNA was extracted from fibroblast cell lines Control #1, Control #2, VCP-R155H #1 and VCP-R155H #2. Briefly, fibroblasts were plated at a density of 4.4 x 10^6 on 10 cm plates and allowed to settle overnight. Next day, fibroblasts were trypsinized and quenched with 8mL of 15% MEM. 1.5mL of trypsinized fibroblasts resuspended in 15% MEM were transferred to a 1.5mL Eppendorf tube and centrifuged

at 135 X g for 5 minutes to pellet the cells. The supernatant was discarded, and the cellular pellet was resuspended in 200μL of SDS-Proteinase K (10 mM Tris-HCl pH 7.4, 10 mM EDTA, 1% SDS (w/v), 1 mg/ml proteinase K) and incubated overnight at 37°C. A combination of 300μL TE, 100μL 5 M NaCl and 500μL phenol were added to the lysate and vortexed at high speed, followed by centrifugation at 21130 X g for 3 minutes. The top layer containing nucleic acids was transferred to fresh 1.5mL Eppendorf tube, 500μL of chloroform was added, the sample was vortexed at high speed and centrifuged at 21130 X g for 3 minutes. The top layer was transferred to a new tube and combined with 500μL isopropanol and mixed before incubation at -20°C for 10 minutes. The sample was centrifuged at 21130 X g for 3 minutes. The resulting supernatant was discarded and the pellet containing genomic DNA was resuspended in 60μL of TE buffer (10 mM Tris-HCL pH 8.0, 1 mM EDTA in ddH_2O).

2.4 PCR

To verify the presence of the R155H mutation in fibroblast cell lines obtained from Coriell Cell Institute Repository, PCR primers were designed to amplify exon 5 of the VCP gene. Primers were designed by Johnson *et al.* to target a roughly 300bp region containing exon 5 (131bp) and flanking introns (forward primer: GAGCTTGGCATTTTGACCC (sense) and reverse primer: CCCAGTCCTGACAGTTACCAC (antisense). PCR conditions were: 30 sec at 94°C for initial denaturation followed by 40 cycles of 15 sec at 94°C, 30 sec at 45°C for annealing and 30 sec at 68°C for extension, with a final extension at 68°C for 5 min.

PCR products were separated on a 2% agarose gel and visualized with ethidium bromide stain. The VCP exon 5 PCR product was sequenced by Ottawa Hospital Research Institute Stemcore Laboratories DNA Sequencing Facility. Sequencing tracings were visualized using FinchTV 1.4.0 (Geospiza, Inc.; Seattle, WA, USA; http://www.geospiza.com) and sequence alignment was completed using Nucleotide Blast [165].

2.5 Crystal Violet Cell Growth Assay

To assess the viability of using serum-free FGM to isolate EVs from cell culture, a crystal violet assay was first performed to assess cell growth. Control #1 and VCP R155H #1 fibroblasts (cell lines: GM23248 and GM21752) were plated at a density of 2.0 X 10^4 in triplicate on 35mm plates and incubated with 2mL of 15% FBS supplemented MEM or Fibroblast Growth Media. Cells were fixed with 4% paraformaldehyde and stained with 0.1% crystal violet dye (Sigma Aldrich) for 30 minutes at 1- ,2- ,3- ,4-days post-seeding, with an empty well to define background from the staining method. Plates were then carefully washed with ddH_2O and allowed to dry overnight. Once dry, 1mL of 10% acetic acid was added to each well and incubated on a bench rocker for 30 minutes to solubilize the dye. Optical density (OD) of each well was measured by a table-top spectrophotometer at 570nm. A standard curve was prepared using serial dilutions of 0.1% crystal violet. The average OD_{570} of the empty wells was subtracted from the OD_{570} of each experimental well to remove background. Each reading was plotted relative to Day 1 values for each cell line. Average relative absorbances and standard deviations were calculated from corrected values and plotted in Graph Pad Prism 7.0. Significance

testing was performed using a Student's T-Test and one-way ANOVA, where $p<0.05$ indicated significance.

2.6 Immunofluorescence and microscopic analysis

Fibroblasts from cell lines Control #1 and VCP-R155H #1 were seeded onto 3-chambered slides at a density of 1.0 X 10^4 and allowed to rest overnight. Cells were subjected to heat shocked using a 42^{o}C incubator for 2-hours and allowed to rest for 4- or 24-hours before being fixed with 4% paraformaldehyde for 10 minutes at 37^{o}C. Slides were then permeablized and blocked with 2% donkey serum albumin in 0.3% Triton X-100 for 1 hour at room temperature. Cells were incubated with primary antibody overnight at 4^o or for 1 hour at room temperature [rabbit anti-TDP 43 (1:250, Abcam,Cambridge, UK), mouse anti-VCP (1:500, Abcam), mouse anti-ß-actin (1:500, Sigma Aldrich), rabbit anti-pan-actin (1:500, Cell Signaling Technology, Massachusetts, USA)]. Secondary antibodies, Alexa Fluor anti-rabbit-IgG 488 (1:5000, Invitrogen), Alexa Fluor anti-rabbit-IgG 594 (1:5000, Invitrogen), Alexa Fluor anti-mouse 488 (1:5000, Invitrogen) and Alexa Fluor anti-mouse-IgG 594 (1:5000, Invitrogen) were added to the slides for 1 hour in the dark at room temperature. Cells were counterstained with 4'-6' diamidino-2-phenylindole (DAPI). Fluorescence images were obtained using a Zeiss Axio Imager M2 upright fluorescent microscope.

ImageJ (FIJI, developed by Wayne Rasband, NIH) was used to quantify immunofluorescent images as follows. Several regions of interest (ROI) were selected in images for whole cell and nucleus using ß-actin and DAPI counterstaining. Mean

fluorescence and other adjacent measurements including background signal were measured for the whole cell and nucleus for all cells in frame, respectively. The corrected total cell fluorescence (CTCF) was calculated using the following formula:

$$CTCF = (area_{total\ cell} \times mean\ fluorescence_{protein\ of\ interest}) - (area_{total\ cell} \times mean\ fluorescence_{background})$$

CTCF was used as the primary measurement of fluorescence. Averages and s.e.m. were calculated for four images with a minimum of 117 total cells per time point and were compared across time points and cell lines. Statistical analysis (2-way ANOVA) was performed with $p<0.05$ indicative of significance. Values of CTCF and s.e.m. were plotted using Graph Pad Prism 7.0 software.

2.7 Cell Fractionation

Fibroblasts from cell lines Control #1 and VCP-R155H #1 (1.1×10^6) were seeded onto 10cm plates and were incubated overnight. Cells were subjected to a 2-hour 42°C heat shock and were allowed to recover at 37°C for either 4- or 24- hours. Cells were fractionated according to Challberg and Kelly [166], and assessed for endogenous TDP-43 in the cytoplasm and nucleus by immunoblot. Purity of fractionated samples was assessed by immunoblot by probing for cytoplasmic and nuclear controls tubulin and H3, respectively. Endogenous TDP-43 signal normalized to H3.

2.8 Immunoblot analysis

Samples in 5x SDS loading buffer (60 mM Tris HCl pH 6.8, 10% glycerol, 2% SDS, 0.01% Bromophenol Blue, 5% β-mercaptoethanol) were heated for 10 minutes at 95°C. Samples (25μL EVs and 10μL cell lysates) were separated by 12 or 15% SDS-PAGE and transferred to a polyvinylidene difluoride membrane (EMD Millipore, Etobicoke, Ontario). The membrane was blocked in Intercept (PBS) Blocking Buffer (LI-COR Biosciences, Nebraska, USA) and the membrane was probed with the following antibodies: rabbit anti-Alix (1:1,000, Abcam), rabbit anti-flotillin-2 (1:1,000, Abcam), rabbit anti-CD63 (1:5,000, Abcam), mouse anti-VCP (1:1000, Abcam), rabbit anti-TDP-43 (1:500, Abcam) rabbit anti-integrin beta-1 (1:1000, Millipore Sigma, Oakville, Ontario), mouse anti-tubulin at (1:10,000, Abcam), rabbit anti-H3 (1:30,000, Abcam). Binding of the primary antibody was detected using fluorescently labeled secondary antibodies (IRDye 1:10,000 anti-mouse 680RD and IRDye 1:10,000 anti-rabbit 800CW, LI-COR) and developed using the Odyssey CLx and visualized using Image Studio 4.0 software. Quantification was completed using LI-COR guidelines and Image Studio 4.0 software and graphed using GraphPad Prism 7.0 software.

2.9 EV isolation by differential ultracentrifugation

To isolate EVs from fibroblast cell lines for proteomic analysis, EVs were isolated from culture media, characterized by immunoblot and NTA and then submitted for proteomic analysis (Figure 3.8A). Briefly, 10cm culture dishes were seeded with fibroblasts and 15% MEM was replaced with FGM the following day. EVs were then allowed to accumulate in the medium over 72 hours to maximize yield. We chose

differential ultracentrifugation to isolate a mixed population of large and small EVs due to cost, compatibility with mass spectrometry and relatively high yield. Many common methods used for EV isolation, differential ultracentrifugation included, result in significant cross-contamination of small and large EVs. For our purposes, we were not concerned about whether a putative biomarker was contained in small or large EV, so we simply utilized a method of isolation that facilitated the collection of both, with the added advantage of a larger yield and greater population from which to identify potential diagnostic, prognostic or predictive biomarkers. In addition, both large and small EVs have been studied as sources of molecular biomarkers and as such were both considered in our study [136,147,167,168]. Common ultracentrifugation methods were adapted by increasing the speed of several centrifugation steps from 100,000 X g to 120,000 X g (Figure 3.8B)[169]. We also excluded a 20,000 X g centrifugation step, eliminating the isolation of a separate population of large EVs.

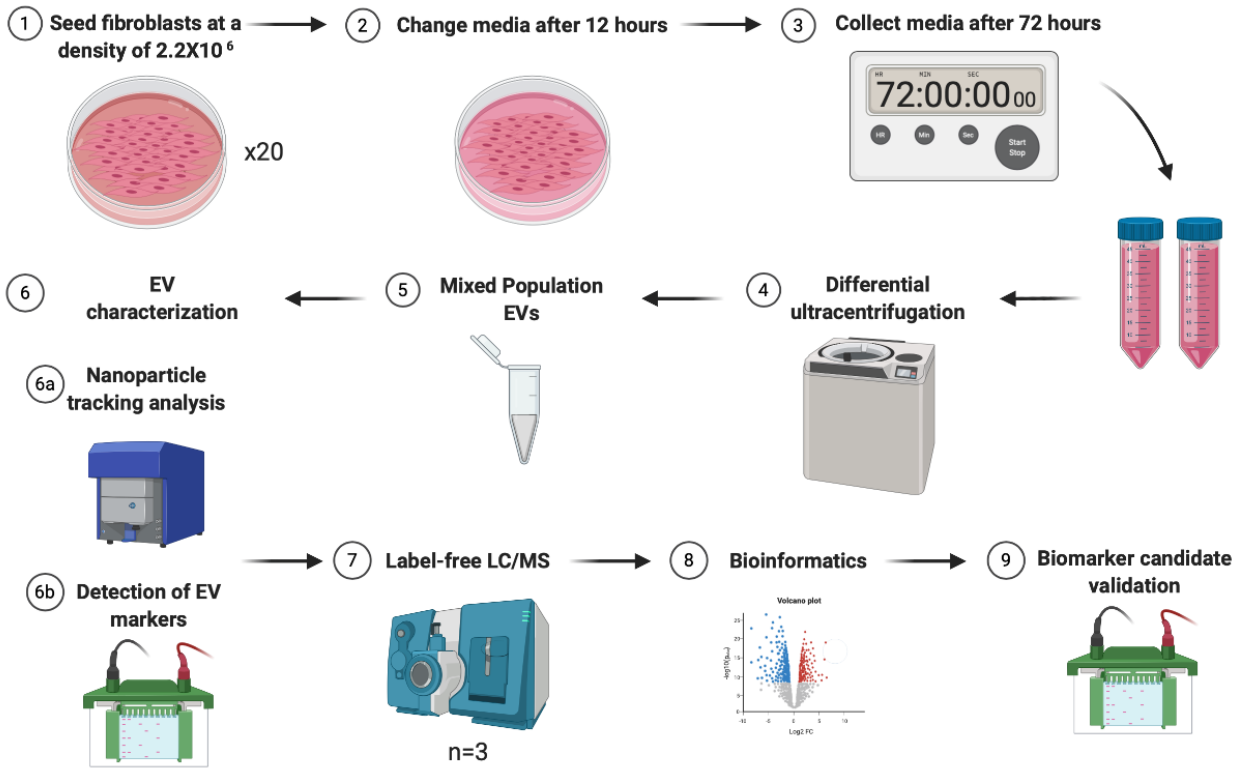

Figure 2.2: Experimental outline. Fibroblasts were plated at a density of 2.2 X 10^6 cells per 10cm dish and allowed to rest overnight. Next day, plates were changed to FGM and EVs were allowed to accumulate in the medium. After 72 hours, a mixed population of large and small EVs were isolated by differential ultracentrifugation. The resulting EVs were characterized by immunoblot and NTA and submitted for proteomic analysis by label free liquid chromatography mass spectrometry. Independent analysis of EV protein content for VCP-R155H and control EVs was performed to identify differentially present proteins in addition to a separate comparative quantitative analysis to generate a list of differentially abundant proteins. Mass spectrometry output was then analyzed using functional enrichment and a list of candidate proteins was constructed for each analysis. Selection of candidate proteins for pilot validation by immunoblot was based in part on the degree of protein differential abundance and on the availability of convenient and specific antibodies. Selected proteins were then validated across EVs from three VCP-R155H and control cell lines using immunoblot and quantitated. Figure created with BioRender.com.

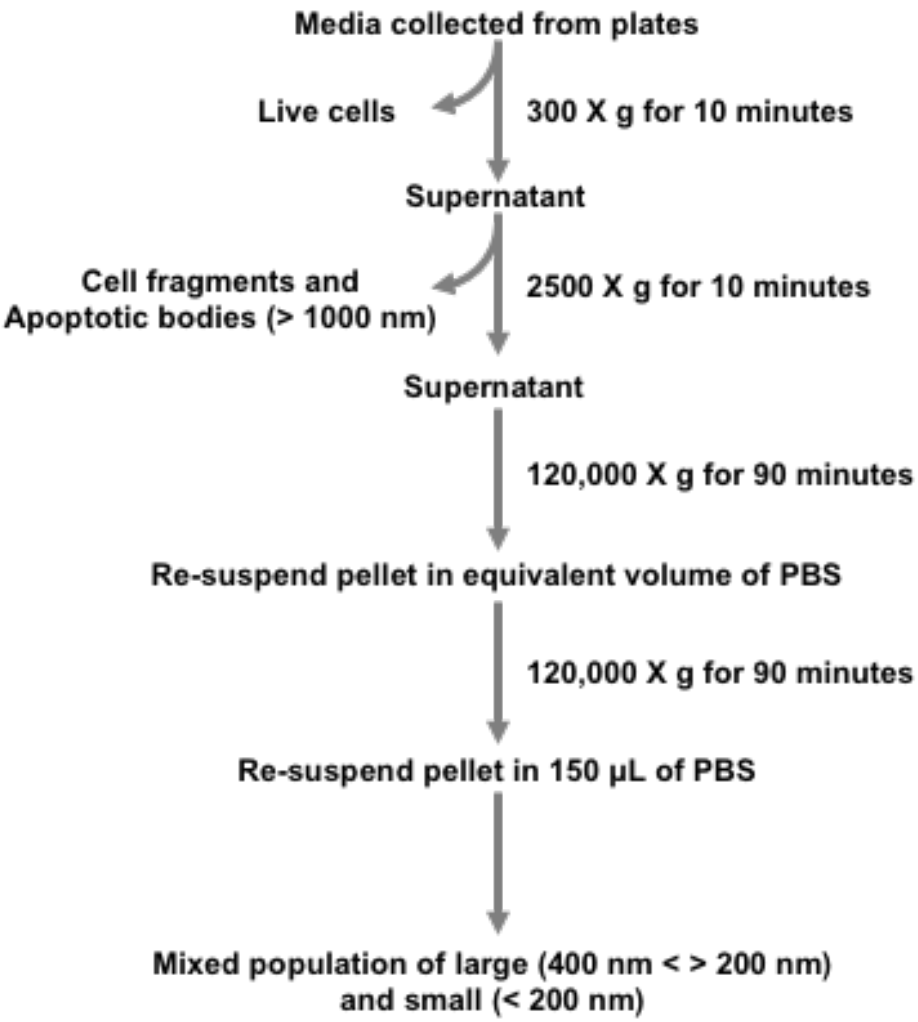

Figure 2.3 Protocol for isolation of a mixed population of large and small EV by differential ultracentrifugation. Briefly, media was collected after 72 hours and subjected to low speed centrifugation at 300 X g for 10 minutes to eliminate cell debris. Media was then subject to an additional low speed centrifugation of 2500 X g for 10 minutes to eliminate apoptotic bodies from the sample. A mixed population of EVs was then isolated from culture media and washed in PBS using two separate 120,000 X g centrifugation steps and the isolated sample was resuspended in 150µL PBS.

EVs were isolated from six cell lines, with a control and VCP-R155H cell line isolated in parallel. Fibroblasts (2.0×10^6) were seeded onto twenty 10 cm plates in MEM supplemented with 15% FBS and incubated overnight. Next day, plates were washed with PBS and changed to FBS-free FGM (10mL per plate) and incubated for 72 hrs. Media

was collected, and the cell debris was removed by low speed centrifugation at 300 X g for 10 minutes. The pellet was discarded, and the resulting supernatant further centrifuged at 2500 X g for 10 minutes to remove apoptotic bodies. The pellet was once again discarded and the supernatant was centrifuged at 120,000 X g for 90 minutes at 4^{o}C using an SW28 rotor to isolate a mixed population of large and small EVs (Beckman Coulter, Mississauga, Ontario). The resulting EV pellet was resuspended in PBS, pooled, and centrifuged again at 120,000 X g for 90 minutes using an SW41 Ti rotor (Beckman Coulter, Mississauga, Ontario). The final EV pellet was resuspended in 150 µL of PBS and stored at -20^{o}C. The size and concentration of the EVs were determined using NTA using a Particle Metrix ZetaView (Cell Guidance Systems, St. Louis, MO). ZetaView software (version 8.04.02, Meerbusch, Germany) was used to capture videos and analyze the particles using 11 camera positions, with videos taken for 2 seconds at a frame rate of 30 fps at 21^{o}C.

2.10 Liquid chromatography mass spectrometry analysis

A mixed population of EVs from fibroblast cell lines Control #1 and VCP-R155H #1 (n=3) were isolated in triplicate and submitted for liquid chromatography-mass spectrometry analysis. In-gel trypsin digestion, mass spectrometry sample preparation and liquid chromatography mass spectrometry was performed under the supervision of Dr. P. Vacratsis at the University of Windsor, as previously described [170,171]. For detailed outline of mass spectrometry methods and settings, please see Appendix I.

2.11 Proteomics Data Analysis

Gene ontology was assigned to the identified EV proteins using g:Profiler software (ELIXIR, 2019 version)[172]. A functional enrichment analysis was performed using g:Profiler to compare the identified proteins in fibroblast EVs cell lines to a reference list to statistically determine classifications (biological processes, pathways, regulatory motifs and protein complexes) that are enriched in the input list compared to the chosen reference lists. For this analysis, we chose data sources GO Biological Process, GO Molecular Function, GO Cellular compartment, KEGG and Reactome. Uploaded protein lists for EVs derived from Control #1 and VCP-R155H #1 were compared to the reference list using a cumulative hypergeometric test. A multiple testing correct termed g:SCS was computed by g:Profiler to produce a corrected p-value (q-value). All terms shown are based on $q < 0.05$. Enriched terms were ordered based on significance and q-values were transformed to a $-\log_{10}$ scale, calculated based on the number of genes in the uploaded dataset divided by the number of genes that would be expected in this category based on the reference dataset. Values of fold-enrichment greater than one are indicative of terms that are overrepresented in control #1 and VCP-R155H #1 EV samples.

Output data from quantitative mass spectrometry analysis performed by Dr. Vacratsis included Protein Accession number, number of unique peptides, confidence score, ANOVA p-value, maximum fold change, protein description and normalized abundance for each replicate. Quantitative data was exported and analyzed using Microsoft Excel software for calculations (2020 Edition). The average protein abundance was calculated from three technical replicates per biological replicate of control and VCP-R155H fibroblast EVs. Reliable quantitation was standardized based on the detection of

at least three unique peptides per protein. Statistical significance, relating to the differences in protein abundance (fmols) between three biological replicates of EVs from control and VCP-R155H fibroblasts, was determined using a student's t-test and were accepted if p-values were <0.05. The p-values obtained were corrected for false-discovery by applying the Benjamini-Hochberg False Discovery Rate to produce a corrected t-test statistic (q-value). To ensure statistical relevance, changes in protein abundance were considered significant only if the q-value <0.05, the ANOVA score <0.05, and the fold-change was >1.3. Statistical data from all quantitated proteins were used to generate a volcano plot. To represent significant changes in protein abundance, the student's t-test scores (q-values) were converted to $-\log_{10}$ p-values (y-axis) and plotted in relation to $\log_2$ fold change (x-axis) using Graph Pad Prism 7.0 software.

Chapter 3: Results

3.1 Coriell fibroblast cell lines are positive for the VCP-R155H mutation

To confirm the presence of the R155H mutation in the fibroblast cell lines obtained from Coriell, we extracted the genomic DNA from each fibroblast cell line via phenol/chloroform protocol and performed PCR to amplify exon 5 of the VCP gene. The VCP exon 5 PCR product was sequenced by Ottawa Hospital Research Institute Stemcore Laboratories DNA Sequencing Facility. Sequence tracings were visualized using FinchTV and sequence alignment was completed using Nucleotide Blast (Figure 3.1).

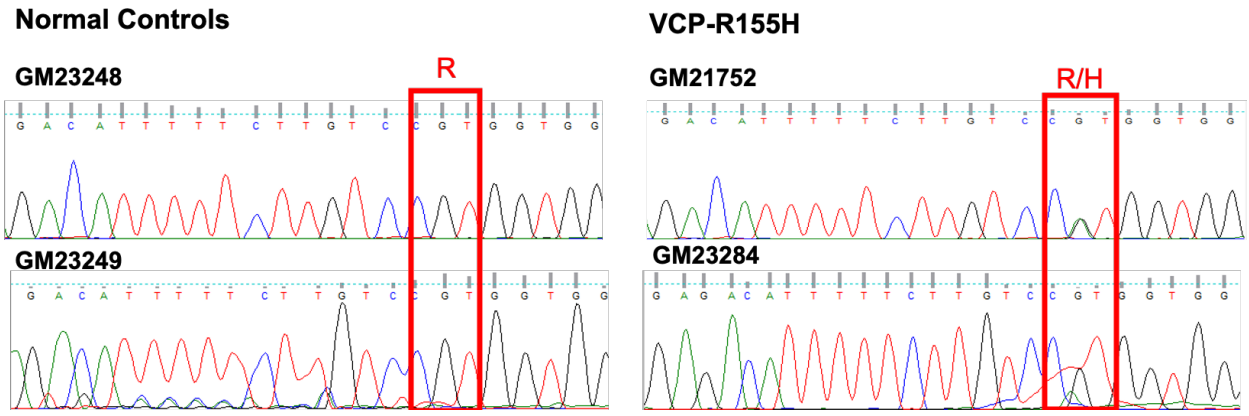

Figure 3.1: VCP gene Exon 5 sequencing tracing

Patients with ALS due to mutation in VCP are typically heterozygous for the mutation as VCP mutations cause early embryonic lethality [173]. Sequence tracings from DNA isolated from the cell lines reported to contain the VCP-R155H mutation detected the wild-type nucleotide, guanine, but also an additional peak at the designated position. Thus, the selected fibroblast cell lines indeed have the G>A substitution conferring the VCP-R155H mutation. Only a single peak is observed at position 464 in the control cell lines, indicating that these cell lines have the wildtype sequence. Based on the

sequencing data above, we were satisfied that two tested VCP-R155H fibroblast cell lines did indeed possess the desired mutation and were suitable for our study. Genomic DNA from cell lines Control #3 and VCP-R155H #3 had been isolated prior to study completion however were unable to be submitted for sequencing due to shut down of the Ottawa Hospital Research Institute Stemcore Laboratories DNA Sequencing Facility during the COVID-19 pandemic.

3.2 VCP-R155H fibroblasts do not experience significant loss of nuclear TDP-43

We next examined our fibroblast cell models for mutation-associated phenotypes. A number of studies have shown the presence of TDP-43 cytoplasmic inclusions in addition to loss of nuclear TDP-43 in a variety of fibroblast models of ALS arising from different genetic mutations [18,63,174,175]. TDP-43 is an RNA/DNA binding protein that accumulates in membraneless RNA-rich structures in the cytoplasm called stress granules when a cell is exposed to stress [176,177]. Impaired stress granule clearance is thought to lead to insoluble TDP-43 containing (TDP-43+) inclusions in the cytoplasm, a common hallmark that is present in 95% of cases of ALS including sporadic and familial ALS subtypes [178]. As a chaperone protein, VCP participates in a number of cellular processes that largely involve maintaining proteostasis, including the clearance of stress granules via autophagy. As such, clearance of cytoplasmic TDP-43, including protein that is localized to stress granules, may be impaired in fibroblasts carrying VCP mutations. To examine TDP-43 dynamics, we conducted a heat shock time course and used immunofluorescence microscopy and subcellular fractionation to visualize the cellular

distribution and nuclear levels of TDP-43 before and after a 2-hr heat shock in Control #1 and VCP-R155H #1 fibroblast cell lines.

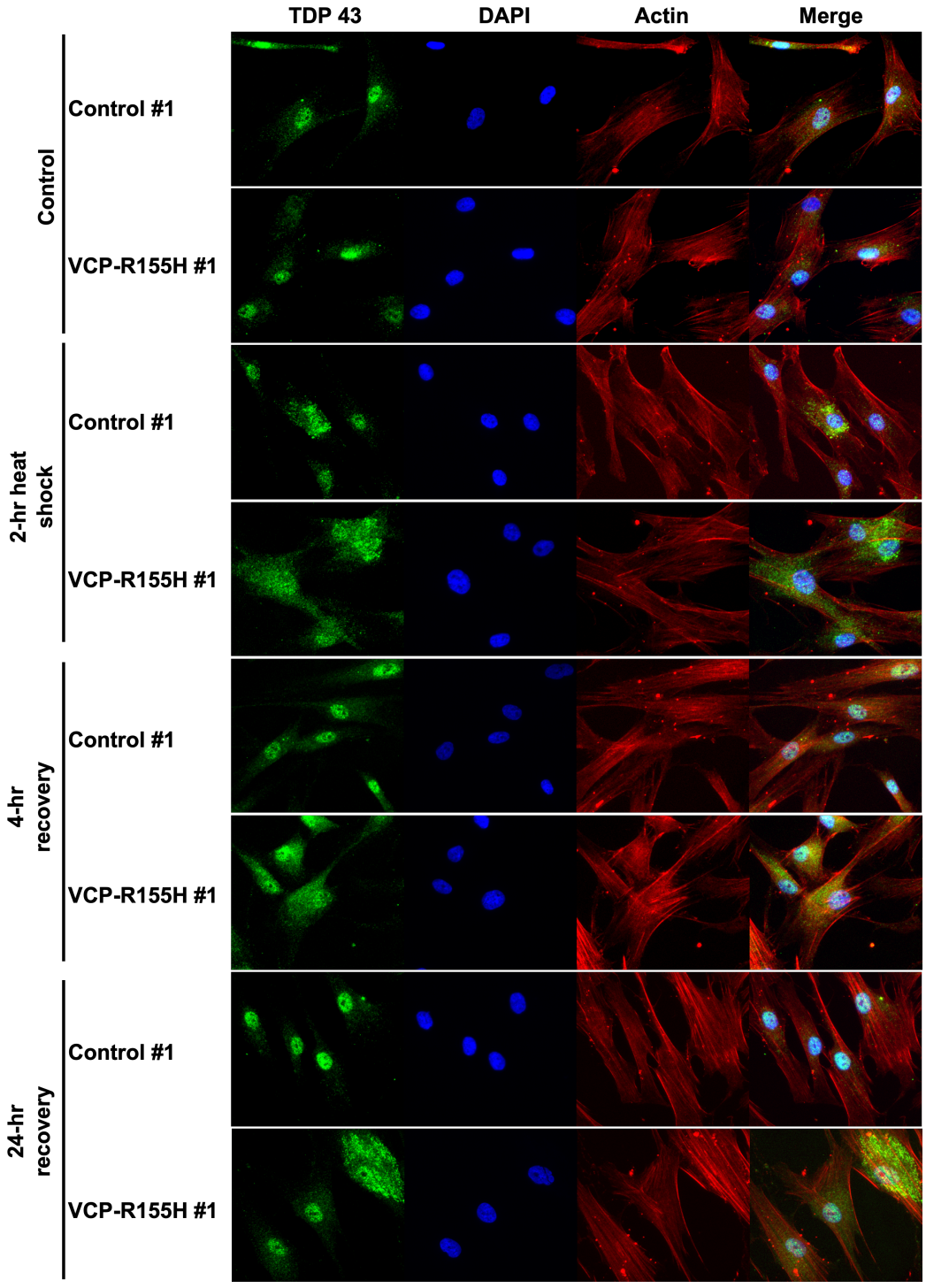

Figure 3.2: Heat stress causes TDP-43 to redistribute and persist in the cytoplasm of VCP-155H #1 fibroblasts, as assessed by fluorescence microscopy. A) Control #1 and VCP-R155H #1 fibroblasts were heat shocked at 42^{o}C and allowed to recover for 4 or 24hours at 37^{o}C. The cells were fixed and analyzed by indirect immunofluorescence for actin and TDP-43. Each image was visualized using a 20X objective with z-stack and extended focus applied.

At rest, imaging of VCP-R155H #1 fibroblasts show a similar distribution of TDP-43 compared to control cells; the majority of TDP-43 is found in the nucleus with a small amount of diffuse staining in the cytoplasm (Figure 3.2). In both cell lines, heat shock treatment caused a portion of nuclear TDP-43 to redistribute to the cytoplasm where it persisted until approximately 4h after treatment. In control #1 fibroblasts, cytoplasmic TDP-43 was no longer observed in the cytoplasm by 24h and cells appeared to have recovered; at 24h, TDP-43 was once again predominantly restricted to nuclei (Figure 3.2). Cytoplasmic TDP-43 appears to persist for longer in VCP-R155H cells, with concentrated staining in the cytoplasm up to 24h after heat shock. Images in Figure 3.2 were quantified using ImageJ (FIJI) software to determine the relative signal intensity of TDP-43 in the nucleus relative to the whole cell using ß-actin and DAPI counterstaining to identify regions of interest (ROI) and measure the signal intensity of TDP-43 in the designated areas (Figure 3.3A). Consistent with our qualitative assessment, we observed decreases in relative nuclear TDP-43 in control and VCP-R155H fibroblast cell lines in response to heat stress, the most severe of which occurred immediately following heat shock treatment (Figure 3.3A). Two-way ANOVA analysis indicated that nuclear TDP-43 changed significantly over the course of the heat shock time course in both cell lines, decreasing with heat shock and slowly increasing over the course of the recovery period, however those differences were similar between wild-type and VCP-R155H fibroblasts (Figure 3.3A). When normalized to levels at time 0 (Control #1), VCP-R155H fibroblasts showed a trend towards slower recovery, however it did not reach statistical significance between the two cell lines (Figure 3.3B).

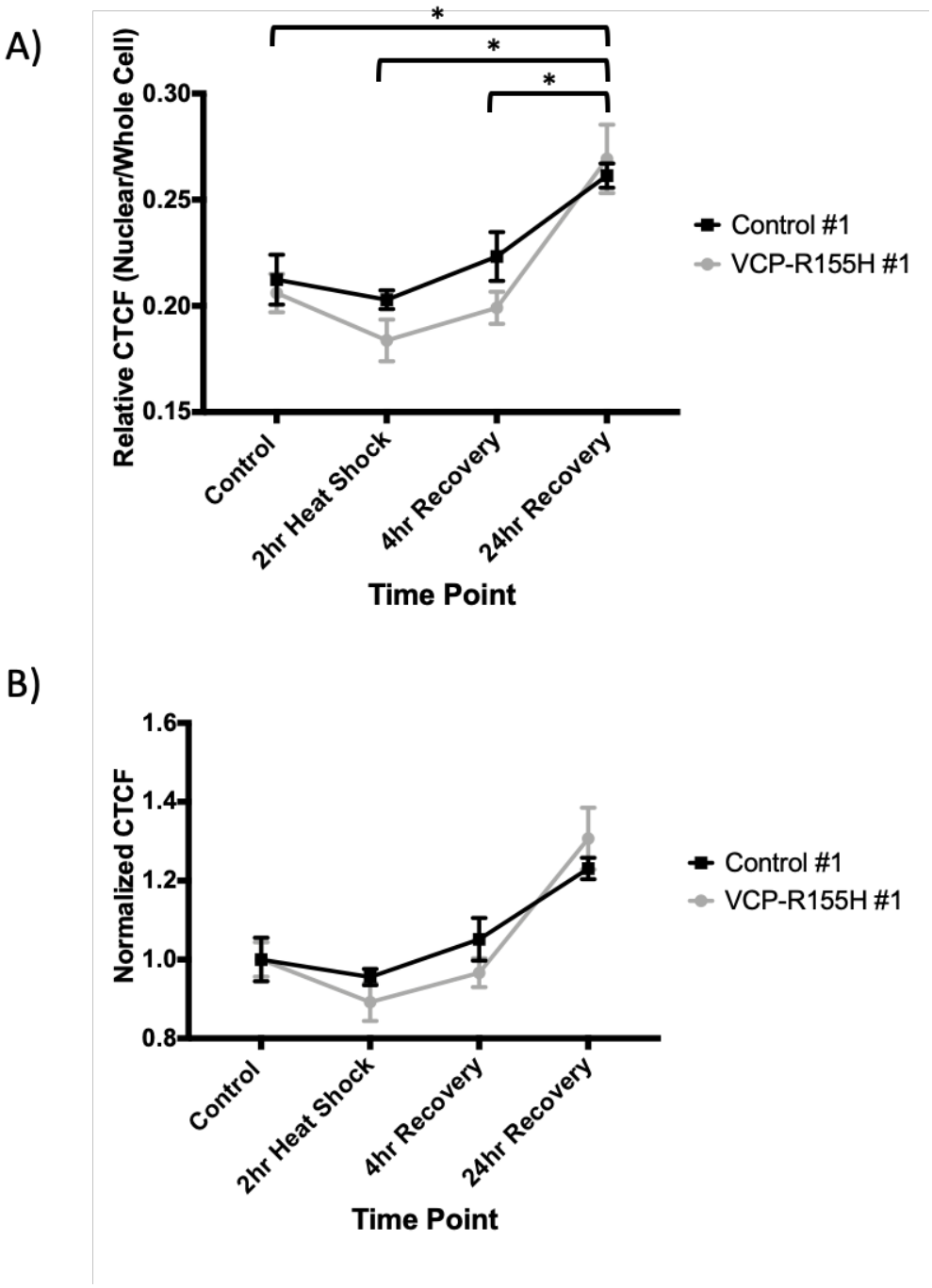

Figure 3.3: Heat stress causes no significant reduction in nuclear TDP-43 in VCP-R155H fibroblasts. Using 4 fluorescent images from the experiment above with a minimum of 117 cells per time point, corrected total cell fluorescence (CTCF) was manually calculated for the nucleus and total cell using FIJI (ImageJ). The proportion of nuclear TDP-43 relative to whole cell content (A) and the proportion of nuclear TDP-43 normalized to baseline concentration of nuclear TDP-43 (C) was compared across time points and between cell lines by 2-way ANOVA (α=0.05). Data presented represents the mean and s.e.m. No significant difference in nuclear TDP-43 was noted between control #1 and VCP-R155H #1 fibroblasts.

We also examined TDP localization by subcellular fractionation followed by immunoblot analysis. Briefly, cells were heat shocked as described for our immunofluorescence study and fractionated to obtain nuclear and cytoplasmic fractions. Prepared fractions were then analyzed by immunoblot to visualize TDP-43 levels in the cytoplasm and nucleus of control and VCP-R155H fibroblast cell lines (n=2) (Figure 3.4). Blots were probed for TDP-43, as well as H3 and tubulin to verify that the fractionation was successful. Nuclear fractions showed minimal tubulin signal and cytoplasmic levels of H3 was below the threshold of detection, indicating minimal cytoplasmic and nuclear contamination in subcellular fractions. As with our immunofluorescence studies, TDP-43 was predominantly localized to the nuclear fractions, with cytoplasmic levels of the protein below the threshold of detection (Figure 3.5). Quantification of TDP-43 levels on immunoblots was performed using ImageStudio software, where TDP-43 signal was normalized to nuclear control, H3 (Figure 3.5A).

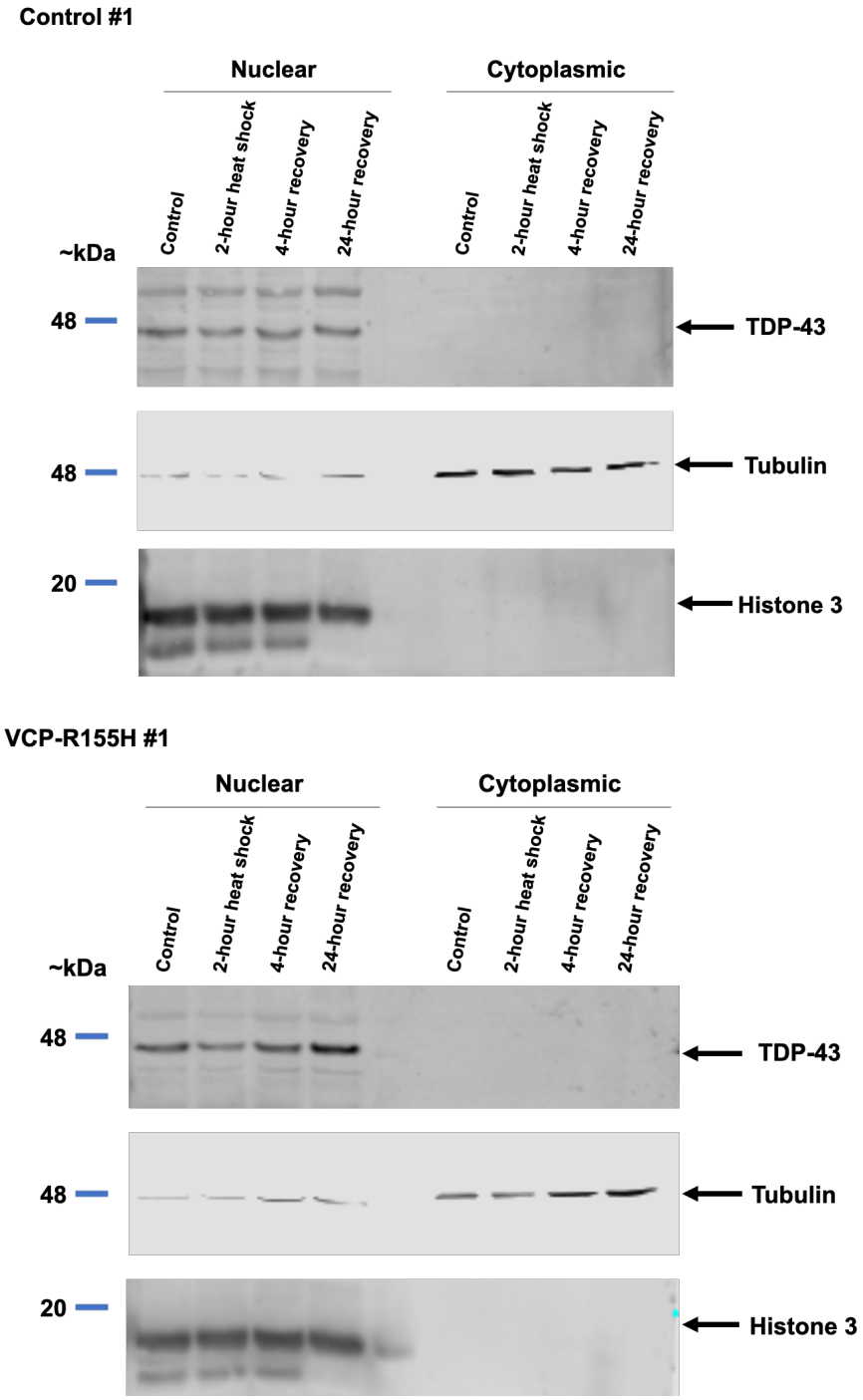

Figure 3.4: Kinetics of nuclear TDP-43 in response to heat stress. A) Control #1 and VCP-R155H #1 fibroblasts were heat shocked at 42°C and allowed to recover for 4 or 24hours at 37°C. Cells were fractionated to prepare nuclear and cytoplasmic fractions. Equal volumes of each fraction were analyzed via immunoblot for the overall protein levels of TDP-43, as well as tubulin (cytoplasmic control protein) and histone 3 (nuclear control protein). Immunoblots representative of n=2 experimental replicates.

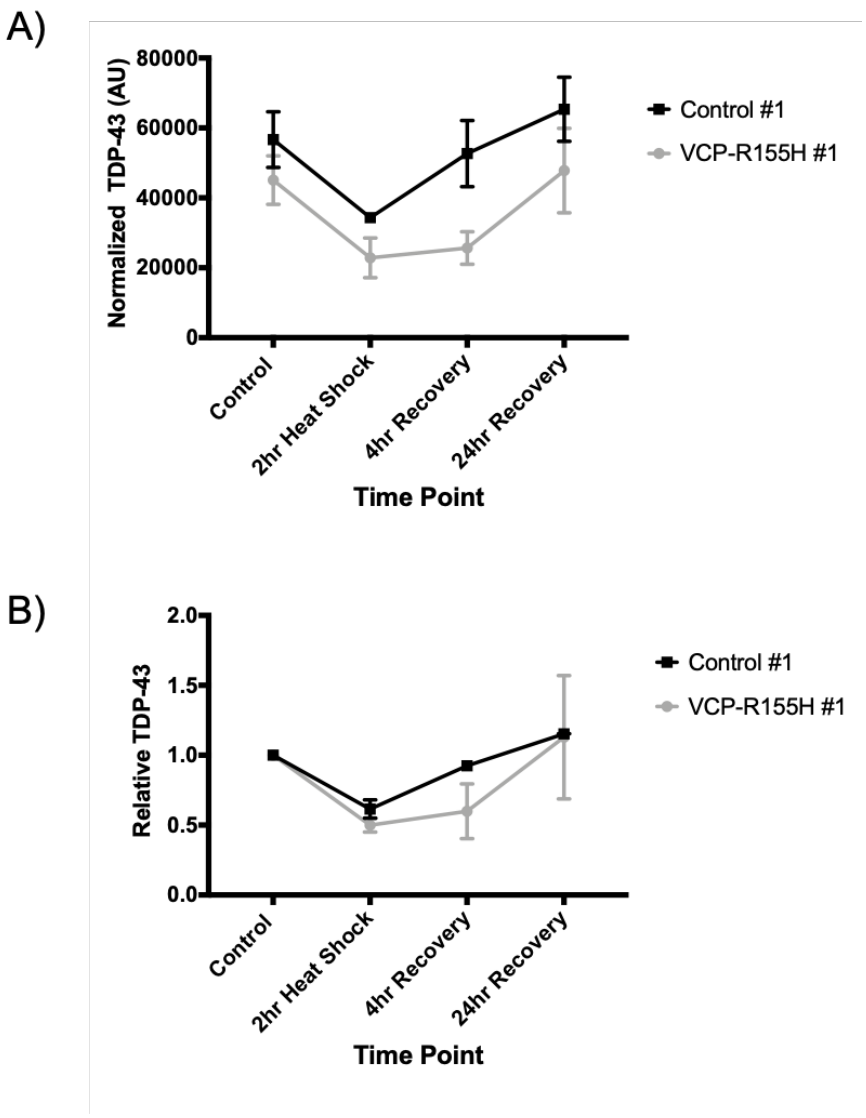

Figure 3.5: Cell fractionation analysis of TDP-43 distribution in response to heat shock in VCP-R155H #1 and control #1 fibroblasts. Fibroblasts were heat shocked at 42°C and allowed to recover for 4 or 24hours at 37°C. Cells were fractionated to prepare nuclear and cytoplasmic fractions and equal volumes were analyzed via immunoblot (Figure 3.5). A) Nuclear TDP-43 levels were quantified using ImageStudio software and normalized to histone 3 signal. B) Normalized nuclear TDP-43 expressed relative to control levels of nuclear TDP-43 for each cell line. Data presented represents mean and s.e.m. Data represents n=2.

The distribution pattern of TDP-43 in control #1 and VCP-R155H #1 fibroblasts in response to heat stress displays a trend towards an initial reduction in nuclear TDP-43 post-heat shock, although it does not reach significance (Figure 3.4, 3.5). In addition,

immunoblot quantitation shows that the recovery of nuclear TDP-43 appears to be slightly delayed in the VCP-R155H fibroblasts relative to control fibroblasts, but again not reaching significance (Figure 3.5B). Therefore, our fluorescence images suggest that there may be a reduced clearance of cytoplasmic aggregates in fibroblasts carrying the VCP-R155H mutation and however, TDP-43 levels fell below level of detection in immunoblot analysis. Thus, the VCP-R155H may show a subtle phenotype similar to those observed in other models of ALS.

3.3 Fibroblast growth media is a viable serum-free alternative for fibroblast cell culture

Typically, EVs are isolated from cell culture models by applying a vesicle-depleted 5%FBS MEM and collecting the medium for isolation after 24-72 hours. However, recent literature indicates laboratory vesicle depletion methods for FBS are limited in their ability to remove bovine EVs from FBS [179]. A recent study using NTA to quantitatively assess the presence of residual EVs in commercially depleted FBS and laboratory depleted FBS found that current methods only deplete up to 75% of EVs [179]. This level of bovine EV contamination may complicate novel biomarker discovery. A new serum-free fibroblast growth media (FGM) supplemented with human fibroblast growth factor and insulin has recently been developed as an alternative to MEM or DMEM supplemented with depleted FBS. We predict that this medium may provide a suitable alternative to traditional 5% FBS-supplemented MEM and eliminate contamination of the sample by FBS-derived proteins during proteomic analysis.

Crystal violet is a triarylmethane dye that can be used to assay the number of adherent cells on a tissue culture dish [180]. To determine whether our cell lines would successfully grow in FGM, we performed a crystal violet cell growth assay over a period of 4 days using both FGM and MEM containing 15% EV-depleted FBS (Figure 3.6). We chose the same cell lines (VCP-R155H #1 and Control #1) used for the previous investigations for TDP-43 mislocalization to maintain continuity throughout the study. Briefly, control and VCP-R155H fibroblasts were plated in 35 mm dishes at $2.0x10^4$ cells per dish in triplicate. Each day, three plates of cells grown in each medium were fixed and stained with 0.1% crystal violet. At the end of the assay, the crystal violet was solubilized in ethanol and the optical density determined by spectrophotometer at 570nm.

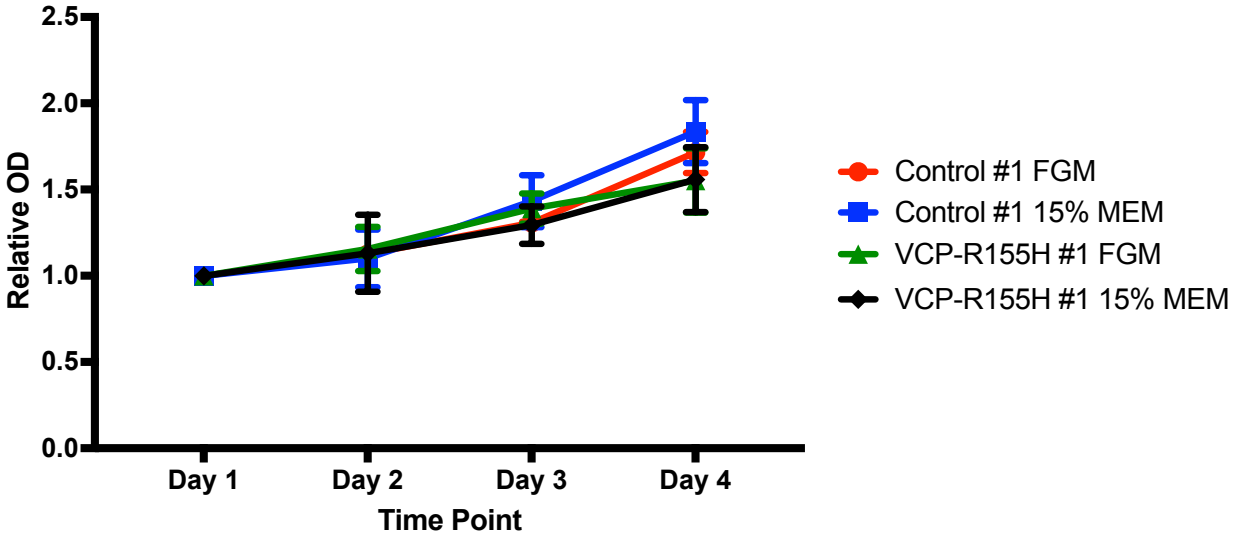

Figure 3.6: There is no difference in fibroblast growth in cells cultured in FGM relative to MEM supplemented with 15% EV-depleted FBS. Fibroblasts were seeded on Day 0 at a density of 2.0 x 10^4 and incubated with MEM supplemented with 15% EV-depleted FBS or FGM. Fibroblasts were fixed at the indicated time points and stained with crystal violet. Optical densities (OD) were assayed with a spectrophotometer at 570nm and assayed against a standard curve. ODs of each time point were calculated relative to Day 1 values for each condition. Data represents n=4 experimental replicates.

As shown in Figure 3.6, an analysis of the growth curves indicates that there are no differences in cell growth between cell lines (control vs VCP-R155H) and media conditions (15% MEM and FGM). Relative OD shows an increase throughout the growth assay, regardless of condition, indicating an increase in cell population growth. Based on these results, FGM showed similar growth kinetics compared to 15% MEM and may serve as a suitable alternative to traditional MEM supplemented with 5% vesicle depleted FBS for growth of our cells.

3.4 Characterization of EVs from fibroblast cells lines

A mixed population of large and small EVs were isolated from fibroblast culture media after 72 hours using sequential differential ultracentrifugation (Figure 2.2B). EV isolates from all six fibroblast cell lines were used for this study (Table 2.1). Once isolated, EVs were characterized by NTA and immunoblot in alignment with MISEV2018 guidelines (Figure 3.7)[112]. Immunoblot analysis was used to assay for the presence of EV and the purity of the samples using a total of three positive markers (flotillin-2, ALIX and CD63), a negative control (H3), and a cytosolic (α-tubulin) control (Figure 3.7A). EV particle concentration and diameter were determined using NTA for EV (Figure 3.7B). EV samples showed the presence of positive EV markers and cytosolic controls as well as the absence of negative EV markers (Figure 3.7A). EV characterization by NTA showed that the EV diameter ranging between ~X-400nm. Therefore, we determined that characteristics of EVs isolated from fibroblast cell lines are consistent with those documented for EV subtypes below 400nm.

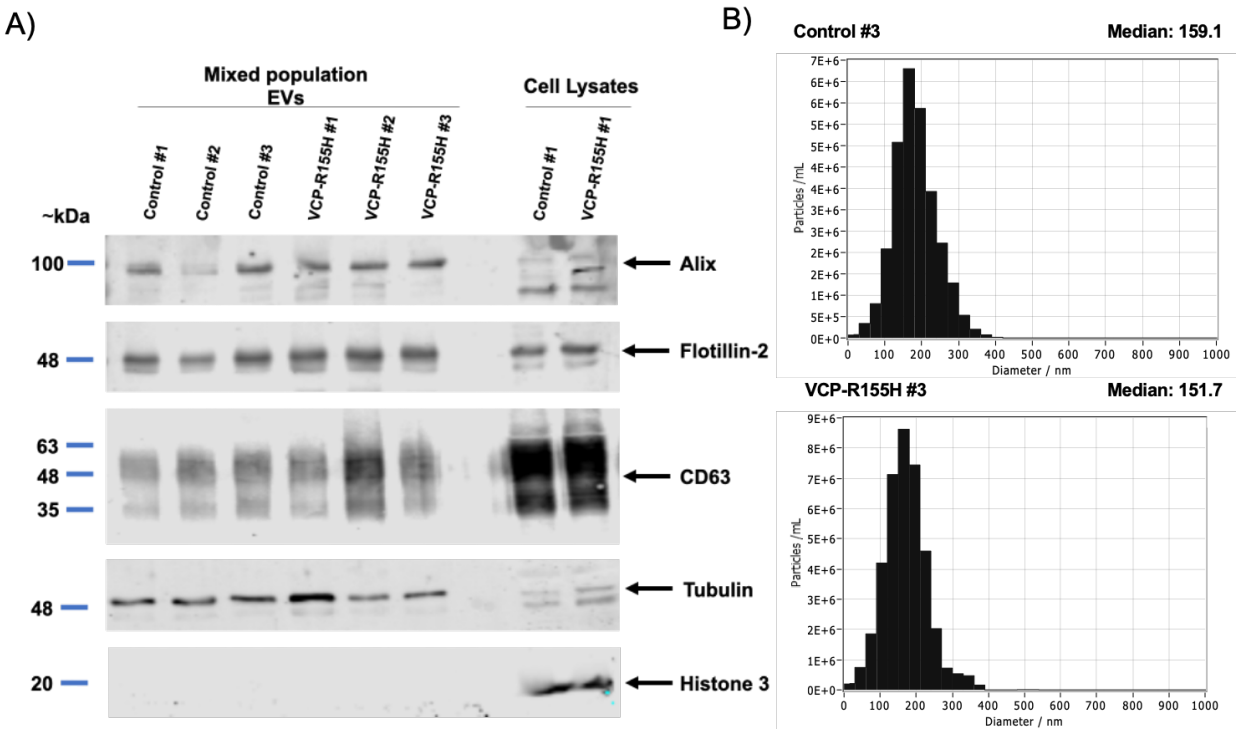

Figure 3.7: A mixed population of large and small EV can be successfully isolated from VCP-R155H and wild-type fibroblasts grown in FGM medium. A) EV were isolated from control and VCP-R155H fibroblasts by differential ultracentrifugation. Equivalent volumes of the isolated EV were separated by SDS-PAGE and analyzed by immunoblot for Alix, flotillin-2, CD-63, Tubulin and histone 3. B) EV size distributions were constructed by assessment of particle diameter in each sample using NTA. Images shown for NTA are a representative example.

3.5 VCP is selectively enriched in EVs derived from VCP-R155H fibroblasts relative to control fibroblasts

To construct a list of candidate biomarker proteins to distinguish between patients with ALS and a healthy population, a two-pronged approach was used. First, we used a biased literature-based candidate approach to generate a list of proteins with established relevance to ALS, whose expression or EV loading may change as a result of VCP mutations. Second, EVs from fibroblast cell lines were subjected to label-free liquid

chromatography (L/C) mass spectrometry analysis to identify proteins that showed differential presentation or abundance in EVs sourced from the VCP- R155H and control fibroblasts. We used immunoblot analysis for pilot validation of protein candidates in both approaches, focusing on proteins that could be readily detected in EV samples by immunoblot analysis. EV content of candidate proteins was then evaluated for each immunoblot using relative abundance to compare the amount of protein in control and VCP-R155H fibroblast EVs.

The candidate-based approach yielded a list of proteins of interest (Table 3.1). These proteins were considered highly relevant to ALS disease pathogenesis, displaying either pathway or mechanistic involvement, and each is directly related to different subtypes of familial ALS. Sproviero *et al.*[136] found that FUS, TDP-43 and SOD1 are all selectively enriched in the EVs isolated from plasma from patients with sporadic forms of ALS, indicating that these proteins may serve as ideal candidates for EV-derived protein biomarkers. TDP-43 and SOD1 in particular show a great deal of promise as biomarkers, as both have been implicated in the spread of ALS pathology through EVs via a prion-like seeding mechanism [21,80,139,141]. VCP was included in our list of candidate proteins because of the nature of our cellular models and the involvement of VCP in stress granule clearance through the process of autophagy, ERAD, UPS and UPR [36,42,44,45,47,49,52,55,57,181]. RNA-binding proteins, TDP-43 and FUS, are both constituents of stress granules and can exhibit pathological mislocalization in cells harbouring pathological VCP mutations [57,59,133].

Table 3.1: Potential protein biomarkers identified by candidate-based approach

Protein	Reference
VCP	Gitcho MA, Strider J, Carter D, et al. VCP mutations causing frontotemporal lobar degeneration disrupt localization of TDP-43 and induce cell death. *J Biol Chem.* 2009;284(18):12384-12398. Ju JS, Fuentealba RA, Miller SE, et al. Valosin-containing protein (VCP) is required for autophagy and is disrupted in VCP disease. *J Cell Biol.* 2009;187(6):875-888. Kustermann M, Manta L, Paone C, et al. Loss of the novel Vcp (valosin containing protein) interactor Washc4 interferes with autophagy-mediated proteostasis in striated muscle and leads to myopathy in vivo. *Autophagy.* 2018;14(11):1911-1927. Ayaki T, Ito H, Fukushima H, et al. Immunoreactivity of valosin-containing protein in sporadic amyotrophic lateral sclerosis and in a case of its novel mutant. *Acta Neuropathol Commun.* 2014;2:172.
FUS	Sproviero D, La Salvia S, Giannini M, et al. Pathological Proteins Are Transported by Extracellular Vesicles of Sporadic Amyotrophic Lateral Sclerosis Patients. *Front Neurosci.* 2018;12:487. Tyzack GE, Luisier R, Taha DM, et al. Widespread FUS mislocalization is a molecular hallmark of amyotrophic lateral sclerosis. *Brain.* 2019.
TDP-43	Feneberg E, Gray E, Ansorge O, Talbot K, Turner MR. Towards a TDP-43-Based Biomarker for ALS and FTLD. *Mol Neurobiol.* 2018;55(10):7789-7801. Sproviero D, La Salvia S, Giannini M, et al. Pathological Proteins Are Transported by Extracellular Vesicles of Sporadic Amyotrophic Lateral Sclerosis Patients. *Front Neurosci.* 2018;12:487. Gitcho MA, Strider J, Carter D, et al. VCP mutations causing frontotemporal lobar degeneration disrupt localization of TDP-43 and induce cell death. *J Biol Chem.* 2009;284(18):12384-12398.
SOD1	Paré B, Lehmann M, Beaudin M, et al. Misfolded SOD1 pathology in sporadic Amyotrophic Lateral Sclerosis. *Sci Rep.* 2018;8(1):14223. Grad LI, Pokrishevsky E, Cashman NR. Intercellular Prion-Like Conversion and Transmission of Cu/Zn Superoxide Dismutase (SOD1) in Cell Culture. *Methods Mol Biol.* 2017;1658:357-367. Sproviero D, La Salvia S, Giannini M, et al. Pathological Proteins Are Transported by Extracellular Vesicles of Sporadic Amyotrophic Lateral Sclerosis Patients. *Front Neurosci.* 2018;12:487.

To investigate EV VCP levels, EVs were isolated from six different VCP-R155H and control fibroblast cell lines (refer to Table 2.1 for cell line characteristics). VCP protein levels were then assessed by immunoblot analysis and evaluated for relative abundance between control and VCP-R155H EVs. In EVs, immunoblot analysis revealed that VCP is enriched in samples derived from fibroblasts carrying the VCP-R155H mutation compared to control fibroblasts (Figure 3.8A). Subsequent quantitative of VCP signal intensity from immunoblot analysis showed that VCP levels were 70% higher in EVs derived from fibroblasts with the VCP-R155H mutation relative to control fibroblasts ($p<0.05$) (Figure 3.8B). Due to the significant difference in levels of VCP in fibroblast EVs, we further investigated cellular expression of VCP in the same fibroblast cell lines by immunoblot (Figure 3.8C). A similar trend was noted in VCP levels in cell lysates of the VCP-R155H fibroblasts, although it did not achieve significance (Figure 3.8 C, D). VCP protein is therefore significantly enriched in fibroblast EVs with no significant difference in the levels of cellular expression however, due to a lack of sample size general conclusions regarding VCP as a biomarker cannot be made and therefore follow up experiments increasing sample size are needed.

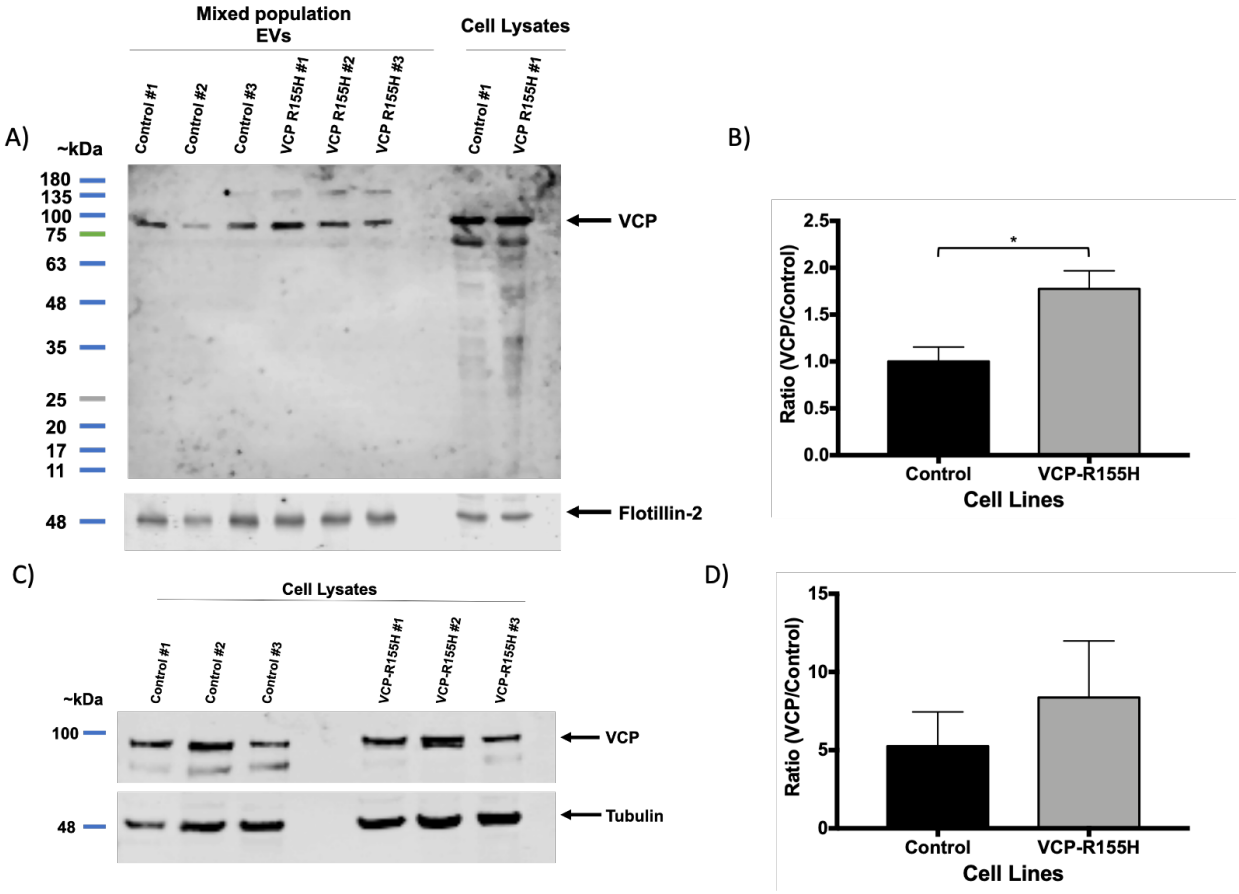

Figure 3.8: VCP protein is enriched in EVs derived from VCP-R155H fibroblasts compared to EVs derived from control cell lines. A) EVs were isolated from six different fibroblast cell lines (three VCP-R155H, three control) and equivalent volumes of isolated EVs were separated by SDS-PAGE to be analyzed by immunoblot for VCP and Flotillin-2. B) VCP and flotillin-2 protein signals were quantified using ImageStudio software. VCP signal was normalized to flotillin-2 and then compared to the average ratio of VCP/flotillin-2 of EVs from control cell lines. C) Equivalent volumes of cell lysates were separated by SDS-PAGE and analyzed by immunoblot for VCP and tubulin. D) VCP protein signal was quantified and normalized relative to tubulin signal using ImageStudio software. Quantitative data in panels B and D represent n=3 experimental replicates with 9 total normalized data points and is presented as average ratio of VCP signal in VCP-R155H:Control. An asterisk (*) indicates significance where $p<0.05$. Statistical analysis was performed using an unpaired t-test.

SOD1 was the second candidate proteins chosen for evaluation. As with previous analysis of VCP, EVs were isolated from six fibroblast cell lines, three control and three

VCP-R155H, and assessed by immunoblot for levels of SOD1 (Figure 3.9). EV levels of SOD1 fell below detectable threshold for immunoblot and was not suitable for reliable signal quantitation.

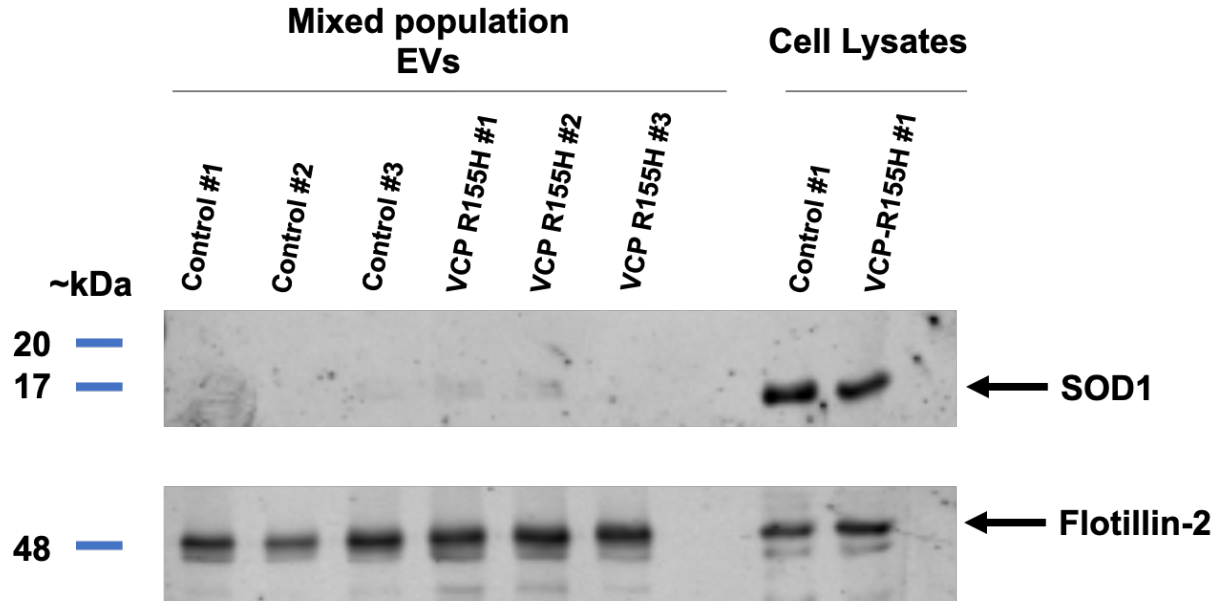

Figure 3.9: SOD1 protein levels fall below detectable threshold for immunoblot. EVs were isolated from six different fibroblast cell lines by differential ultracentrifugation and equivalent volumes of isolated EVs were separated by SDS-PAGE to be analyzed by immunoblot for SOD1 and Flotillin-2.

3.6 Proteomics analysis identifies differentially abundant proteins in EVs derived from fibroblast cell models.

We next used liquid chromatography mass spectrometry to identify proteins that were present in fibroblast EVs. For the sake of continuity throughout our study, we submitted EVs isolated from the same two cell lines that were used in previous immunofluorescence and cell fractionation studies, Control #1 and VCP-R155H #1. Three technical replicates per cell line were submitted for label-free L/C mass spectrometry analysis. Two independent modes of proteomic analysis were performed using the same data output from L/C mass spectrometry analysis to identify protein content in our EV

samples; the first was a preliminary analysis simply to identify proteins present in the EVs and the second was a quantitative proteomic analysis to identify a subset of differentially abundant proteins from EVs isolated from the two cell lines.

To identify proteins in the samples, L/C mass spectrometry output from individual sample analysis using EVs from Control #1 and VCP-R155H fibroblasts were submitted for protein identification to generate a list of protein hits. In total, 197 proteins were identified: 57 were unique to control fibroblast EVs and 29 unique to VCP-R155H fibroblast EVs (Figure 3.10). A complete list of all proteins exclusive to control and VCP-R155H fibroblast EVs is available below in Table 3.2.

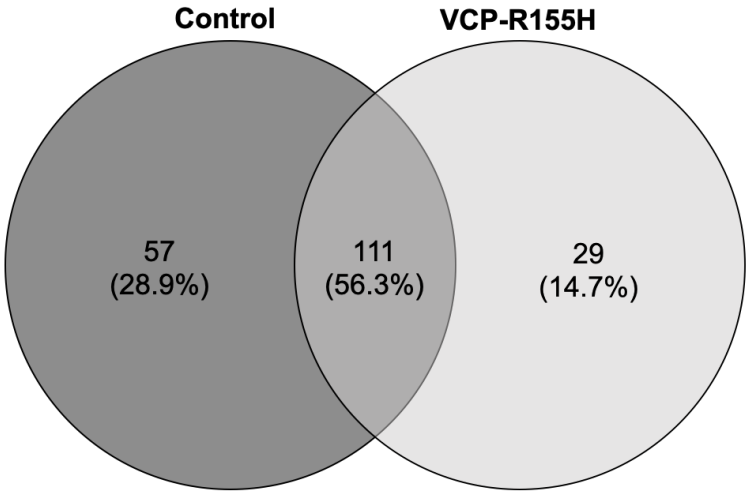

Figure 3.10: Mass spectrometry identifies 197 proteins from EVs isolated from media from control #1 and VCP-R155H #1 fibroblasts. Venn diagram of protein identified through mass spectrometry analysis of EV protein content. Data represents n=3 biological replicates.

Table 3.2: Differentially present proteins identified by mass spectrometry in EVs isolated from culture medium of Control #1 and VCP-R155H #1 fibroblasts.

Accession Number	Protein Description	Condition
Q9P1U1.1	Actin-related protein 3B	VCP-R155H
Q53H12.2	Acylglycerol kinase_ mitochondrial	VCP-R155H
Q8N6T3.2	ADP-ribosylation factor GTPase-activating protein 1	VCP-R155H
P01023.3	Alpha-2-macroglobulin	VCP-R155H
Q08043.2	Alpha-actinin-3	VCP-R155H
O43707.2	Alpha-actinin-4	VCP-R155H
P25705.1	ATP synthase subunit alpha_ mitochondrial	VCP-R155H
Q8N8U9.3	BMP-binding endothelial regulator protein	VCP-R155H
P04040.3	Catalase	VCP-R155H
Q03135.4	Caveolin-1	VCP-R155H
P56539.1	Caveolin-3	VCP-R155H
P12110.4	Collagen alpha-2(VI) chain	VCP-R155H
P13639.4	Elongation factor 2	VCP-R155H
Q13642.4	Four and a half LIM domains protein 1	VCP-R155H
P05062.2	Fructose-bisphosphate aldolase B	VCP-R155H
P47929.2	Galectin-7	VCP-R155H
Q86X29.4	Lipolysis-stimulated lipoprotein receptor	VCP-R155H
Q14764.4	Major vault protein	VCP-R155H
P14649.1	Myosin light chain 6B	VCP-R155H
P60660.2	Myosin light polypeptide 6	VCP-R155H
P83859.1	Orexigenic neuropeptide QRFP	VCP-R155H
Q13835.2	Plakophilin-1	VCP-R155H
P02545.1	Prelamin-A/C	VCP-R155H
P49756.3	RNA-binding protein 25	VCP-R155H
P02787.3	Serotransferrin	VCP-R155H
Q15464.2	SH2 domain-containing adapter protein B	VCP-R155H
Q01995.4	Transgelin	VCP-R155H
P68366.1	Tubulin alpha-4A chain	VCP-R155H
Q5T200.1	Zinc finger CCCH domain-containing protein 13	VCP-R155H
P31946.3	14-3-3 protein eta	Control
P09543.2	2'_3'-cyclic-nucleotide 3'-phosphodiesterase	Control
P21589.1	5'-nucleotidase	Control
O43491.1	Band 4.1-like protein 2	Control
Q9Y2J2.2	Band 4.1-like protein 3	Control
Q562R1.2	Beta-actin-like protein 2	Control
P50747.1	Biotin--protein ligase	Control
Q86T13.1	C-type lectin domain family 14 member A	Control
Q05682.3	Caldesmon	Control
Q6YHK3.2	]CD109 antigen	Control
P16070.3	CD44 antigen	Control
Q8IVM0.1	Coiled-coil domain-containing protein 50	Control
P12109.3	Collagen alpha-1(VI) chain	Control
P08123.7	Collagen alpha-2(I) chain	Control
Q53TN4.1	Cytochrome b reductase 1	Control
Q6UVY6.1	DBH-like monooxygenase protein 1	Control
Q14240.2	Eukaryotic initiation factor 4A-II	Control
Q16658.3	Fascin	Control
Q9Y4F1.1	FERM_ RhoGEF and pleckstrin domain-containing protein 1	Control
Q14192.3	Four and a half LIM domains protein 2	Control
P41250.3	Glycine--tRNA ligase	Control
P09471.4	Guanine nucleotide-binding protein G(o) subunit alpha	Control
P38405.1	Guanine nucleotide-binding protein G(olf) subunit alpha	Control
P63092.1	Guanine nucleotide-binding protein G(s) subunit alpha isoforms short	Control
Q5JWF2.2	Guanine nucleotide-binding protein G(s) subunit alpha isoforms Xlas	Control
P11488.5	Guanine nucleotide-binding protein G(t) subunit alpha-1	Control
A8MTJ3.2	Guanine nucleotide-binding protein G(t) subunit alpha-3	Control
Q03113.4	Guanine nucleotide-binding protein subunit alpha-12	Control
Q14344.2	Guanine nucleotide-binding protein subunit alpha-13	Control
P01834.1	Ig kappa chain C region	Control
P17301.1	Integrin alpha-2	Control
P07864.4	L-lactate dehydrogenase C chain	Control
Q9BTT6.1	Leucine-rich repeat-containing protein 1	Control
Q96S90.1	LysM and putative peptidoglycan-binding domain-containing protein 1	Control
O14786.3	Neuropilin-1	Control
Q15758.2	Neutral amino acid transporter B(0)	Control
Q14197.1	Peptidyl-tRNA hydrolase ICT1_ mitochondrial	Control
Q06830.1	Peroxiredoxin-1	Control
Q9Y617.2	Phosphoserine aminotransferase	Control
Q8WUM4.1	Programmed cell death 6-interacting protein	Control
O14910.2	Protein lin-7 homolog A	Control
Q9HAP6.1	Protein lin-7 homolog B	Control
Q9NUP9.1	Protein lin-7 homolog C	Control
Q9BZQ8.1	Protein Niban	Control
Q04941.1	Proteolipid protein 2	Control
P30613.2	Pyruvate kinase PKLR	Control
Q9ULC3.1	Ras-related protein Rab-23	Control
P20336.1	Ras-related protein Rab-3A	Control
P20337.2	Ras-related protein Rab-3B	Control
Q96E17.1	Ras-related protein Rab-3C	Control
O95716.1	Ras-related protein Rab-3D	Control
P51148.2	Ras-related protein Rab-5C	Control
O00186.2	Syntaxin-binding protein 3	Control
Q13769.2	THO complex subunit 5 homolog	Control
O60701.1	UDP-glucose 6-dehydrogenase	Control
O00159.4	Unconventional myosin-Ic	Control
Q8N5A5.3	Zinc finger CCCH-type with G patch domain-containing protein	Control

We performed an enrichment analysis using g.Profiler to determine functional enrichment in the total protein lists generated from control and VCP-R155H fibroblast EVs (Figure 3.11). Lists of identified proteins from analysis of EVs derived from Control #1 and VCP-R155H #1 fibroblasts were uploaded separately to g.Profiler for analysis. Enrichment analysis indicated enrichment of total EV protein lists for numerous EV-associated components including “extracellular vesicle”, “extracellular exosome”, “vesicle-mediated transport” and “exocytosis” (Figure 3.11). Therefore the populations of EV proteins identified in this study are enriched for genes pertinent to cellular compartments and biological processes that are associated with previously established EV functions, biogenesis or release.

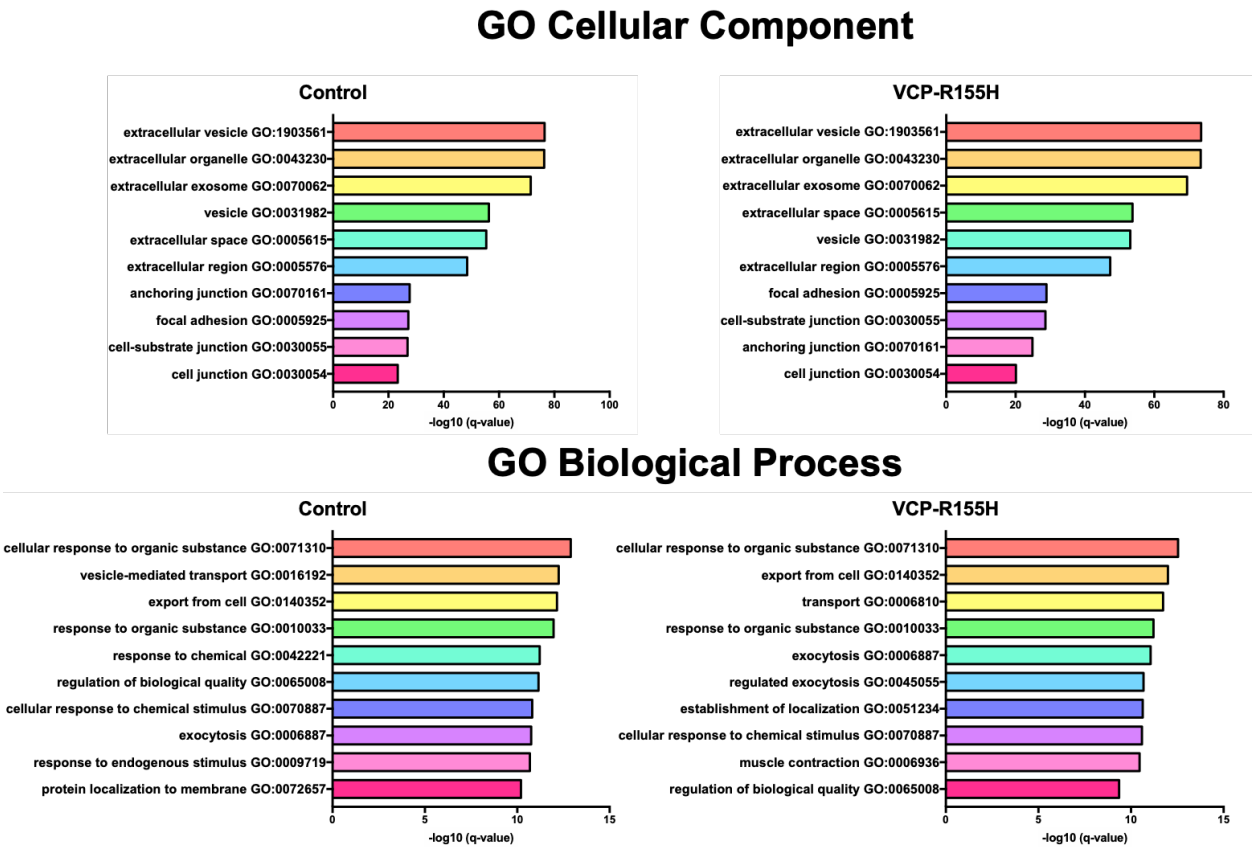

Figure 3.11: Functional enrichment analysis of proteins identified in EVs isolated from control #1 and VCP-R155H #1. Enrichment analysis was performed using g.Profiler using proteins identified in EVs derived from control #1 or VCP-R155H #1 fibroblasts. Protein lists identified from EVs for each cell line were independently submitted to g.Profiler to determine functional enrichment. Significance threshold was 0.05. p-values were corrected for multiple comparisons by g.Profiler and transformed to a $-\log_{10}$ scale and plotted using Prism. Graphics depict the top 10 annotations for GO Cellular Component and GO Biological Process ontologies for each cell line.

The second approach used to identify EV-derived protein biomarkers was quantitative mass spectrometry. Quantitative analysis was achieved by using label-free L/C mass spectrometry to analyze each EV technical replicate in triplicate. Protein quantification was based on the three most abundant peptides per protein and normalized using spiked Hi3 internal standard peptides. Quantitative mass spectrometry analysis of fibroblast EVs identified a total of 166 differentially abundant proteins, 55 of which were

identified using three unique peptides and could be reliably quantitated. Mean normalized abundance was calculated for each cell line from all replicates and used as the primary indicator of protein abundance. A t-test was performed to assess statistical differences in EV protein abundance between control and VCP-R155H fibroblast cell lines. The p-values obtained from t-test were corrected for false-discovery by applying the Benjamini-Hochberg method of analysis to produce a corrected t-test statistic (q-value). The fold change was then calculated as the ratio of VCP-R155H EV protein abundance relative to control levels. All proteins with q-values < 0.05 and fold change greater than 50% (> 1.3) were considered significant. A Volcano-plot was constructed plotting the log_2fold change (x-axis) in relation to the -Log_{10}p-value (y-axis) to visualize EV differential protein abundance (Figure 3.12).

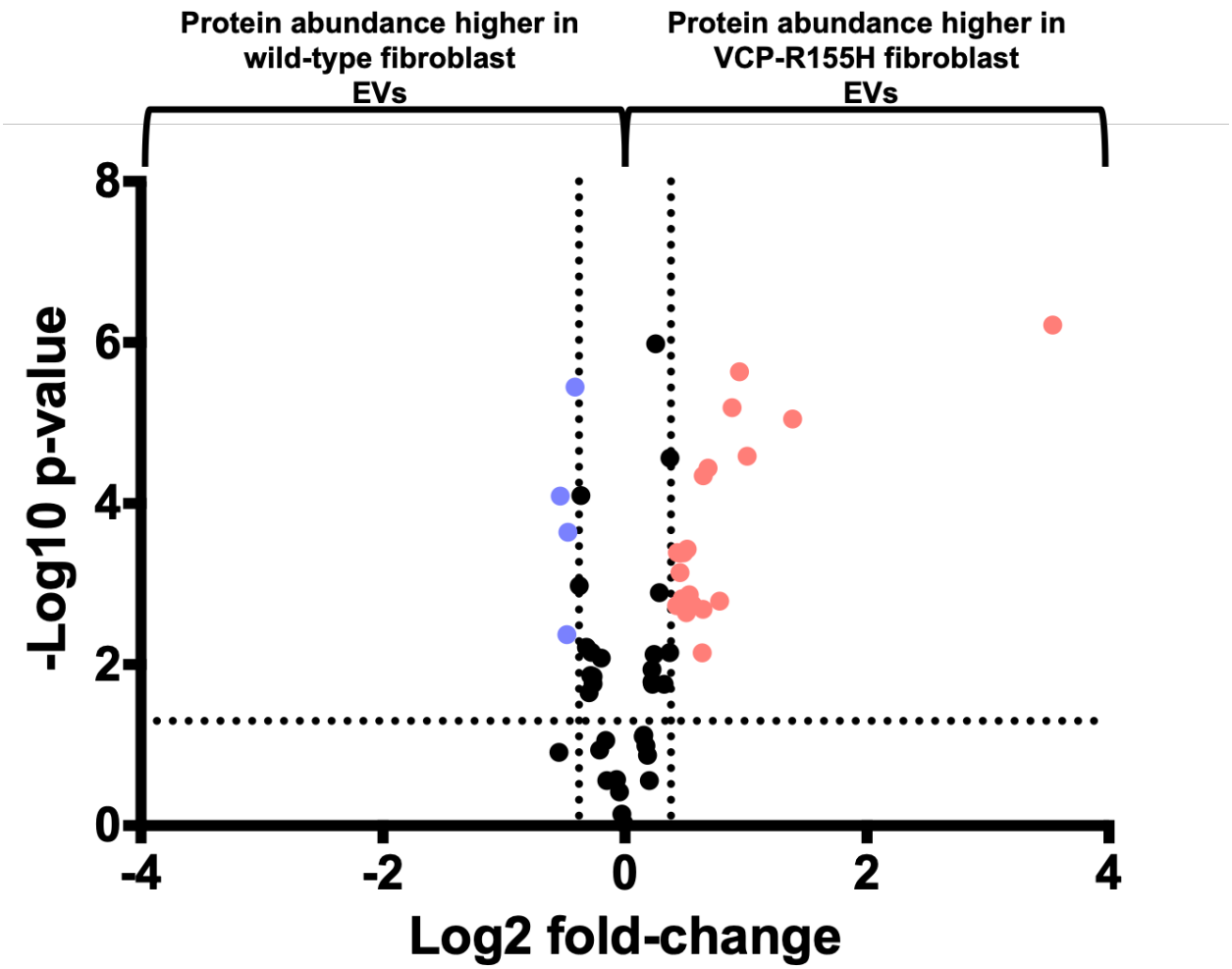

Figure 3.12: A volcano plot illustrating differentially abundant proteins in fibroblast EVs. Proteins achieving significance ($q<0.05$ and fold change > 1.3) are indicated by the colours red and blue, where red indicates proteins elevated in VCP-R155H fibroblast EVs and blue indicates proteins elevated in control fibroblast EVs. Data is based on n=3 biological replicates per cell line analyzed in triplicate.

A total of 24 differentially abundant proteins out the 55 quantitated in EV samples achieved significance; 20 proteins were elevated and 4 were decreased in VCP-R155H fibroblast EVs (Figure 3.12). All quantitated proteins that achieved significance were taken into consideration as candidate biomarkers (Table 3.3).

Table 3.3: Identity of differentially abundant proteins between control #1 and VCP-R155H #1 fibroblast EVs

Accession number	Protein Description	Confidence score	Elevated Condition	Max fold change	p-value	q-value
P68431.2	Histone H3.1	28.9415	VCP-R155H	11.60565645	6.09454E-07	0.0009091
P06396.1	Gelsolin	26.1298	VCP-R155H	2.61376291	8.90891E-06	0.0054546
Q05682.3	Caldesmon	21.5543	VCP-R155H	2.013728297	2.59454E-05	0.0063636
P07355.2	Annexin A2	72.7446	VCP-R155H	1.92719705	2.3136E-06	0.0027273
P09525.4	Annexin A4	44.791	VCP-R155H	1.84758205	6.44616E-06	0.0045455
P62258.1	14-3-3 protein epsilon	65.8358	VCP-R155H	1.719625251	0.001627807	0.0209091
P06733.2	Alpha-enolase	26.8218	VCP-R155H	1.609194512	3.64007E-05	0.0081818
P68104.1	Elongation factor 1-alpha 1	43.6571	VCP-R155H	1.566379753	4.5185E-05	0.0090909
P60709.1	Beta-actin	23.7776	VCP-R155H	1.564260454	0.002057645	0.0236364
P00338.2	L-lactate dehydrogenase A chain	41.7399	VCP-R155H	1.556180717	0.007154707	0.0290909
P15311.4	Ezrin	16.5725	VCP-R155H	1.473481921	0.001804214	0.0218182
P08133.3	Annexin A6	49.0989	VCP-R155H	1.445302818	0.00136049	0.0190909
O00299.4	Chloride intracellular channel protein 1	18.0697	VCP-R155H	1.427476215	0.00036814	0.0127273
P60174.3	Triosephosphate isomerase	16.976	VCP-R155H	1.421437839	0.002281857	0.0245455
Q99536.2	Synaptic vesicle membrane protein VAT-1 homolog	56.3727	VCP-R155H	1.400941622	0.000409679	0.0145455
P08670.4	Vimentin	59.5502	VCP-R155H	1.388687086	0.001525234	0.02
P18206.4	Vinculin	111.4219	VCP-R155H	1.371250416	0.000720808	0.0163636
O94832.2	Unconventional myosin-Id	99.3652	VCP-R155H	1.368555166	0.000412493	0.0154546
P35579.4	Myosin-9	107.7576	VCP-R155H	1.350800155	0.000407094	0.0136364
P31946.3	14-3-3 protein beta/alpha	29.0536	VCP-R155H	1.344593352	0.001861081	0.0227273
P05556.2	Integrin beta-1	28.0859	Control	1.44898076	8.08962E-05	0.0109091
O00159.4	Unconventional myosin-Ic	20.5671	Control	1.394186355	0.004267375	0.0254546
P0CG47.1	Polyubiquitin-B	26.3463	Control	1.38629889	0.000227135	0.0118182
P11142.1	Heat shock cognate 71 kDa protein	27.9633	Control	1.330255079	3.59682E-06	0.0036364

In short, proteomic analysis of EVs from VCP-R155H and control fibroblasts allowed for the creation of an unbiased list of candidate protein biomarkers for ALS. Mass spectrometry analysis of EV protein content allowed for identification of proteins differentially present in EVs from control and VCP-R155H fibroblasts, in addition to the quantitation of proteins with differential abundance in EVs from both cell types. In total, label-free L/C mass spectrometry analysis identified 106 as candidate biomarkers of ALS, 20 with significant differential abundance in both cell lines (see above significance criteria) and 86 differentially present in control and VCP-R155H fibroblast EVs. While proteins identified in this analysis of EV content may represent valuable potential biomarkers for ALS, further validation in EVs derived from multiple independent fibroblast cell lines is required to determine significance of identified hits.

3.7 Pilot validation by immunoblot analysis shows that Integrin-beta 1 is elevated in VCP-R155H fibroblast EVs

To validate our findings of mass spectrometry analysis and test their applicability in other VCP-R155H and control cell lines, we isolated EVs from three different VCP-R155H and control fibroblast cell lines (see Table 3.1 for phenotypic characteristics) and assessed the levels of the candidate proteins by immunoblot quantitation. For pilot validation of protein candidates, we focused on proteins that would be easily detectable via EV immunoblot analysis. Label-free mass spectrometry analysis of EV content yielded 106 proteins differentially present and 24 differentially abundant proteins that could act as potential EV-sourced protein biomarkers for ALS (Table 3.2 and Table 3.3). Of these 106 proteins, four proteins were selected for pilot validation via immunoblot: H3, prelamin A/C, gelsolin and integrin beta 1. Selection of these proteins was based in part on the degree of protein differential abundance and on the availability of convenient and specific antibodies. Selection of these proteins for validation was based largely on antibody availability. Mass spectrometry analysis identified H3, gelsolin and integrin beta 1 as differentially abundant, while prelamin A/C was solely detected in VCP-R155H fibroblast EVs.

H3 was the top hit for differentially abundant proteins, showing 11.6-fold enrichment in VCP-R155H fibroblasts. Interestingly, H3 was previously used during EV characterization as a negative control for EV samples and fell below detectable levels in immunoblot analysis of EV samples from control and VCP-R155H fibroblasts (Figure 3.7A. A similar phenomenon was apparent with fellow nuclear protein prelamin A/C, which

mass spectrometry analysis found was solely detected in VCP-R155H fibroblast EVs. Prelamin A/C, a precursor protein cleaved for form lamin A/C, can be detected by immunoblot using an antibody for lamin A/C. Immunoblot analysis of control and VCP-R155H fibroblast EVs revealed that prelamin A/C could not be detected in EV samples, despite the conflicting results of proteomic analysis (Figure 3.13). Thus, despite proteomic analysis reporting the presence of prelamin A/C in VCP-R155H EV samples, levels of prelamin A/C fall below the detectable threshold and was therefore excluded from further analysis.

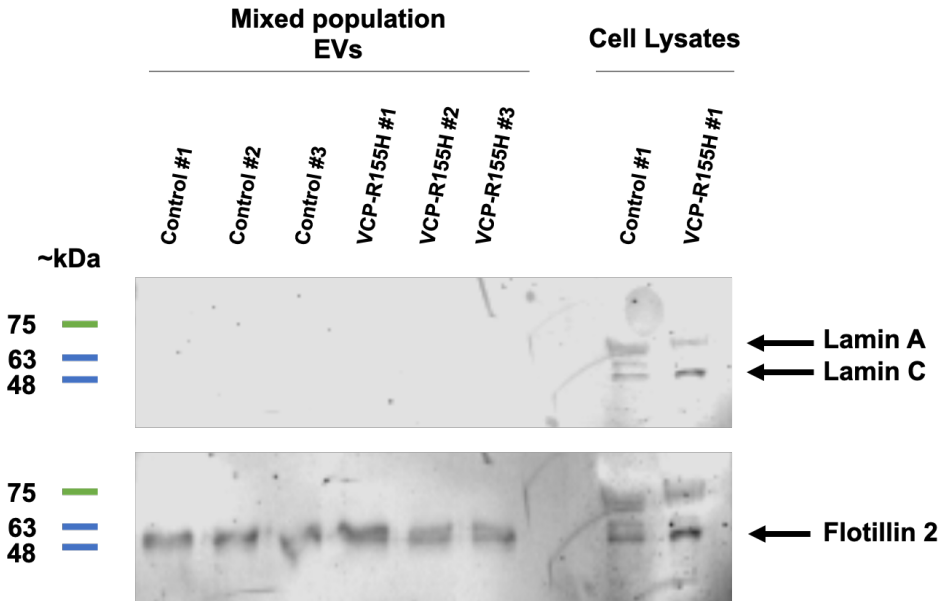

Figure 3.13: Neither prelamin A/C nor lamin A/C can be detected fibroblast EVs by immunoblot. EVs were isolated from six different fibroblast cell lines by differential ultracentrifugation and equivalent volumes of isolated EVs were separated by SDS-PAGE to be analyzed by immunoblot and probed with antibodies for lamin A/C and flotillin-2. Immunoblot was probed with anti-lamin a/c, developed using Odyssey CLx and then re-probed with anti-flotillin-2 as a loading control and developed for a second time. Blot represents n=1 experimental replicate.

Gelsolin, an actin binding protein, was another protein selected for pilot validation as an EV-derived protein biomarker for ALS. In VCP-R155H fibroblast EVs, quantitative proteomic analysis found that gelsolin showed a 2.6-fold higher level relative to control EVs and, in fact, was the second greatest differentially abundant protein identified during quantitative mass spectrometry analysis (Table 3.3). Although multiple immunoblots were performed with multiple EV samples from different isolations, gelsolin signal was highly variable and unreliably detected in EVs, ranging from definitive signal in multiple lanes to falling below detectable limits for the same samples (Figure 3.14). In the immunoblot where gelsolin was detected, it appeared enriched in EVs derived from VCP-R155H fibroblasts and was consistent with results of proteomic analysis (Figure 3.14). Although incomplete, preliminary efforts for pilot validation showed differences in EV levels of gelsolin protein in EVs derived from Control and VCP-R155H fibroblasts which appear to be in line with those reported from quantitative mass spectrometry analysis.

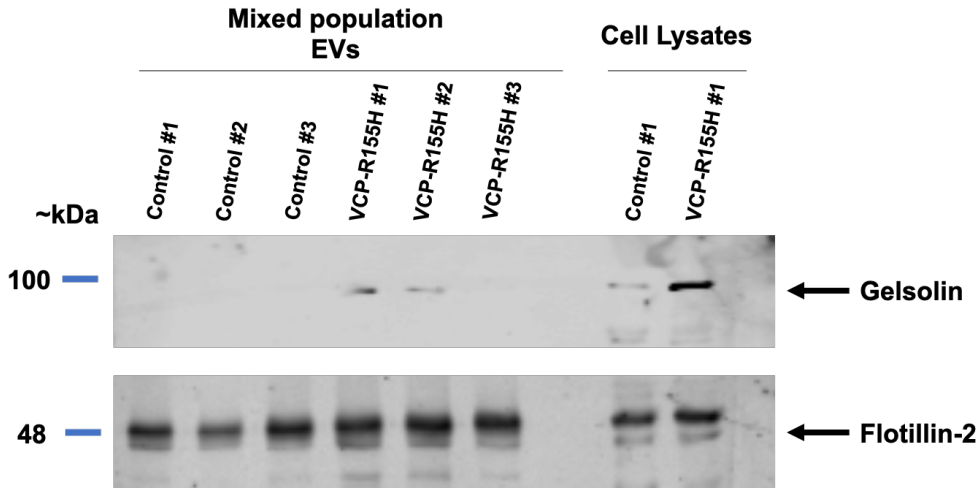

Figure 3.14: Analysis of gelsolin in EV isolated from VCP and control cell lines. EVs were isolated from six different fibroblast cell lines by differential ultracentrifugation and equivalent volumes of isolated EVs were separated by SDS-PAGE to be analyzed by immunoblot and probed with antibodies for gelsolin and flotillin-2. Blot is a representative image from repeated (n=3) experiments.

The final protein selected for pilot validation was integrin beta 1. Quantitative mass spectrometry reports a 40% decrease in VCP-R155H fibroblast EVs relative to controls (Table 3.3). We performed immunoblot analysis on EV samples isolated from six different fibroblast cell lines and probed with antibodies for integrin beta and flotillin-2 to validate the findings from proteomic analysis. In total, three separate immunoblots were performed using 3 independent EV isolations from the cell lines. Contrary to the results of proteomic analysis, our immunoblot analysis showed significantly ($p<0.05$) higher levels of integrin beta 1 protein in VCP-R155H fibroblast EVs relative to controls (Figure 3.15). Therefore, pilot validation by immunoblot confirmed the significant enrichment of integrin beta-1 and suspected enrichment of gelsolin in EVs derived from VCP-R155H+ fibroblasts in comparison to healthy controls. Further validation must be performed to confirm the enrichment of these proteins and to assess their utility as biomarkers for ALS14.

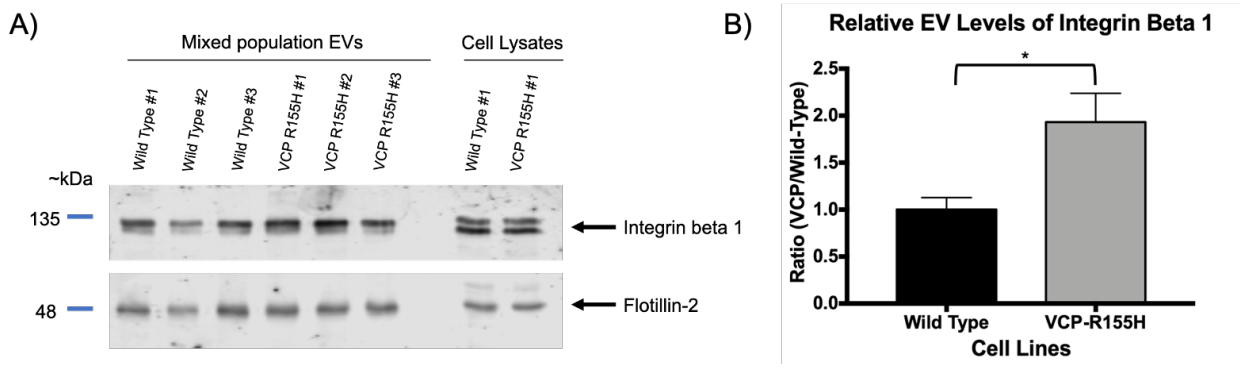

Figure 3.15: Analysis of integrin 1 beta in EV isolated from VCP and control cell lines. A) EVs were isolated by differential ultracentrifugation and equivalent volumes of the isolated EVs were separated by SDS-PAGE and analyzed by immunoblot for integrin beta 1 and flotillin-2. Image is a representative blot. B) VCP signal was quantified and normalized relative to flotillin-2 signal using ImageStudio software. Data represents n=3 experimental replicates. An asterisk (*) indicates significance where $p<0.05$. Statistical analysis was performed using an unpaired t-test.

Chapter 4: Discussion

ALS is a devastating neuromuscular illness caused by the degeneration of motor neurons in the brain and spinal cord [61]. Despite being the most common adult-onset motor neuron disease with an incidence of 3.8 per 100,000 people, there is no cure or effective form of treatment for ALS [1]. Neuromuscular symptoms aside, ALS patients may also present with FTD, and language and cognitive impairments, which can further delay the diagnostic process and onset of treatment. One of the central limitations in the development of potential diagnostic and therapeutic advances for ALS is that patients become symptomatic well after significant motor neuron degeneration has already occurred, hindering the ability of researchers and clinicians to study the preclinical phase and identify key pre-symptomatic biomarkers. The preclinical phase includes from the time of birth until the time of symptom manifestation, where the presence of a mutation, environmental factors or epigenetic changes may cause an individual to become increasingly susceptible to insults including excitotoxicity, neuroinflammation, oxidative stress and mitochondrial dysfunction [26]. Recent approval by Health Canada of the drug Edaravone, the first new ALS treatment in 20 years, has provided a valuable addition to the clinical arsenal, however current studies indicate treatment with Edaravone does not significantly increase life expectancy [70,74,75]. With a projected global increases in the number of ALS cases, but also innovation of novel therapeutics, there is urgent need for sensitive and reliable biomarkers to aid in diagnosis, track disease progression and monitor the efficacy of current and groundbreaking medications [182].

EVs provide an appealing source of molecular biomarkers because they are easily isolated from a multitude of biofluids including serum, plasma, CSF and saliva, and contain a miscellany of selectively-enriched cellular components including lipids, a variety of nucleic acids (non-coding RNA, microRNA, mRNA) and protein that directly reflect the cells from which they are derived. Previous work by a number of groups has solidified the value of harnessing EVs as a potential source of biomarkers for a number of diseases including ALS, cardiovascular disease, Parkinson's, Spinal Muscular Atrophy, hypertension and cancer [86,147,167,168,183-186]. In this study, we successfully identified protein biomarkers for ALS from a targeted candidate search and proteomic analysis of control and VCP-R155H fibroblast derived EVs (Table 3.2-3.3). We further demonstrated that proteins VCP, integrin beta-1 and gelsolin are enriched in EVs from VCP-R155H fibroblast cell lines (Figure 3.9 and 3.16). These results suggest that gelsolin, integrin beta-1 and VCP protein content in exosomes may represent novel biomarkers for ALS14.

4.1 Cytoskeletal proteins as biomarkers for ALS14

A total of 106 proteins were identified as potential biomarkers of the ALS disease state from proteomic analysis of control and VCP-R155H fibroblast EV content. Included in the differentially abundant and differentially present proteins were a number of structural proteins including vinculin, β-actin, vimentin and tubulin α-4A chain, indicating that the structural stability of the cell may be compromised in ALS14. Although many cytoskeletal proteins are considered common contaminants in mass spectrometry analysis, previous studies indicate that disruptions of cellular cytoskeleton may contribute to some forms of ALS pathogenesis [9,187-190]. The actin-binding protein gelsolin, which has

previously been proposed as a plasma biomarker for ALS [191,192], was selectively enriched in proteomics and immunoblot analysis in our study. Unfortunately, the levels of gelsolin protein contained in EVs appears to be low, and further validation and testing is required for gelsolin to be deemed a good potential biomarker for ALS.

4.2 Integrin β-1 as a biomarker for ALS14

Integrins, which are one of the primary mediators of interaction between the cell and its environment, also play a role in linking the actin cytoskeleton to the extracellular matrix [193]. Integrin beta-1 was identified through proteomic analysis as differentially expressed in EVs of control and VCP-R155H fibroblast EVs. Integrins are transmembrane receptors that are commonly found on the surface of EVs; disruption of integrin signaling has been shown to promote cancer and inflammation[132,193] . A recent study implicated integrin signaling in ALS using a combined-tissue and fluid proteomics approach to elucidate mechanisms of phenotypic variability in ALS pathogenesis, although how integrins directly contributes to the disease state has yet to be determined [132].

4.3 VCP as a potential biomarker for ALS14

VCP is involved in many functions within the cell and mutations in VCP directly contribute to disruptions in proteostasis observed in ALS14. We determined that VCP is enriched in the EVs isolated from culture media of VCP-R155H fibroblasts and may serve as a potential biomarker of the ALS disease state (Figure 3.8). VCP forms homohexameric complexes to perform various functions in the cell, which ultimately become compromised in cells harboring mutant VCP. Expression of VCP appeared

elevated in R155H mutant fibroblasts relative to controls, although it did not achieve significance, potentially as a compensatory mechanism (Figure 3.8). The protein caveolin-1 (CAV-1) was also noted among differentially identified proteins in VCP-R155H EVs (Table 3.2). CAV-1 is a recognized binding partner of VCP protein [44]. Localized to the membrane of late endosomes, CAV-1 is responsible for binding VCP, which then transports CAV-1 to the endolysosomes for degradation [44]. Previous studies determined that when VCP-CAV-1 binding is blocked chemically or by mutation, CAV-1 accumulates on the limiting membrane of the late endosome of patient fibroblasts harbouring the VCP-R155H and VCP-L198W mutations [44]. Moreover, the binding of Cav-1 is directly compromised by the presence of the VCP-R155H mutation and may impact endosomal trafficking in patients with IBMPFD/ALS [44].

4.4 Extracellular Histones

Protein H3 was significantly enriched in VCP-R155H EVs by 11.6-fold according to proteomic analysis (Table 3.3). This result was surprising, given that H3 was used in previous analysis as a marker of EV sample purity when characterizing isolated EV samples to rule out sample contamination with nuclear and extracellular proteins as well as cell debris, and the levels of H3 in EV fell below threshold of detection for immunoblot analysis (Figure 3.7A). While one possibility for the presence of H3 in our samples is contamination of the EV with larger apoptotic bodies, further review of the literature revealed multiple proteomic studies in which histones were largely abundant in the EVs from a number of cell types including B16 melanoma cells, sebocytes, mast cells as well as human and murine monocyte derived dendritic cells [194-197]. Histones are localized to

the nucleus, and are intimately involved in transcriptional regulation, chromatin stability and nucleosome remodelling [198]. Apoptotic cell death can cause histones to dissociate from genomic DNA, translocate to the cytoplasm of the cell, and are subsequently released into the extracellular space [199]. The release of histones into the extracellular space can lead to an inflammatory response [200]. Although sample contamination with apoptotic bodies is possible, we consider this unlikely given the first two centrifugation steps in our EV isolation protocol (300g X 10minutes and 2500g X 10minutes) are designed to eliminate the majority of extra-large vesicles. Moreover, we did not detect large vesicles in our NTA analysis (Figure 3.7b). H3 protein may have been present in our EV samples analyzed by immunoblot but were below the level of detection. Alternatively, the detection of H3 in our proteomic analysis may be a false positive [201]. Regardless, given that H3 fell below the threshold of detection for immunoblot validation, it was not further pursued in this study.

4.5 Primary fibroblast cultures as a model of ALS

The primary objective of this study was to identify protein biomarkers for ALS using primary fibroblasts carrying the VCP-R155H mutation through candidate search and proteomic analysis of EV content. VCP mutations cause a rare form of autosomal dominant familial ALS that falls into the IBMPFD/ALS spectrum of disease. IBMPFD/ALS affects brain, heart and bone and is therefore well-suited for *in vitro* studies in a number of different culture model systems [34]. As a major part of connective tissue, fibroblasts are present throughout the body and allow us to identify and characterize key disease-relevant pathologies that may extend to other, potentially overlooked, biological systems

in disease pathogenesis. Moreover, primary fibroblast cultures may be able to recapitulate early pathological changes present in the brains of ALS patients [174,202]. In the context of neurodegenerative disease, primary fibroblast culture models have been crucial in the examination of early pathological changes, with the benefit of incorporating the biological aging of patients according to their genetic predisposition, chronological age and environment [202]. Studies of a number of neurodegenerative diseases have shown that may disease features can be recapitulated in fibroblast cell models carrying disease-relevant pathological mutations, such as impaired mitochondrial function, proteostasis and bioenergetics in Huntington's disease, Parkinson's disease and Alzheimer's disease [18,147,202-206]. Of relevance to ALS, previous studies showed that fibroblasts from patients carrying mutations associated with familial ALS experience a decrease in nuclear TDP-43 relative to controls even in the absence of cellular stress [174,207]. While a marked decrease of nuclear TDP-43 was not readily observed in our VCP-R155H fibroblast cell models relative to controls, we did observe a trend toward slower recovery of nuclear TDP-43 in VCP-R155H fibroblasts relative to controls , potentially due to impaired nucleocytoplasmic shuttling of TDP-43 and delayed reestablishment of proteostasis due to prolongation of the cellular stress response (Figures 3.3 and 3.5). In addition, we observed increased cytoplasmic localization of TDP-43 in immunofluorescent images of VCP-R155H #1 fibroblasts, where TDP-43 inclusions persisted until the final time-point at 24 hours post-heat shock (Figure 3.2). This finding is in agreement with previous studies indicating that VCP mutations led to increased cytoplasmic localization of TDP-43 and supports that TDP-43 toxicity is mediated by a toxic gain of function in the cytoplasm [208]. Future work should examine the impact of VCP

on TDP-43 and stress granule dynamics, particularly in the context of fibroblasts and motor neurons.

4.6 Study limitations

The ideal outcome of this study was to identify EV-derived protein biomarkers in a cell culture model of ALS that could later be translated into clinical studies involving patients with various forms of ALS. Blood or plasma is among the first biofluids tested during the diagnostic process for ALS patients and is among the least invasive to obtain [88]. In peripheral blood samples, the majority of EVs originate from platelets, erythrocytes, leukocytes and endothelial cell types, however recent literature suggests that EVs originating from cell types in the brain may also be detected [209,210]. While the notion of using peripheral cell types, such as fibroblasts, as a means to identify EV-derived biomarkers is exciting, it also brings about the question of applicability to the disease state. Whether or not protein biomarkers identified in this study will be applicable to EVs isolated from plasma of VCP patients remains to be determined. Although fibroblasts can recapitulate important phenotypes and give insight into potential mechanisms of disease pathogenesis, it is important to acknowledge that they are not representative of the disease state as a whole, nor is their EV content necessarily reflective of the content of circulating EVs in biofluids such as plasma. Although pilot validation was performed on EVs sourced from three fibroblast cell lines and their corresponding controls, mass spectrometry analysis of EVs was restricted to a single cell line with a technical triplicate. The small sample size used during this study prevent significant conclusions from being drawn.

4.7 Future Directions

Despite recent advances, there is still a distinct lack of effective therapeutics and sensitive, non-invasive biomarkers for ALS. Therefore, there is a dire need for non-invasive and sensitive biomarkers for ALS that can distinguish between healthy, at-risk and affected individuals. In this work we have shown that EVs derived from fibroblasts carrying the VCP-R155H mutation may serve as a simplified source of protein biomarkers. Although this study has generated a number of potential novel biomarkers for ALS14, it is important to note that these efforts are preliminary and there is much work to be done before a new biomarker for ALS can be declared (Figure 4.1). Pilot validation was performed by immunoblot and future studies would benefit from validation through the use of single vesicle analysis. EV fractions are often contaminated with similar sized protein aggregates that are co-isolated during the EV purification procedure [211]. This is a problem for mass spectrometry-based proteomics investigation, which can detect and report artefactual results based on detection of these contaminating protein aggregates [212]. To address this limitation, EV samples could be examined by immunogold-labelling for the protein of interest and electron microscopy, to confirm that the proteins were indeed contained within EVs [112]. Proteins not located with EVs would be excluded from further study.

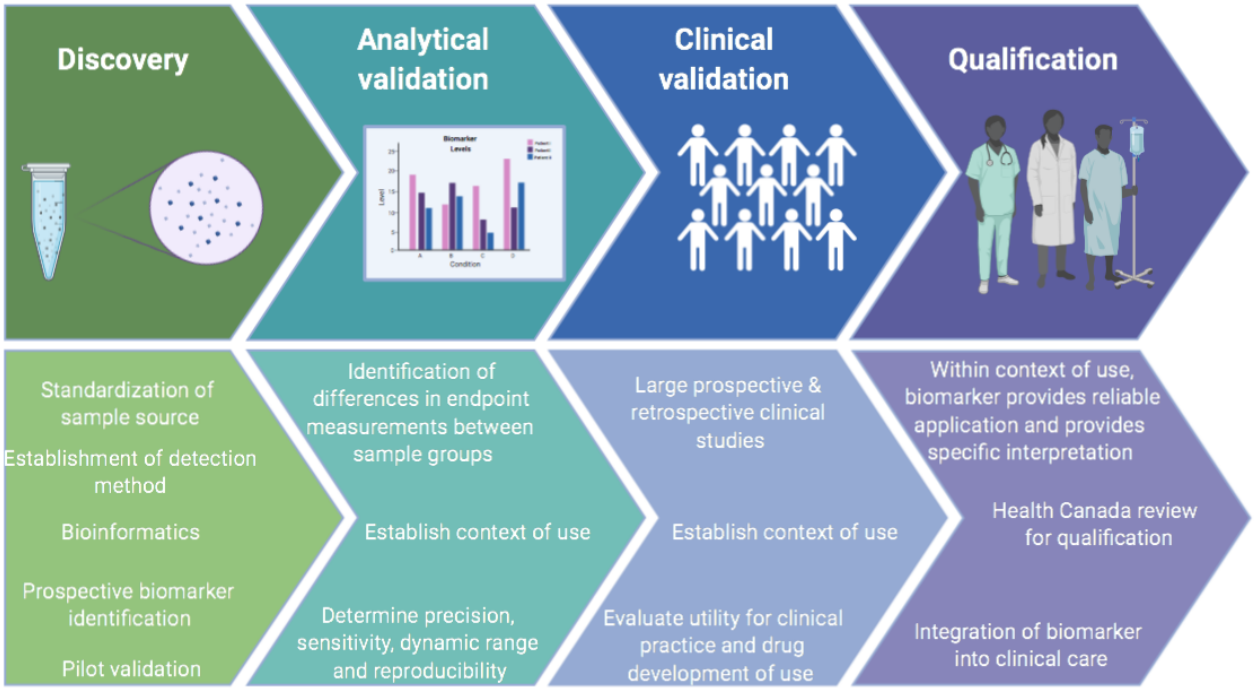

Figure 4.1: Pipeline for the discovery and integration of novel biomarkers into clinical care.

While fibroblasts may not be representative of the ALS disease state as a whole, we believe future studies should strive to further validate the biomarkers identified in this study in EVs derived from plasma and CSF samples taken from patients with IBMPFD/ALS and other forms of sporadic and familial ALS. To assess the wider applicability of identified EV-derived biomarkers, blood and CSF samples should be drawn from individual patients and care should be taken to document patient's age, gender, presence of any disease-relevant mutations and disease progression at the time when the sample was taken. These parameters will aid in determining whether the biomarker is indicative of the disease state, applies to single or multiple forms of ALS, changes with disease progression, or changes with gender. The levels of each candidate protein should be compared between samples from the same individual and among other individuals. For gelsolin, particular care should be taken to identify which of the two

gelsolin isoforms is indicative of the disease state; cytosolic or plasma [213]. Plasma gelsolin has been previously put forward as a potential biomarker of the ALS disease, however cytosolic and plasma gelsolin can both be packaged into EVs [214]. Ideally, the levels of a potential protein biomarker within plasma-derived EVs would be similar to CSF-derived EVs, as obtaining blood is much less invasive than obtaining CSF, thus allowing for repeated sampling during the course of disease progression or treatment.

Should the levels of VCP, integrin beta-1 or gelsolin from patient-derived EVs prove to be effective diagnostic biomarkers, these proteins should be further examined as prognostic biomarkers in individuals carrying mutations associated with other forms of familial ALS. To assess the prognostic capabilities of identified biomarkers and identify novel prognostic EV-derived protein biomarkers, CSF and plasma would need to be sampled from asymptomatic patients prior to disease onset, which occurs on average at 55 years of age, although disease onset is largely dependent on familial subtype [8,88]. Annual CSF and plasma sampling could be performed on asymptomatic carriers from the age of approximately 40 years onwards to identify crucial changes in EV protein levels that that may precede disease onset. If EV-levels of previously identified protein biomarkers or novel biomarkers are able to identify individuals at risk for development of ALS or individuals in the pre-clinical disease state, this could be further explored in symptomatic individuals with sporadic forms of the disease to allow for the amelioration of early detection strategies and improve the overall diagnostic process for ALS patients. Ideally, EV-derived protein biomarkers identified in familial ALS patients would apply in cases of sporadic ALS and could be incorporated into preventative clinical care.

In the event that EV VCP, Integrin beta-1 or gelsolin levels prove to be indicators of the ALS disease state in patient-derived EVs, these proteins should be further examined as biomarkers of ALS therapeutic efficacy. Riluzole and edaravone are the only two approved treatments for ALS; riluzole is administered in tablet form at a recommended dosage of 100mg/day and edaravone is administered by intravenous infusion in six cycles, each of which consists of 28 days (10-14 days with treatment followed by 14 days without treatment) [215]. Currently, therapeutic efficacy is indirectly monitored through the use of the ALSFRS-R, which provides a numerical score of disease severity [216]. To examine the predictive capabilities of validated protein biomarkers, patient blood and CSF would be sampled upon ALS diagnosis, prior to treatment onset to establish a baseline measurement. Samples could be drawn every month for patients taking Riluzole or at the beginning of each treatment cycle for those taking edaravone. Although it is unknown how the EV levels of each candidate biomarker would change with treatment, they would ideally normalize to indicate the slowing of disease progression with the administration of therapeutic agents.

Chapter 5: Conclusion

I have shown that EVs can be isolated from fibroblast culture models and may be used as a source of protein biomarkers for ALS14. I have also shown that protein biomarkers identified from carriers of VCP-155H mutations can be validated across multiple fibroblast cell lines. Despite these findings, there exists major barriers to the translation of pre-clinical investigations of EV biomarkers for ALS, specifically the differentiation between natural variance in EV protein content and those reflective of pathological processes relevant to the disease state. While there is a lack of biological replication to make significant conclusions, experiments using fibroblasts sourced from individual patient (VCP-R155H#1) with a technical triplicate were successful in identifying proteins that were significantly different in their EVs compared to healthy controls. Therefore, an unbiased approach may be a meaningful way to examine novel biomarkers in EVs derived from patient samples and follow up experiments should be done to increase sample size to see if these proteins remain significant. Future studies should focus on the validation and identification of novel EV biomarkers. Specifically, analyses should be performed in EVs derived from patient plasma and CSF in order to determine novel biomarkers and accurately assess the utility and contribution of previously identified protein biomarkers to the ALS disease state. By identifying and validating novel biomarkers for ALS, a more streamlined diagnostic process and the innovation of novel treatment strategies will be achieved, ultimately improving patient outcomes.

Appendix I

Liquid chromatography mass spectrometry analysis

EV samples were suspended in 6x SDS loading dye (10% SDS w/v, 0.5 M Tris-HCl pH 6.8, 40% glycerol (v/v), and 30 mM DTT), boiled for 10 minutes and separated by 15% SDS-PAGE. Protein in digested samples was visualized using Imperial Coomassie stain (Thermo Fisher Scientific) following the manufacturer's protocol. Individual lanes were excised and dissected into three parts in siliconized tubes (Fisher Scientific) and destained as per *Gombar et al.* prior to in-gel trypsin [170]. Samples were digested overnight at 37 °C with 0.8 µg of mass spectrometry grade trypsin (Promega) prepared in 50 mM NH_4HCO_3 (Thermo Fisher Scientific) to a final concentration of 0.04 µg/µL. Trypsin digestion was quenched with 5% formic acid (Sigma) and peptides were extracted using 60% acetonitrile (Burdick and Jackson), 1% formic acid in HPLC grade water (Burdick and Jackson). Peptide extracts for each biological replicate were pooled together to yield three fractions and concentrated to dryness using vacuum centrifugation. Samples were reconstituted in 0.1% formic acid solution, and Hi3 standard peptides (Waters) (12.5 fmol/ µL) were added for relative protein quantitation.

The resulting peptides were injected on a 1.8 µm HSS T3 75 µm × 150 mm reverse-phase column (Waters) using a nanoAcquity UPLC system (Waters) at a flow rate of 0.3 µL/min. Mobile phase A (0.1 % formic acid in H_2O) and mobile phase B (acetonitrile with 0.1% formic acid) were then used to equilibrate the column and peptides were loaded into the column at a ratio of 97:3 (A/B). Peptides were then separated on a 120 min gradient (3-25% B for 70 min, 25-50% B for 20 min, 50-85% B for 9 min, 85-3% for 2 min, 3% B for 20 min) and electrosprayed into a SYNAPT G2-Si mass spectrometer

(Waters). The mass spectrometer was operated in data independent acquisition mode employing ion mobility separation ($HDMS^E$) alternating between low energy (4 eV) and high energy (20-45 eV) scans in positive resolution mode, scanning from 50 – 2000 m/z with a scan rate of 0.6 s. [Glu1]- fibrinopeptide B (50 fmol/µL) was used as the lock mass external calibrant. Cone voltage was set to 30 V, and the capillary voltage was set at 3 kV. MassLynx (version 4.1) was used to collect the data.

Processing was performed for EV protein identification using ProteinLynx Global Server (PLGS) software. The following processing parameters were used: low energy noise reduction thresholds-135, high-energy threshold-30, and intensity threshold-750, with data lock mass corrected post acquisition. Search parameters included a maximum protein mass of 250 kDa, a minimum of two matched peptides per protein, a minimum of seven fragment ion matches per protein, a minimum of three fragment ion matches per peptide, a maximum of two missed cleavages (trypsin). The false-discovery rate was estimated to be below 1% using a decoy database. Variable modifications for carbamidomethylated cysteine and oxidation of methionine were specified.

Processing was performed for quantitative analysis using Progenesis QI (Nonlinear Dynamics) for peptide identification analysis and the *Homo sapiens* subset of the Uniprot/Swissprot Human Database (updated 2018). The following processing parameters were used: low energy noise reduction thresholds-135, high-energy threshold-30, and intensity threshold-750, with data lock mass corrected post acquisition. Search parameters included a maximum protein mass of 250 kDa, a minimum of two matched peptides per protein, a minimum of seven fragment ion matches per protein, a

minimum of three fragment ion matches per peptide, a maximum of two missed cleavages (trypsin). The false-discovery rate was estimated to be below 1% using a decoy database. Variable modifications for carbamidomethylated cysteine and oxidation of methionine were specified. Three technical replicates for each of the three biological replicates were analyzed per tactic (30 total measurements). Quantitation was determined using the three most abundant peptides per protein (including the internal standard) and normalized using the Progenesis QI software. The normalization processing utilized a reference chromatography run and spiked Hi3 internal standard peptides (50 fmol on column) to convert raw abundance values to absolute measurements (fmol on column).

References

1. Longinetti E, Fang F. Epidemiology of amyotrophic lateral sclerosis: an update of recent literature. *Curr Opin Neurol.* 2019;32(5):771-776.
2. Consortium PMAS. Project MinE: study design and pilot analyses of a large-scale whole-genome sequencing study in amyotrophic lateral sclerosis. *Eur J Hum Genet.* 2018;26(10):1537-1546.
3. Rowland LP, Shneider NA. Amyotrophic lateral sclerosis. *N Engl J Med.* 2001;344(22):1688-1700.
4. de Majo M, Topp SD, Smith BN, et al. ALS-associated missense and nonsense TBK1 mutations can both cause loss of kinase function. *Neurobiol Aging.* 2018;71:266.e261-266.e210.
5. Nguyen HP, Van Broeckhoven C, van der Zee J. ALS Genes in the Genomic Era and their Implications for FTD. *Trends Genet.* 2018;34(6):404-423.
6. Keith JL, Swinkin E, Gao A, et al. Neuropathologic description of *CHCHD10* mutated amyotrophic lateral sclerosis. *Neurol Genet.* 2020;6(1):e394.
7. Yu Y, Nakagawa T, Morohoshi A, et al. Pathogenic mutations in the ALS gene CCNF cause cytoplasmic mislocalization of Cyclin F and elevated VCP ATPase activity. *Hum Mol Genet.* 2019;28(20):3486-3497.
8. Li HF, Wu ZY. Genotype-phenotype correlations of amyotrophic lateral sclerosis. *Transl Neurodegener.* 2016;5:3.
9. Smith BN, Vance C, Scotter EL, et al. Novel mutations support a role for Profilin 1 in the pathogenesis of ALS. *Neurobiol Aging.* 2015;36(3):1602.e1617-1627.
10. Gros-Louis F, Larivière R, Gowing G, et al. A frameshift deletion in peripherin gene associated with amyotrophic lateral sclerosis. *J Biol Chem.* 2004;279(44):45951-45956.
11. Smith BN, Ticozzi N, Fallini C, et al. Exome-wide rare variant analysis identifies TUBA4A mutations associated with familial ALS. *Neuron.* 2014;84(2):324-331.
12. Brenner D, Müller K, Wieland T, et al. NEK1 mutations in familial amyotrophic lateral sclerosis. *Brain.* 2016;139(Pt 5):e28.
13. Nicolas A, Kenna KP, Renton AE, et al. Genome-wide Analyses Identify KIF5A as a Novel ALS Gene. *Neuron.* 2018;97(6):1268-1283.e1266.
14. Smith BN, Topp SD, Fallini C, et al. Mutations in the vesicular trafficking protein annexin A11 are associated with amyotrophic lateral sclerosis. *Sci Transl Med.* 2017;9(388).
15. Volk AE, Weishaupt JH, Andersen PM, Ludolph AC, Kubisch C. Current knowledge and recent insights into the genetic basis of amyotrophic lateral sclerosis. *Med Genet.* 2018;30(2):252-258.
16. Mehta SG, Watts GD, Adamson JL, et al. APOE is a potential modifier gene in an autosomal dominant form of frontotemporal dementia (IBMPFD). *Genet Med.* 2007;9(1):9-13.
17. Chiò A, Calvo A, Mazzini L, et al. Extensive genetics of ALS: a population-based study in Italy. *Neurology.* 2012;79(19):1983-1989.

18. Riancho J, Castanedo-Vázquez D, Gil-Bea F, et al. ALS-derived fibroblasts exhibit reduced proliferation rate, cytoplasmic TDP-43 aggregation and a higher susceptibility to DNA damage. *J Neurol.* 2020.
19. Cykowski MD, Powell SZ, Appel JW, Arumanayagam AS, Rivera AL, Appel SH. Phosphorylated TDP-43 (pTDP-43) aggregates in the axial skeletal muscle of patients with sporadic and familial amyotrophic lateral sclerosis. *Acta Neuropathol Commun.* 2018;6(1):28.
20. Logroscino G, Piccininni M. Amyotrophic Lateral Sclerosis Descriptive Epidemiology: The Origin of Geographic Difference. *Neuroepidemiology.* 2019;52(1-2):93-103.
21. Paré B, Lehmann M, Beaudin M, et al. Misfolded SOD1 pathology in sporadic Amyotrophic Lateral Sclerosis. *Sci Rep.* 2018;8(1):14223.
22. Lai SL, Abramzon Y, Schymick JC, et al. FUS mutations in sporadic amyotrophic lateral sclerosis. *Neurobiol Aging.* 2011;32(3):550.e551-554.
23. Majounie E, Renton AE, Mok K, et al. Frequency of the C9orf72 hexanucleotide repeat expansion in patients with amyotrophic lateral sclerosis and frontotemporal dementia: a cross-sectional study. *Lancet Neurol.* 2012;11(4):323-330.
24. ARMITAGE P, DOLL R. The age distribution of cancer and a multi-stage theory of carcinogenesis. *Br J Cancer.* 1954;8(1):1-12.
25. Al-Chalabi A, Calvo A, Chio A, et al. Analysis of amyotrophic lateral sclerosis as a multistep process: a population-based modelling study. *Lancet Neurol.* 2014;13(11):1108-1113.
26. Chiò A, Mazzini L, D'Alfonso S, et al. The multistep hypothesis of ALS revisited: The role of genetic mutations. *Neurology.* 2018;91(7):e635-e642.
27. Zhang M, McKeever PM, Xi Z, et al. DNA methylation age acceleration is associated with ALS age of onset and survival. *Acta Neuropathol.* 2020.
28. Chen K, Bennett SA, Rana N, et al. Neurodegenerative Disease Proteinopathies Are Connected to Distinct Histone Post-translational Modification Landscapes. *ACS Chem Neurosci.* 2018;9(4):838-848.
29. Peters S, Visser AE, D'Ovidio F, et al. Effect modification of the association between total cigarette smoking and ALS risk by intensity, duration and time-since-quitting: Euro-MOTOR. *J Neurol Neurosurg Psychiatry.* 2020;91(1):33-39.
30. Tai H, Cui L, Shen D, Li D, Cui B, Fang J. Military service and the risk of amyotrophic lateral sclerosis: A meta-analysis. *J Clin Neurosci.* 2017;45:337-342.
31. Johnson JO, Mandrioli J, Benatar M, et al. Exome sequencing reveals VCP mutations as a cause of familial ALS. *Neuron.* 2010;68(5):857-864.
32. Abramzon Y, Johnson JO, Scholz SW, et al. Valosin-containing protein (VCP) mutations in sporadic amyotrophic lateral sclerosis. *Neurobiol Aging.* 2012;33(9):2231.e2231-2231.e2236.
33. Miller TD, Jackson AP, Barresi R, et al. Inclusion body myopathy with Paget disease and frontotemporal dementia (IBMPFD): clinical features including sphincter disturbance in a large pedigree. *J Neurol Neurosurg Psychiatry.* 2009;80(5):583-584.

34. Al-Obeidi E, Al-Tahan S, Surampalli A, et al. Genotype-phenotype study in patients with valosin-containing protein mutations associated with multisystem proteinopathy. *Clin Genet.* 2018;93(1):119-125.
35. Brody MJ, Vanhoutte D, Bakshi CV, et al. Disruption of valosin-containing protein activity causes cardiomyopathy and reveals pleiotropic functions in cardiac homeostasis. *J Biol Chem.* 2019;294(22):8918-8929.
36. Meyer H, Weihl CC. The VCP/p97 system at a glance: connecting cellular function to disease pathogenesis. *J Cell Sci.* 2014;127(Pt 18):3877-3883.
37. Ayaki T, Ito H, Fukushima H, et al. Immunoreactivity of valosin-containing protein in sporadic amyotrophic lateral sclerosis and in a case of its novel mutant. *Acta Neuropathol Commun.* 2014;2:172.
38. Zhao N, Attrebi ON, Ren Y, et al. APOE4 exacerbates α-synuclein pathology and related toxicity independent of amyloid. *Sci Transl Med.* 2020;12(529).
39. Konttinen H, Cabral-da-Silva MEC, Ohtonen S, et al. PSEN1ΔE9, APPswe, and APOE4 Confer Disparate Phenotypes in Human iPSC-Derived Microglia. *Stem Cell Reports.* 2019;13(4):669-683.
40. Huang YA, Zhou B, Wernig M, Südhof TC. ApoE2, ApoE3, and ApoE4 Differentially Stimulate APP Transcription and Aβ Secretion. *Cell.* 2017;168(3):427-441.e421.
41. Spina S, Van Laar AD, Murrell JR, et al. Phenotypic variability in three families with valosin-containing protein mutation. *Eur J Neurol.* 2013;20(2):251-258.
42. Wójcik C, Rowicka M, Kudlicki A, et al. Valosin-containing protein (p97) is a regulator of endoplasmic reticulum stress and of the degradation of N-end rule and ubiquitin-fusion degradation pathway substrates in mammalian cells. *Mol Biol Cell.* 2006;17(11):4606-4618.
43. Hänzelmann P, Schindelin H. The structural and functional basis of the p97/valosin-containing protein (VCP)-interacting motif (VIM): mutually exclusive binding of cofactors to the N-terminal domain of p97. *J Biol Chem.* 2011;286(44):38679-38690.
44. Ritz D, Vuk M, Kirchner P, et al. Endolysosomal sorting of ubiquitylated caveolin-1 is regulated by VCP and UBXD1 and impaired by VCP disease mutations. *Nat Cell Biol.* 2011;13(9):1116-1123.
45. Buchan JR, Kolaitis RM, Taylor JP, Parker R. Eukaryotic stress granules are cleared by autophagy and Cdc48/VCP function. *Cell.* 2013;153(7):1461-1474.
46. Seguin SJ, Morelli FF, Vinet J, et al. Inhibition of autophagy, lysosome and VCP function impairs stress granule assembly. *Cell Death Differ.* 2014;21(12):1838-1851.
47. Wang T, Xu W, Qin M, et al. Pathogenic Mutations in the Valosin-containing Protein/p97(VCP) N-domain Inhibit the SUMOylation of VCP and Lead to Impaired Stress Response. *J Biol Chem.* 2016;291(27):14373-14384.
48. Bastola P, Neums L, Schoenen FJ, Chien J. VCP inhibitors induce endoplasmic reticulum stress, cause cell cycle arrest, trigger caspase-mediated cell death and synergistically kill ovarian cancer cells in combination with Salubrinal. *Mol Oncol.* 2016;10(10):1559-1574.
49. Kustermann M, Manta L, Paone C, et al. Loss of the novel Vcp (valosin containing protein) interactor Washc4 interferes with autophagy-mediated

proteostasis in striated muscle and leads to myopathy in vivo. *Autophagy.* 2018;14(11):1911-1927.
50. Hou X, Wei H, Rajagopalan C, et al. Dissection of the Role of VIMP in Endoplasmic Reticulum-Associated Degradation of CFTRΔF508. *Sci Rep.* 2018;8(1):4764.
51. Harding HP, Calfon M, Urano F, Novoa I, Ron D. Transcriptional and translational control in the Mammalian unfolded protein response. *Annu Rev Cell Dev Biol.* 2002;18:575-599.
52. Shah PP, Beverly LJ. Regulation of VCP/p97 demonstrates the critical balance between cell death and epithelial-mesenchymal transition (EMT) downstream of ER stress. *Oncotarget.* 2015;6(19):17725-17737.
53. Rabinovich E, Kerem A, Fröhlich KU, Diamant N, Bar-Nun S. AAA-ATPase p97/Cdc48p, a cytosolic chaperone required for endoplasmic reticulum-associated protein degradation. *Mol Cell Biol.* 2002;22(2):626-634.
54. Jarosch E, Taxis C, Volkwein C, et al. Protein dislocation from the ER requires polyubiquitination and the AAA-ATPase Cdc48. *Nat Cell Biol.* 2002;4(2):134-139.
55. Lim PJ, Danner R, Liang J, et al. Ubiquilin and p97/VCP bind erasin, forming a complex involved in ERAD. *J Cell Biol.* 2009;187(2):201-217.
56. Yu L, Chen Y, Tooze SA. Autophagy pathway: Cellular and molecular mechanisms. *Autophagy.* 2018;14(2):207-215.
57. Ju JS, Fuentealba RA, Miller SE, et al. Valosin-containing protein (VCP) is required for autophagy and is disrupted in VCP disease. *J Cell Biol.* 2009;187(6):875-888.
58. Kobayashi T, Manno A, Kakizuka A. Involvement of valosin-containing protein (VCP)/p97 in the formation and clearance of abnormal protein aggregates. *Genes Cells.* 2007;12(7):889-901.
59. Gitcho MA, Strider J, Carter D, et al. VCP mutations causing frontotemporal lobar degeneration disrupt localization of TDP-43 and induce cell death. *J Biol Chem.* 2009;284(18):12384-12398.
60. Rycenga HB, Wolfe KB, Yeh ES, Long DT. Uncoupling of p97 ATPase activity has a dominant negative effect on protein extraction. *Sci Rep.* 2019;9(1):10329.
61. Turner MR, Bowser R, Bruijn L, et al. Mechanisms, models and biomarkers in amyotrophic lateral sclerosis. *Amyotroph Lateral Scler Frontotemporal Degener.* 2013;14 Suppl 1:19-32.
62. Jain S, Wheeler JR, Walters RW, Agrawal A, Barsic A, Parker R. ATPase-Modulated Stress Granules Contain a Diverse Proteome and Substructure. *Cell.* 2016;164(3):487-498.
63. Orrù S, Coni P, Floris A, et al. Reduced stress granule formation and cell death in fibroblasts with the A382T mutation of TARDBP gene: evidence for loss of TDP-43 nuclear function. *Hum Mol Genet.* 2016;25(20):4473-4483.
64. Buchan JR, Parker R. Eukaryotic stress granules: the ins and outs of translation. *Mol Cell.* 2009;36(6):932-941.
65. Molliex A, Temirov J, Lee J, et al. Phase separation by low complexity domains promotes stress granule assembly and drives pathological fibrillization. *Cell.* 2015;163(1):123-133.

66. Kedersha N, Ivanov P, Anderson P. Stress granules and cell signaling: more than just a passing phase? *Trends Biochem Sci.* 2013;38(10):494-506.
67. Guo W, Chen Y, Zhou X, et al. An ALS-associated mutation affecting TDP-43 enhances protein aggregation, fibril formation and neurotoxicity. *Nat Struct Mol Biol.* 2011;18(7):822-830.
68. Prasad A, Bharathi V, Sivalingam V, Girdhar A, Patel BK. Molecular Mechanisms of TDP-43 Misfolding and Pathology in Amyotrophic Lateral Sclerosis. *Front Mol Neurosci.* 2019;12:25.
69. Khalfallah Y, Kuta R, Grasmuck C, Prat A, Durham HD, Vande Velde C. TDP-43 regulation of stress granule dynamics in neurodegenerative disease-relevant cell types. *Sci Rep.* 2018;8(1):7551.
70. Breiner A, Zinman L, Bourque PR. Edaravone for amyotrophic lateral sclerosis: barriers to access and lifeboat ethics. *CMAJ.* 2020;192(12):E319-E320.
71. Jaiswal MK. Riluzole But Not Melatonin Ameliorates Acute Motor Neuron Degeneration and Moderately Inhibits SOD1-Mediated Excitotoxicity Induced Disrupted Mitochondrial Ca. *Front Cell Neurosci.* 2016;10:295.
72. Miller RG, Mitchell JD, Lyon M, Moore DH. Riluzole for amyotrophic lateral sclerosis (ALS)/motor neuron disease (MND). *Cochrane Database Syst Rev.* 2002(2):CD001447.
73. Qi X, Okuma Y, Hosoi T, Nomura Y. Edaravone protects against hypoxia/ischemia-induced endoplasmic reticulum dysfunction. *J Pharmacol Exp Ther.* 2004;311(1):388-393.
74. Ito H, Wate R, Zhang J, et al. Treatment with edaravone, initiated at symptom onset, slows motor decline and decreases SOD1 deposition in ALS mice. *Exp Neurol.* 2008;213(2):448-455.
75. Luo L, Song Z, Li X, et al. Efficacy and safety of edaravone in treatment of amyotrophic lateral sclerosis-a systematic review and meta-analysis. *Neurol Sci.* 2019;40(2):235-241.
76. Zhao B, Marciniuk K, Gibbs E, Yousefi M, Napper S, Cashman NR. Therapeutic vaccines for amyotrophic lateral sclerosis directed against disease specific epitopes of superoxide dismutase 1. *Vaccine.* 2019;37(35):4920-4927.
77. Ma J, Gao J, Wang J, Xie A. Prion-Like Mechanisms in Parkinson's Disease. *Front Neurosci.* 2019;13:552.
78. Marciniuk K, Taschuk R, Napper S. Evidence for prion-like mechanisms in several neurodegenerative diseases: potential implications for immunotherapy. *Clin Dev Immunol.* 2013;2013:473706.
79. Sibilla C, Bertolotti A. Prion Properties of SOD1 in Amyotrophic Lateral Sclerosis and Potential Therapy. *Cold Spring Harb Perspect Biol.* 2017;9(10).
80. Grad LI, Pokrishevsky E, Cashman NR. Intercellular Prion-Like Conversion and Transmission of Cu/Zn Superoxide Dismutase (SOD1) in Cell Culture. *Methods Mol Biol.* 2017;1658:357-367.
81. Marciniuk K, Määttänen P, Taschuk R, et al. Development of a multivalent, PrP(Sc)-specific prion vaccine through rational optimization of three disease-specific epitopes. *Vaccine.* 2014;32(17):1988-1997.

82. Taschuk R, Griebel P, Napper S. Carrier protein significantly alters the magnitude, duration and type of antibody response to a peptide epitope from a self-protein. *J Immol and Vacc.* 2015;1(1):101.
83. Kirk SE, Tracey TJ, Steyn FJ, Ngo ST. Biomarkers of Metabolism in Amyotrophic Lateral Sclerosis. *Front Neurol.* 2019;10:191.
84. Verber NS, Shepheard SR, Sassani M, et al. Biomarkers in Motor Neuron Disease: A State of the Art Review. *Front Neurol.* 2019;10:291.
85. Califf RM. Biomarker definitions and their applications. *Exp Biol Med (Maywood).* 2018;243(3):213-221.
86. Rosengren LE, Karlsson JE, Karlsson JO, Persson LI, Wikkelsø C. Patients with amyotrophic lateral sclerosis and other neurodegenerative diseases have increased levels of neurofilament protein in CSF. *J Neurochem.* 1996;67(5):2013-2018.
87. Joyce NC, Carter GT. Electrodiagnosis in persons with amyotrophic lateral sclerosis. *PM R.* 2013;5(5 Suppl):S89-95.
88. Matharan M, Mathis S, Bonabaud S, Carla L, Soulages A, Le Masson G. Minimizing the Diagnostic Delay in Amyotrophic Lateral Sclerosis: The Role of Nonneurologist Practitioners. *Neurol Res Int.* 2020;2020:1473981.
89. Fang J, Cui LY, Liu MS, et al. F Wave Study in Amyotrophic Lateral Sclerosis: Assessment of Segmental Motoneuronal Dysfunction. *Chin Med J (Engl).* 2015;128(13):1738-1742.
90. Liu MS, Niu JW, Li Y, Guan YZ, Cui LY. Quantitating Changes in Jitter and Spike Number Using Concentric Needle Electrodes in Amyotrophic Lateral Sclerosis Patients. *Chin Med J (Engl).* 2016;129(9):1036-1040.
91. Ishaque A, Mah D, Seres P, et al. Corticospinal tract degeneration in ALS unmasked in T1-weighted images using texture analysis. *Hum Brain Mapp.* 2019;40(4):1174-1183.
92. Kassubek J, Müller HP, Del Tredici K, et al. Imaging the pathoanatomy of amyotrophic lateral sclerosis in vivo: targeting a propagation-based biological marker. *J Neurol Neurosurg Psychiatry.* 2018;89(4):374-381.
93. Benatar M, Wuu J, Andersen PM, Lombardi V, Malaspina A. Neurofilament light: A candidate biomarker of presymptomatic amyotrophic lateral sclerosis and phenoconversion. *Ann Neurol.* 2018;84(1):130-139.
94. Benatar M, Wuu J, Lombardi V, et al. Neurofilaments in pre-symptomatic ALS and the impact of genotype. *Amyotroph Lateral Scler Frontotemporal Degener.* 2019;20(7-8):538-548.
95. Poesen K, De Schaepdryver M, Stubendorff B, et al. Neurofilament markers for ALS correlate with extent of upper and lower motor neuron disease. *Neurology.* 2017;88(24):2302-2309.
96. Gaetani L, Blennow K, Calabresi P, Di Filippo M, Parnetti L, Zetterberg H. Neurofilament light chain as a biomarker in neurological disorders. *J Neurol Neurosurg Psychiatry.* 2019;90(8):870-881.
97. Siller N, Kuhle J, Muthuraman M, et al. Serum neurofilament light chain is a biomarker of acute and chronic neuronal damage in early multiple sclerosis. *Mult Scler.* 2018:1352458518765666.

98. Lewczuk P, Ermann N, Andreasson U, et al. Plasma neurofilament light as a potential biomarker of neurodegeneration in Alzheimer's disease. *Alzheimers Res Ther.* 2018;10(1):71.
99. Gaiani A, Martinelli I, Bello L, et al. Diagnostic and Prognostic Biomarkers in Amyotrophic Lateral Sclerosis: Neurofilament Light Chain Levels in Definite Subtypes of Disease. *JAMA Neurol.* 2017;74(5):525-532.
100. Hansson O, Janelidze S, Hall S, et al. Blood-based NfL: A biomarker for differential diagnosis of parkinsonian disorder. *Neurology.* 2017;88(10):930-937.
101. Darras BT, Crawford TO, Finkel RS, et al. Neurofilament as a potential biomarker for spinal muscular atrophy. *Ann Clin Transl Neurol.* 2019;6(5):932-944.
102. Kasai T, Kojima Y, Ohmichi T, et al. Combined use of CSF NfL and CSF TDP-43 improves diagnostic performance in ALS. *Ann Clin Transl Neurol.* 2019.
103. Forgrave LM, Ma M, Best JR, DeMarco ML. The diagnostic performance of neurofilament light chain in CSF and blood for Alzheimer's disease, frontotemporal dementia, and amyotrophic lateral sclerosis: A systematic review and meta-analysis. *Alzheimers Dement (Amst).* 2019;11:730-743.
104. Liu Y, Chen Q. 150 years of Darwin's theory of intercellular flow of hereditary information. *Nat Rev Mol Cell Biol.* 2018;19(12):749-750.
105. Wolf P. The nature and significance of platelet products in human plasma. *Br J Haematol.* 1967;13(3):269-288.
106. Konoshenko MY, Lekchnov EA, Vlassov AV, Laktionov PP. Isolation of Extracellular Vesicles: General Methodologies and Latest Trends. *Biomed Res Int.* 2018;2018:8545347.
107. Latifkar A, Hur YH, Sanchez JC, Cerione RA, Antonyak MA. New insights into extracellular vesicle biogenesis and function. *J Cell Sci.* 2019;132(13).
108. Rayyan M, Zheutlin A, Byrd JB. Clinical research using extracellular vesicles: insights from the International Society for Extracellular Vesicles 2018 Annual Meeting. *J Extracell Vesicles.* 2018;7(1):1535744.
109. Nabhan JF, Hu R, Oh RS, Cohen SN, Lu Q. Formation and release of arrestin domain-containing protein 1-mediated microvesicles (ARMMs) at plasma membrane by recruitment of TSG101 protein. *Proc Natl Acad Sci U S A.* 2012;109(11):4146-4151.
110. Tricarico C, Clancy J, D'Souza-Schorey C. Biology and biogenesis of shed microvesicles. *Small GTPases.* 2017;8(4):220-232.
111. Yi YW, Lee JH, Kim SY, et al. Advances in Analysis of Biodistribution of Exosomes by Molecular Imaging. *Int J Mol Sci.* 2020;21(2).
112. Théry C, Witwer KW, Aikawa E, et al. Minimal information for studies of extracellular vesicles 2018 (MISEV2018): a position statement of the International Society for Extracellular Vesicles and update of the MISEV2014 guidelines. *J Extracell Vesicles.* 2018;7(1):1535750.
113. Anand S, Samuel M, Kumar S, Mathivanan S. Ticket to a bubble ride: Cargo sorting into exosomes and extracellular vesicles. *Biochim Biophys Acta Proteins Proteom.* 2019;1867(12):140203.
114. Chiou NT, Kageyama R, Ansel KM. Selective Export into Extracellular Vesicles and Function of tRNA Fragments during T Cell Activation. *Cell Rep.* 2018;25(12):3356-3370.e3354.

115. Tosar JP, Gámbaro F, Sanguinetti J, Bonilla B, Witwer KW, Cayota A. Assessment of small RNA sorting into different extracellular fractions revealed by high-throughput sequencing of breast cell lines. *Nucleic Acids Res.* 2015;43(11):5601-5616.
116. Nolte-'t Hoen EN, Buermans HP, Waasdorp M, Stoorvogel W, Wauben MH, 't Hoen PA. Deep sequencing of RNA from immune cell-derived vesicles uncovers the selective incorporation of small non-coding RNA biotypes with potential regulatory functions. *Nucleic Acids Res.* 2012;40(18):9272-9285.
117. Nazarenko I, Rana S, Baumann A, et al. Cell surface tetraspanin Tspan8 contributes to molecular pathways of exosome-induced endothelial cell activation. *Cancer Res.* 2010;70(4):1668-1678.
118. van Niel G, Charrin S, Simoes S, et al. The tetraspanin CD63 regulates ESCRT-independent and -dependent endosomal sorting during melanogenesis. *Dev Cell.* 2011;21(4):708-721.
119. Katzmann DJ, Babst M, Emr SD. Ubiquitin-dependent sorting into the multivesicular body pathway requires the function of a conserved endosomal protein sorting complex, ESCRT-I. *Cell.* 2001;106(2):145-155.
120. Babst M, Katzmann DJ, Estepa-Sabal EJ, Meerloo T, Emr SD. Escrt-III: an endosome-associated heterooligomeric protein complex required for mvb sorting. *Dev Cell.* 2002;3(2):271-282.
121. Azmi I, Davies B, Dimaano C, et al. Recycling of ESCRTs by the AAA-ATPase Vps4 is regulated by a conserved VSL region in Vta1. *J Cell Biol.* 2006;172(5):705-717.
122. Babst M, Katzmann DJ, Snyder WB, Wendland B, Emr SD. Endosome-associated complex, ESCRT-II, recruits transport machinery for protein sorting at the multivesicular body. *Dev Cell.* 2002;3(2):283-289.
123. Wollert T, Wunder C, Lippincott-Schwartz J, Hurley JH. Membrane scission by the ESCRT-III complex. *Nature.* 2009;458(7235):172-177.
124. Colombo M, Moita C, van Niel G, et al. Analysis of ESCRT functions in exosome biogenesis, composition and secretion highlights the heterogeneity of extracellular vesicles. *J Cell Sci.* 2013;126(Pt 24):5553-5565.
125. Larios J, Mercier V, Roux A, Gruenberg J. ALIX- and ESCRT-III-dependent sorting of tetraspanins to exosomes. *J Cell Biol.* 2020;219(3).
126. Wang T, Gilkes DM, Takano N, et al. Hypoxia-inducible factors and RAB22A mediate formation of microvesicles that stimulate breast cancer invasion and metastasis. *Proc Natl Acad Sci U S A.* 2014;111(31):E3234-3242.
127. Muralidharan-Chari V, Clancy J, Plou C, et al. ARF6-regulated shedding of tumor cell-derived plasma membrane microvesicles. *Curr Biol.* 2009;19(22):1875-1885.
128. Bolukbasi MF, Mizrak A, Ozdener GB, et al. miR-1289 and "Zipcode"-like Sequence Enrich mRNAs in Microvesicles. *Mol Ther Nucleic Acids.* 2012;1:e10.
129. Wang Q, Lu Q. Plasma membrane-derived extracellular microvesicles mediate non-canonical intercellular NOTCH signaling. *Nat Commun.* 2017;8(1):709.
130. Kuipers ME, Hokke CH, Smits HH, Nolte-'t Hoen ENM. Pathogen-Derived Extracellular Vesicle-Associated Molecules That Affect the Host Immune System: An Overview. *Front Microbiol.* 2018;9:2182.

131. Neumann M, Sampathu DM, Kwong LK, et al. Ubiquitinated TDP-43 in frontotemporal lobar degeneration and amyotrophic lateral sclerosis. *Science.* 2006;314(5796):130-133.
132. Leoni E, Bremang M, Mitra V, et al. Combined Tissue-Fluid Proteomics to Unravel Phenotypic Variability in Amyotrophic Lateral Sclerosis. *Sci Rep.* 2019;9(1):4478.
133. Tyzack GE, Luisier R, Taha DM, et al. Widespread FUS mislocalization is a molecular hallmark of amyotrophic lateral sclerosis. *Brain.* 2019.
134. Vaccaro A, Tauffenberger A, Aggad D, Rouleau G, Drapeau P, Parker JA. Mutant TDP-43 and FUS cause age-dependent paralysis and neurodegeneration in C. elegans. *PLoS One.* 2012;7(2):e31321.
135. Shibata N, Hirano A, Kobayashi M, et al. Cu/Zn superoxide dismutase-like immunoreactivity in Lewy body-like inclusions of sporadic amyotrophic lateral sclerosis. *Neurosci Lett.* 1994;179(1-2):149-152.
136. Sproviero D, La Salvia S, Giannini M, et al. Pathological Proteins Are Transported by Extracellular Vesicles of Sporadic Amyotrophic Lateral Sclerosis Patients. *Front Neurosci.* 2018;12:487.
137. Iguchi Y, Eid L, Parent M, et al. Exosome secretion is a key pathway for clearance of pathological TDP-43. *Brain.* 2016;139(Pt 12):3187-3201.
138. Grad LI, Yerbury JJ, Turner BJ, et al. Intercellular propagated misfolding of wild-type Cu/Zn superoxide dismutase occurs via exosome-dependent and -independent mechanisms. *Proc Natl Acad Sci U S A.* 2014;111(9):3620-3625.
139. Silverman JM, Christy D, Shyu CC, et al. CNS-derived extracellular vesicles from superoxide dismutase 1 (SOD1). *J Biol Chem.* 2019;294(10):3744-3759.
140. Peng X, Cashman NR, Plotkin SS. Prediction of Misfolding-Specific Epitopes in SOD1 Using Collective Coordinates. *J Phys Chem B.* 2018;122(49):11662-11676.
141. Ayers JI, Cashman NR. Prion-like mechanisms in amyotrophic lateral sclerosis. *Handb Clin Neurol.* 2018;153:337-354.
142. Smethurst P, Risse E, Tyzack GE, et al. Distinct responses of neurons and astrocytes to TDP-43 proteinopathy in amyotrophic lateral sclerosis. *Brain.* 2020;143(2):430-440.
143. Nonaka T, Masuda-Suzukake M, Arai T, et al. Prion-like properties of pathological TDP-43 aggregates from diseased brains. *Cell Rep.* 2013;4(1):124-134.
144. Franzmann TM, Alberti S. Prion-like low-complexity sequences: Key regulators of protein solubility and phase behavior. *J Biol Chem.* 2019;294(18):7128-7136.
145. Barranco I, Padilla L, Parrilla I, et al. Extracellular vesicles isolated from porcine seminal plasma exhibit different tetraspanin expression profiles. *Sci Rep.* 2019;9(1):11584.
146. van Herwijnen MJC, Driedonks TAP, Snoek BL, et al. Abundantly Present miRNAs in Milk-Derived Extracellular Vesicles Are Conserved Between Mammals. *Front Nutr.* 2018;5:81.
147. Sproviero D, La Salvia S, Colombo F, et al. Leukocyte Derived Microvesicles as Disease Progression Biomarkers in Slow Progressing Amyotrophic Lateral Sclerosis Patients. *Front Neurosci.* 2019;13:344.

148. Abu-Rumeileh S, Steinacker P, Polischi B, et al. CSF biomarkers of neuroinflammation in distinct forms and subtypes of neurodegenerative dementia. *Alzheimers Res Ther.* 2019;12(1):2.
149. Welton JL, Loveless S, Stone T, von Ruhland C, Robertson NP, Clayton A. Cerebrospinal fluid extracellular vesicle enrichment for protein biomarker discovery in neurological disease; multiple sclerosis. *J Extracell Vesicles.* 2017;6(1):1369805.
150. Sun Y, Xia Z, Shang Z, et al. Facile preparation of salivary extracellular vesicles for cancer proteomics. *Sci Rep.* 2016;6:24669.
151. Garcia-Vives E, Solé C, Moliné T, et al. The Urinary Exosomal miRNA Expression Profile is Predictive of Clinical Response in Lupus Nephritis. *Int J Mol Sci.* 2020;21(4).
152. Ohmichi T, Mitsuhashi M, Tatebe H, Kasai T, Ali El-Agnaf OM, Tokuda T. Quantification of brain-derived extracellular vesicles in plasma as a biomarker to diagnose Parkinson's and related diseases. *Parkinsonism Relat Disord.* 2019;61:82-87.
153. Wang S, Kojima K, Mobley JA, West AB. Proteomic analysis of urinary extracellular vesicles reveal biomarkers for neurologic disease. *EBioMedicine.* 2019;45:351-361.
154. Ebrahimkhani S, Vafaee F, Young PE, et al. Exosomal microRNA signatures in multiple sclerosis reflect disease status. *Sci Rep.* 2017;7(1):14293.
155. Serio A, Patani R. Concise Review: The Cellular Conspiracy of Amyotrophic Lateral Sclerosis. *Stem Cells.* 2018;36(3):293-303.
156. Smethurst P, Newcombe J, Troakes C, et al. In vitro prion-like behaviour of TDP-43 in ALS. *Neurobiol Dis.* 2016;96:236-247.
157. Otake K, Kamiguchi H, Hirozane Y. Identification of biomarkers for amyotrophic lateral sclerosis by comprehensive analysis of exosomal mRNAs in human cerebrospinal fluid. *BMC Med Genomics.* 2019;12(1):7.
158. Wu QY, Zhu YY, Liu Y, et al. CUEDC2, a novel interacting partner of the SOCS1 protein, plays important roles in the leukaemogenesis of acute myeloid leukaemia. *Cell Death Dis.* 2018;9(7):774.
159. Zachau AC, Landén M, Mobarrez F, Nybom R, Wallén H, Wetterberg L. Leukocyte-derived microparticles and scanning electron microscopic structures in two fractions of fresh cerebrospinal fluid in amyotrophic lateral sclerosis: a case report. *J Med Case Rep.* 2012;6:274.
160. Saucier D, Wajnberg G, Roy J, et al. Identification of a circulating miRNA signature in extracellular vesicles collected from amyotrophic lateral sclerosis patients. *Brain Res.* 2019;1708:100-108.
161. Katsu M, Hama Y, Utsumi J, et al. MicroRNA expression profiles of neuron-derived extracellular vesicles in plasma from patients with amyotrophic lateral sclerosis. *Neurosci Lett.* 2019;708:134176.
162. Diekstra FP, Van Deerlin VM, van Swieten JC, et al. C9orf72 and UNC13A are shared risk loci for amyotrophic lateral sclerosis and frontotemporal dementia: a genome-wide meta-analysis. *Ann Neurol.* 2014;76(1):120-133.

163. van Es MA, Veldink JH, Saris CG, et al. Genome-wide association study identifies 19p13.3 (UNC13A) and 9p21.2 as susceptibility loci for sporadic amyotrophic lateral sclerosis. *Nat Genet.* 2009;41(10):1083-1087.
164. Ross PJ, Parks RJ. Construction of First–generation Adenoviral Vectors. In: Friedman T, Rossi J, eds. *Gene Transfer: Delivery and Expression of DNA and RNA, A Laboratory Manual.* Cold Spring Harbor, New York: Cold Spring Harbor Laboratory Press; 2007.
165. Altschul SF, Gish W, Miller W, Myers EW, Lipman DJ. Basic local alignment search tool. *J Mol Biol.* 1990;215(3):403-410.
166. Challberg MD, Kelly TJ. Adenovirus DNA replication in vitro. *Proc Natl Acad Sci U S A.* 1979;76(2):655-659.
167. França CN, Izar MC, Amaral JB, Tegani DM, Fonseca FA. Microparticles as potential biomarkers of cardiovascular disease. *Arq Bras Cardiol.* 2015;104(2):169-174.
168. Usta Atmaca H, Akbas F, Aral H. Relationship between circulating microparticles and hypertension and other cardiac disease biomarkers in the elderly. *BMC Cardiovasc Disord.* 2019;19(1):164.
169. Burger D, Viñas JL, Akbari S, et al. Human endothelial colony-forming cells protect against acute kidney injury: role of exosomes. *Am J Pathol.* 2015;185(8):2309-2323.
170. Gombar R, Pitcher TE, Lewis JA, Auld J, Vacratsis PO. Proteomic characterization of seminal plasma from alternative reproductive tactics of Chinook salmon (Oncorhynchus tswatchysha). *J Proteomics.* 2017;157:1-9.
171. Eshraghi M, Gombar R, De Repentigny Y, Vacratsis PO, Kothary R. Pathologic Alterations in the Proteome of Synaptosomes from a Mouse Model of Spinal Muscular Atrophy. *J Proteome Res.* 2019;18(8):3042-3051.
172. Raudvere U, Kolberg L, Kuzmin I, et al. g:Profiler: a web server for functional enrichment analysis and conversions of gene lists (2019 update). *Nucleic Acids Res.* 2019;47(W1):W191-W198.
173. Müller JM, Deinhardt K, Rosewell I, Warren G, Shima DT. Targeted deletion of p97 (VCP/CDC48) in mouse results in early embryonic lethality. *Biochem Biophys Res Commun.* 2007;354(2):459-465.
174. Sabatelli M, Zollino M, Conte A, et al. Primary fibroblasts cultures reveal TDP-43 abnormalities in amyotrophic lateral sclerosis patients with and without SOD1 mutations. *Neurobiol Aging.* 2015;36(5):2005.e2005-2005.e2013.
175. Yang S, Zhang KY, Kariawasam R, et al. Evaluation of Skin Fibroblasts from Amyotrophic Lateral Sclerosis Patients for the Rapid Study of Pathological Features. *Neurotox Res.* 2015;28(2):138-146.
176. Chen Y, Cohen TJ. Aggregation of the nucleic acid-binding protein TDP-43 occurs via distinct routes that are coordinated with stress granule formation. *J Biol Chem.* 2019;294(10):3696-3706.
177. Freibaum BD, Chitta RK, High AA, Taylor JP. Global analysis of TDP-43 interacting proteins reveals strong association with RNA splicing and translation machinery. *J Proteome Res.* 2010;9(2):1104-1120.

178. Kabashi E, Valdmanis PN, Dion P, et al. TARDBP mutations in individuals with sporadic and familial amyotrophic lateral sclerosis. *Nat Genet.* 2008;40(5):572-574.
179. Lehrich BM, Liang Y, Khosravi P, Federoff HJ, Fiandaca MS. Fetal Bovine Serum-Derived Extracellular Vesicles Persist within Vesicle-Depleted Culture Media. *Int J Mol Sci.* 2018;19(11).
180. Feoktistova M, Geserick P, Leverkus M. Crystal Violet Assay for Determining Viability of Cultured Cells. *Cold Spring Harb Protoc.* 2016;2016(4):pdb.prot087379.
181. Shih YT, Hsueh YP. The involvement of endoplasmic reticulum formation and protein synthesis efficiency in VCP- and ATL1-related neurological disorders. *J Biomed Sci.* 2018;25(1):2.
182. Arthur KC, Calvo A, Price TR, Geiger JT, Chiò A, Traynor BJ. Projected increase in amyotrophic lateral sclerosis from 2015 to 2040. *Nat Commun.* 2016;7:12408.
183. Nash LA, McFall ER, Perozzo AM, et al. Survival Motor Neuron Protein is Released from Cells in Exosomes: A Potential Biomarker for Spinal Muscular Atrophy. *Sci Rep.* 2017;7(1):13859.
184. Kitamura Y, Kojima M, Kurosawa T, et al. Proteomic Profiling of Exosomal Proteins for Blood-based Biomarkers in Parkinson's Disease. *Neuroscience.* 2018;392:121-128.
185. Kosaka N, Kogure A, Yamamoto T, et al. Exploiting the message from cancer: the diagnostic value of extracellular vesicles for clinical applications. *Exp Mol Med.* 2019;51(3):1-9.
186. Roy J, Saucier D, O'Connell C, Morin PJ. Extracellular vesicles and their diagnostic potential in amyotrophic lateral sclerosis. *Clin Chim Acta.* 2019;497:27-34.
187. Giampetruzzi A, Danielson EW, Gumina V, et al. Modulation of actin polymerization affects nucleocytoplasmic transport in multiple forms of amyotrophic lateral sclerosis. *Nat Commun.* 2019;10(1):3827.
188. Hensel N, Claus P. The Actin Cytoskeleton in SMA and ALS: How Does It Contribute to Motoneuron Degeneration? *Neuroscientist.* 2018;24(1):54-72.
189. Wang M, You J, Bemis KG, Tegeler TJ, Brown DP. Label-free mass spectrometry-based protein quantification technologies in proteomic analysis. *Brief Funct Genomic Proteomic.* 2008;7(5):329-339.
190. Higgs RE, Knierman MD, Gelfanova V, Butler JP, Hale JE. Comprehensive label-free method for the relative quantification of proteins from biological samples. *J Proteome Res.* 2005;4(4):1442-1450.
191. Xu Z, Lee A, Nouwens A, Henderson RD, McCombe PA. Mass spectrometry analysis of plasma from amyotrophic lateral sclerosis and control subjects. *Amyotroph Lateral Scler Frontotemporal Degener.* 2018;19(5-6):362-376.
192. Mohanty L, Henderson RD, McCombe PA, Lee A. Levels of clusterin, CD5L, ficolin-3, and gelsolin in ALS patients and controls. *Amyotroph Lateral Scler Frontotemporal Degener.* 2020:1-4.
193. Anderson LR, Owens TW, Naylor MJ. Structural and mechanical functions of integrins. *Biophys Rev.* 2014;6(2):203-213.

194. Muhsin-Sharafaldine MR, Saunderson SC, Dunn AC, Faed JM, Kleffmann T, McLellan AD. Procoagulant and immunogenic properties of melanoma exosomes, microvesicles and apoptotic vesicles. *Oncotarget.* 2016;7(35):56279-56294.
195. Kowal J, Arras G, Colombo M, et al. Proteomic comparison defines novel markers to characterize heterogeneous populations of extracellular vesicle subtypes. *Proc Natl Acad Sci U S A.* 2016;113(8):E968-977.
196. Théry C, Boussac M, Véron P, et al. Proteomic analysis of dendritic cell-derived exosomes: a secreted subcellular compartment distinct from apoptotic vesicles. *J Immunol.* 2001;166(12):7309-7318.
197. Nagai A, Sato T, Akimoto N, Ito A, Sumida M. Isolation and identification of histone H3 protein enriched in microvesicles secreted from cultured sebocytes. *Endocrinology.* 2005;146(6):2593-2601.
198. Jang CW, Shibata Y, Starmer J, Yee D, Magnuson T. Histone H3.3 maintains genome integrity during mammalian development. *Genes Dev.* 2015;29(13):1377-1392.
199. Wu D, Ingram A, Lahti JH, et al. Apoptotic release of histones from nucleosomes. *J Biol Chem.* 2002;277(14):12001-12008.
200. Allam R, Kumar SV, Darisipudi MN, Anders HJ. Extracellular histones in tissue injury and inflammation. *J Mol Med (Berl).* 2014;92(5):465-472.
201. Li W, Wypych J, Duff RJ. Improved sequence variant analysis strategy by automated false positive removal. *MAbs.* 2017;9(6):978-984.
202. Auburger G, Klinkenberg M, Drost J, et al. Primary skin fibroblasts as a model of Parkinson's disease. *Mol Neurobiol.* 2012;46(1):20-27.
203. Pérez MJ, Ponce DP, Osorio-Fuentealba C, Behrens MI, Quintanilla RA. Mitochondrial Bioenergetics Is Altered in Fibroblasts from Patients with Sporadic Alzheimer's Disease. *Front Neurosci.* 2017;11:553.
204. Gray NE, Quinn JF. Alterations in mitochondrial number and function in Alzheimer's disease fibroblasts. *Metab Brain Dis.* 2015;30(5):1275-1278.
205. Teves JMY, Bhargava V, Kirwan KR, et al. Parkinson's Disease Skin Fibroblasts Display Signature Alterations in Growth, Redox Homeostasis, Mitochondrial Function, and Autophagy. *Front Neurosci.* 2017;11:737.
206. Gardiner SL, Milanese C, Boogaard MW, et al. Bioenergetics in fibroblasts of patients with Huntington disease are associated with age at onset. *Neurol Genet.* 2018;4(5):e275.
207. Lee SM, Asress S, Hales CM, et al. TDP-43 cytoplasmic inclusion formation is disrupted in *C9orf72*-associated amyotrophic lateral sclerosis/frontotemporal lobar degeneration. *Brain Commun.* 2019;1(1):fcz014.
208. Liu G, Byrd A, Warner AN, et al. Cdc48/VCP and Endocytosis Regulate TDP-43 and FUS Toxicity and Turnover. *Mol Cell Biol.* 2020;40(4).
209. Arraud N, Linares R, Tan S, et al. Extracellular vesicles from blood plasma: determination of their morphology, size, phenotype and concentration. *J Thromb Haemost.* 2014;12(5):614-627.
210. Shi M, Sheng L, Stewart T, Zabetian CP, Zhang J. New windows into the brain: Central nervous system-derived extracellular vesicles in blood. *Prog Neurobiol.* 2019;175:96-106.

211. Gardiner C, Di Vizio D, Sahoo S, et al. Techniques used for the isolation and characterization of extracellular vesicles: results of a worldwide survey. *J Extracell Vesicles.* 2016;5:32945.
212. Ludwig N, Whiteside TL, Reichert TE. Challenges in Exosome Isolation and Analysis in Health and Disease. *Int J Mol Sci.* 2019;20(19).
213. Kwiatkowski DJ, Stossel TP, Orkin SH, Mole JE, Colten HR, Yin HL. Plasma and cytoplasmic gelsolins are encoded by a single gene and contain a duplicated actin-binding domain. *Nature.* 1986;323(6087):455-458.
214. Asare-Werehene M, Nakka K, Reunov A, et al. The exosome-mediated autocrine and paracrine actions of plasma gelsolin in ovarian cancer chemoresistance. *Oncogene.* 2020;39(7):1600-1616.
215. Jaiswal MK. Riluzole and edaravone: A tale of two amyotrophic lateral sclerosis drugs. *Med Res Rev.* 2019;39(2):733-748.
216. Cedarbaum JM, Stambler N, Malta E, et al. The ALSFRS-R: a revised ALS functional rating scale that incorporates assessments of respiratory function. BDNF ALS Study Group (Phase III). *J Neurol Sci.* 1999;169(1-2):13-21.

Contributions of Collaborators

All of the data presented herein were generated by the author. Kathy Poulin provided some technical assistance. Dr. Dylan Burger contributed to the experimental design, troubleshooting of EV isolations and provided advice regarding EV characterization. Dr. Panayotis Vacratsis and his student Justin Roberto performed all liquid chromatography mass spectrometry analysis of EV samples. Antibodies for Prelamin A/C, Integrin beta-1 and gelsolin were generously gifted by Dr. Tesson, Dr. Kothary and Dr. Megeney. Dr. Robin Parks, my graduate supervisor, provided guidance and feedback throughout my training. Dr. Parks also provided editorial comments on this work.

Curriculum Vitae

Charlotte Manser

EDUCATION

University of Ottawa (2018-2020)
Master of Science, Biochemistry
Anticipated Graduation: September 2020

Carleton University (2014-2018)
Bachelor of Science Joint Honours in Biology and Neuroscience
Graduated (with distinction): June 2018

SCHOLARSHIPS & AWARDS

- uOttawa CNMD Scholarships in Translational Research (STaR) Award (2019 - declined)
- Admission Scholarship-Master's (2018-2020)
- Dean's Honour List (2018)
- Dean's Honour List (2017)
- J. Lorne Gray Scholarship (2017)

RESEARCH EXPERIENCE

- Lab of Dr. Robin J. Parks
  Master in Biochemistry (May 2018-August 2020
  Project Title: Extracellular vesicles and the quest for molecular biomarkers in amyotrophic lateral sclerosis
- Lab of Dr. Johnny K. Ngsee
  Undergraduate Honours Project (September 2017-April 2018)
  Project Title: Characterizing the Unfolded Protein Response in a cellular model of ALS8

TALKS

- Manser, C., Poulin, K., Warman Chardon, J., Burger, D. and Parks, R. J. Extracellular Vesicles and the quest for molecular biomarkers in amyotrophic lateral sclerosis. University of Ottawa Day of Medicine, Ottawa ON, May 2019

CONFERENCES AND PRESENTATIONS

- Manser, C., Poulin, K., Warman Chardon, J., Burger, D. and Parks, R. J. Extracellular Vesicles and the quest for molecular biomarkers in amyotrophic lateral sclerosis. OHRI Research Day, Ottawa ON, November 2019.
- Manser, C., Poulin, K., Warman Chardon, J., Burger, D. and Parks, R. J. Extracellular Vesicles and the quest for molecular biomarkers in amyotrophic lateral sclerosis. 15th André-Delambre Symposium on ALS, Montreal QC, September 2019.
- Manser, C., Poulin, K., Warman Chardon, J., Burger, D. and Parks, R. J. Extracellular Vesicles and the quest for molecular biomarkers in amyotrophic lateral sclerosis. Biochemistry, Microbiology and Immunology Poster Day, Ottawa ON, May 2019.
- Manser, C., Poulin, K., Warman Chardon, J., Burger, D. and Parks, R. J. Extracellular Vesicles and the quest for molecular biomarkers in amyotrophic lateral sclerosis. ALS Canada Research Forum, Toronto ON, April 2019.
- Manser, C and Parks, R. Identification of protein biomarkers in extracellular vesicles derived from patients with ALS. The Ottawa Hospital Research Institute Research Day, Ottawa ON, November 2018.
- Manser, C and Ngsee, J. Characterization of the Unfolded Protein Response in a Cellular Model of ALS8. Carleton University Undergraduate Neuroscience Research Day, Ottawa ON, April 2018.

VOLUNTEER ACTIVITIES

- Team Captain- The Éric Poulin Centre for Neuromuscular Disease, WALK TO END ALS (Ottawa ON) (June 2020) – Personal fundraising total: $3820
- Team Captain- The Éric Poulin Centre for Neuromuscular Disease, WALK TO END ALS (Ottawa ON) (June 2019) – Personal fundraising total: $2600
- Walk for Muscular Dystrophy (June 2019)
- WALK TO END ALS (Ottawa ON) (June 2018) – Personal fundraising total: $2166
- Walk for Muscular Dystrophy (June 2018)
- Participant in WALK TO END ALS (2013-2015)

PROFESSIONAL ACTIVITIES

- ALS Canada Global Citation Analysis project (June 2018-August 2019)

AREAS OF INTERESTS

- Investigation into the biological basis for selective neuron vulnerability associated with amyotrophic lateral sclerosis and other neuromuscular disease.
- Examining protein aggregation and interruptions of proteostasis and their contribution to the disease state in the context of neuromuscular disease.
- Identification of novel prognostic, diagnostic and pharmacodynamic molecular biomarkers associated with amyotrophic lateral sclerosis.